Charging, Aggregation, and Aggregate Strength of Colloidal Particles: Effect of Hydrophobicity and Solution pH

July 2019

Azizul HAKIM

Charging, Aggregation, and Aggregate Strength of Colloidal Particles: Effect of Hydrophobicity and Solution pH

A dissertation Submitted to
the Graduate School of Life and Environmental Sciences,
the University of Tsukuba
in partial Fulfillment of the Requirements
for the Degree of Doctor of Philosophy in Bioresource Engineering
(Doctoral Program in Appropriate Technology and Sciences for Sustainable Development)

Azizul HAKIM

Table of Contents

List of Figures

List of Tables

List of symbols and abbreviations

Symbol	Designation
a	Particle radius
A	Elongation rate
C_s	Bulk concentration of TPP^+ ion
C^I_s	Charge reversal concentration of TPP ion or concentration at IEP
D_f	Fractal dimension
d_{maj}	Major length of the best-fit ellipse
d_{min}	Minor length of the best-fit ellipse
e	Elementary charge
I	Scattered light intensity
m	Scaled ionic drag coefficients of counterions
$\bar{m}$	Scaled ionic drag coefficients of co-ions
m_i	Scaled drag coefficient of *i-th* ion specie
N_A	Avogadro number
n	Refractive index
Q	Scattering vector
Q	Volumetric flow rate
R	Radius of the capillary tube
r_s	Radius of adsorbed TPP^+ ion
S	The surface area of aggregate
S_{max}	The maximum surface area of an aggregate
ψ_0	Surface potential
ψ_d	Diffuse layer potential
σ_0	Surface charge density
$1/\kappa$	Debye length
n_0	Concentration (number density) of electrolyte
ε_r	Relative permittivity of liquid
ε_0	Vacuum permittivity
k_B	The Boltzmann constant
T	The absolute temperature
μ	Electrophoretic mobility
ζ	Zeta potential
$\bar{\zeta}$	Scaled zeta potential magnitude
Γ_s	The adsorbed amount of TPP ion in the Stern layer
Φ	Chemical/intrinsic adsorption energy per TPP ion
σ_s	Stern layer charge density
σ_d	Diffuse layer charge
σ_k	Electrokinetic surface charge density
x_s	The distance to the slipping plane
η	Viscosity of the medium
μ	Viscosity of fluid/ water (≈ 0.001 pa.s) at 20 °C
λ_i	Ionic drag coefficient of the *i-th* ion species
Λ_i^0	Limiting equivalent conductance of *i-th* ion specie
z_i	The valence of the *i-th* ion specie

λ	Wavelength
θ	Scattering angle
F_{hyd}	Hydrodynamic rupturing force
$F_{aggregate}$	Aggregate strength
$A_{c,max}$	Maximum elongation rate of flow
C_{hyd}	A constant depending on floc/ aggregate shape

Abbreviation Explanation

AFM	Atomic force microscopy
DLS	Dynamic light scattering
NOM	Natural organic matters
HSs	Humic substances
IEP/ iep	Iso-electric point
SRFA	Suwannee river fulvic acid
SRHA	Suwannee river humic acid
LHA	Leonardite humic acid
PSL	Polystyrene sulfate latex
TPPCl	Tetraphenylphosphonium chloride
CPC	Cetylpyridinium chloride
DPC	Dodecylpyridinium chloride
CMC	Critical micelle concentration
HB	Percentage of hydrophobic carbon
HI	Percentage of hydrophilic carbon

Chapter 1

General introduction and research goal

1.1 General introduction

1.1.1 Colloidal particles in the environment

Colloidal particles, a few nm to a few µm sized particles, and their dispersions are found in many agricultural and industrial areas. A large diversity of materials such as metal oxides, polymers, clays, carbon derivatives are included in the colloidal domain. Usually, the natural environment has a diversity of colloidal particles originated from soil minerals and organic matters (Molina, 2014). These natural colloidal particles usually carry electric charge in their surfaces, and the amount and type of charge vary depending on the environmental conditions (Molina, 2014). The charge of natural mineral colloid particles comes from the isomorphous substitution called permanent charge, and sometimes it comes from the broken edges of colloidal mineral surface layers. Additionally, the surface of the minerals and organic colloids have chargeable groups (e.g., hydroxyl (-OH), carboxyl (-COOH), amine ($-NH_2$), etc.) (Sposito, 1984; Stevenson, 1982), which also contribute in the total amount of charge or surface functionality of these colloidal materials.

The soil and water solutions are complex in nature, consisting of various types of ions and colloidal particles. Nowadays, different types of synthetic colloidal particles and chemicals are used in many industrial and agricultural purposes. These synthetic colloidal particles are discharged to the surrounding environment with some other exogenic contaminants. Upon their existence in the natural environment, they undergo different types of physical and chemical processes. The common physical and chemical processes of colloidal materials with synthetic chemicals and colloids in the natural environment are adsorption, coagulation, aggregation, dispersion, and subsequently affect the transport behavior, hydraulic properties and chemical activities (Fig. 1.1). For the understanding of

the complex phenomena in a complex system of the natural environment, it is essential to characterize the colloidal particles in respect of their size, charge, shape, structure and the changes of their behaviors during this physicochemical process.

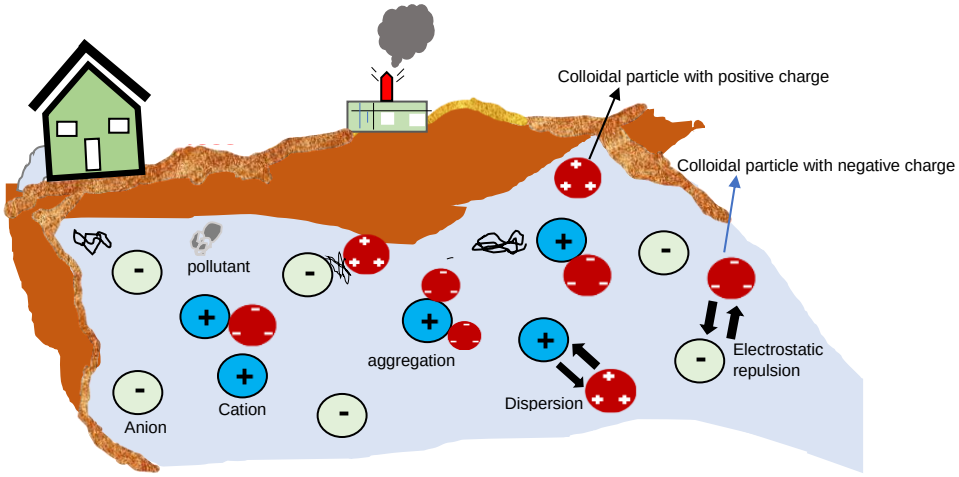

Figure 1.1. Schematic representation of different activities of colloidal particles in natural environmental condition.

It has been shown in the above schematic illustration (Fig. 1.1) that the natural colloidal particles in water environments are interacting with ionic substances by some attractive forces and form aggregates, while the interactions between the same charge of ions and colloids are usually in dispersing state due to electrostatic repulsion. Ions and particles interacting with each other by means of some attractive and repulsive forces, and the total interactions between colloidal particles could be described according to the classical DLVO (Derjaguin, Landau, Verwey, Overbeek) theory (Darjaguin and Landau, 1941). But this DLVO theory could not explain the interaction forces when considering the specific chemical nature of particles such as particles hydrophobicity. This also means that some specific ions affect the interaction between particles in electrolyte solutions, which considerably differ from the results of the DLVO. Since the natural environment has many organic solutes from different sources and multivalent ions, we need to consider some other

non-DLVO interactions and forces like hydration forces (Leneveu et al. 1977), hydrophobic forces (Israelachvili and Pashley, 1982), and charge correlation forces (Miklavic et al., 1994).

1.1.2 Aggregation and charging of colloidal particles

To characterize the colloidal particles and the processes they perform in natural environmental conditions, it is necessary to know the surface activity especially the charging behavior in different environmental conditions. This charging is one of the fundamental aspect affecting aggregation and dispersions. Upon adsorption of oppositely charged ions or particles, colloid shows charge reversal or overcharging. And the aggregation is usually taking place at charge neutralization or near around charge neutralization, usually called IEP (iso-electric point) (Fig. 1.2). Adsorption of some multivalent ions, polyelectrolytes, clays, and surfactants induces the neutralization of the particle charge and triggers aggregation (Fig. 1.2). The subsequent over-sorption and/ or overcompensation of oppositely charged ions or chemicals causes charge reversal or overcharging. This overcharging is driven by some specific ion binding, ion-ion correlations, and hydrophobic interactions (Lyklema, 2006; Jimenez et al., 2012; Nishiya et al., 2016; Hakim et al., 2016, Hakim et al., 2018).

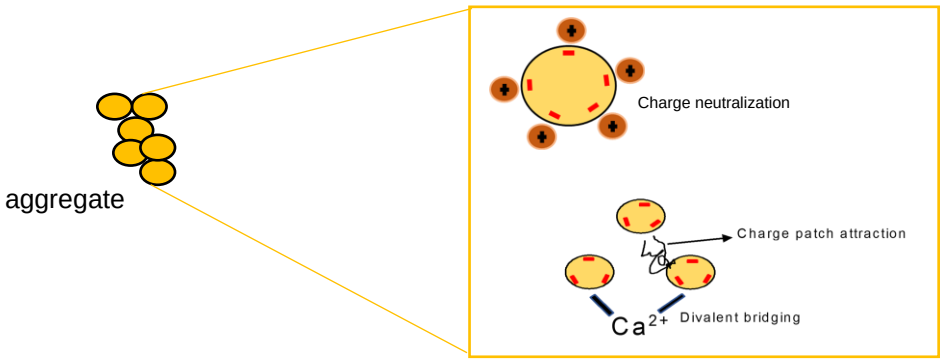

Figure 1.2. Some established mechanism for aggregation in the colloidal system

Moreover, these days a lot of hydrophobic organic dyes, surfactants, synthetic hydrophobic colloids (latex particles in paint and pigments) are released to the surrounding

natural soil and water environments and are interacted with natural organic colloids (NOC) and/or humic substances (HS) in the presence of mono and multivalent ions (Koopal et al., 2004; Ibrahim et al., 2006; Ivanković et al., 2010; Bafana et al., 2011; Olubukola et al., 2018). Therefore, these contaminants interaction with the natural organic matter or natural colloid must be paid attention to consider. These kinds of interactions induce the adsorption and binding of pollutants and big organic hydrophobic ions to colloidal materials or particles forming aggregates, which is controlling the transport and distributions of nutrient ions and pollutants in the flow system (Fig. 1.3). During the transport, the colloidal particles are subjected to the several physicochemical interactions (Fig.1.1 and Fig. 1.3) and collision between the primary particles also plays an important role in the aggregation of these colloidal particles (Russel et. al., 1989) (Fig.1.3). The collision between primary particles and their interaction depend on the shear in the flow field or turbulent flows (Adachi, 1995; Kobayashi et al., 2004; Winterwrep, 1998; Sugimoto et al., 2014) (Fig. 1.3). Hydrophobic interaction is one of the attractive forces and depends on the particle surface composition and solution chemistry (Elimelech et al.,1995). In the natural environment, the surface of the particle is not homogenous like model synthetic colloid (polystyrene latex). The surface of natural colloids (HSs and NOC) is rough and the charge distribution is also heterogeneous. Depending on the particle surface charge, energy of binding or intrinsic energy of adsorption varies (Hakim et. al. 2016, Sugimoto et al., 2017).

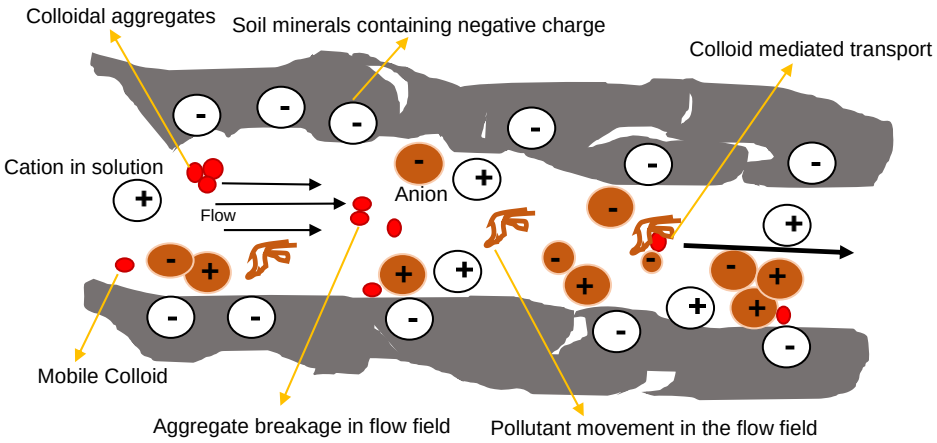

Figure 1.3. Schematic representation of colloidal aggregates in natural flow field subjected to breakage and colloid mediated transport

Figure 1.4 shows the energy of adsorption on a smooth surface of colloids. Usually, the higher the energy of adsorption is, the more the binding force of ions and chemicals on the particle surfaces is. Though the surface of natural colloid is rough, porous and soft along with the surface charge heterogeneity, our purpose is to reveal the effect of ionic strength and solution pH on the aggregation, charging, strength and structure of natural HSs aggregates.

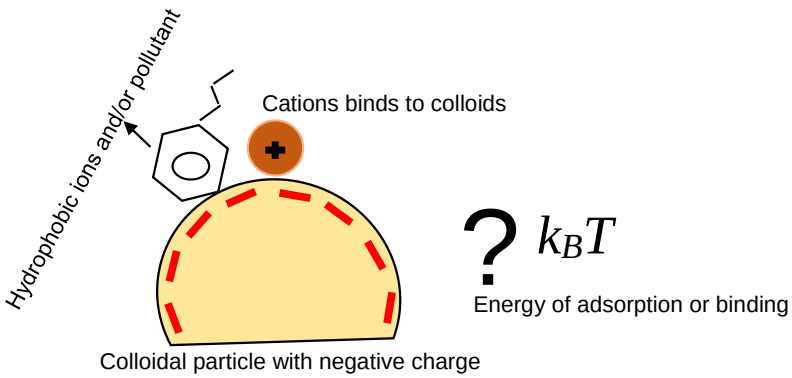

Figure 1.4. The schematic representation of the adsorption energy or binding of hydrophobic ions and simple cations on the colloid surface.

1.1.3 Aggregate breakage and aggregate strength

The aggregates of colloidal particles in the natural flow field are subjected to breakage depending on the magnitude of hydrodynamic force applied during the flow in r shear or velocity gradient in the water environment (Figure 1.5). The more the binding force acting among the particles is, the stronger the aggregate against breakage under laminar shear is. Some of the previous studies measured the force of methyl-methyl (CH_3–CH_3) tip-surface pair interaction in water and alginate hydrogels on self-assembled monolayers (SAMs), expressing as adhesion force using some sophisticated instrumental setup like atomic force microscopy (AFM) of the various synthetic colloidal system in the pure medium. They discussed that the probable cause of this adhesion force is hydrophobic interaction, local electrostatic attraction, hydrogen bonding, and so on (Warszyński et al., 2003; Helfricht et al., 2017; Noy et al., 1997). Kobayashi (2005) measured the aggregate strength expressed as force or force among the particles of floc (F_{floc}) of a natural soil particle in the presence of specific soil ions using laminar converging flow and discussed the origin of force from the attractive electric double layer. In another investigation using polystyrene (PS) microsphere, Kobayashi (2004) measured the magnitude of the floc strength. The strength was comparable with the measured value of adhesion of PS particles by AFM and elucidated the origin of force as interparticle interactions (Kobayashi, 2004).

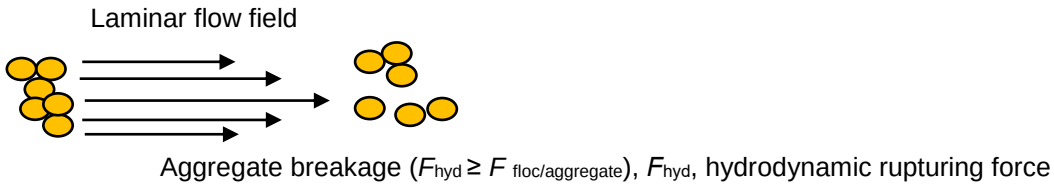

Figure 1. 5. Aggregate breakage in the laminar flow where $F_{hyd} \geq F_{floc/aggregate}$

In the case of natural soil particles and specific soil ions, interactions to form natural soil flocs are probably due to bridging by divalent ions or ion-ion correlation inducing strong attraction in the floc formation (Kobayashi, 2005; Sobeck and Higgins, 2002; Kjellander et al., 1990). The HSs are natural organic molecules, which act as natural soil colloids, and is our concern to evaluate the forces among particles and HSs molecules in aggregate in the presence of some specific ions and organic counter ions or molecules. In this situation we need to explore the strength or the forces among particles in an aggregate of HSs and the charging behavior in different environmental conditions. The factors of considerations to the non-DLVO interactions of particles specially the hydrophobic interactions of colloidal HSs is still unclear.

In addition, we also need to focus on the interactions of some hydrophobic ions with hydrophobic colloids and their effect on aggregation behavior along with charging and aggregate strength considering the natural environmental conditions and surface property of colloidal particles especially the surface charge.

1.2 A note to the factor of humic substances hydrophobicity

Humic substances (HSs) are the most common natural organic matter (NOM) in soil and water environment and are called natural colloid (Jones and Bryan, 1998) or nano-colloid. This HSs usually have a negative surface charge in natural environmental condition. This charged macromolecule has hydrophobic and hydrophilic moieties in their structure (Tipping, 2002). A solute hydrophobicity is usually the preference of the solutes to a nonaqueous solvent over the aqueous environment. The hydrophobic interaction and humic substances hydrophobicity play an important role for the binding of cationic surfactants and hydrophobic monovalent organic ions to HSs (Hakim and Kobayashi, 2019; Hakim et al. 2018; Matsuda et al., 2009; Ishiguro et. al., 2007; Treeby et. al., 2005). Nevertheless, the

effect of HSs hydrophobicity and the effect of hydrophobic interactions on the aggregation, charging, and strength of HSs aggregates are still unclear. In this investigation, we focused on the hydrophobicity factor of humic substances in the aggregation, charging, and aggregate strength of HSs in chapters 3, 4, and 5.

The hydrophobicity of amino acids hydrophobic side chains was measured from the free energy of transfer to ethanol and dioxane (Nozaki and Tanford, 1971). Bandyopadhyay and Mehler (2008) proposed another method depending on the protein structure-based scale of hydrophobicity. Another recent method characterizes the hydrophobicity of amino acid side chains in a protein environment by measuring the contact angle of water nanodroplet on the 2D peptide networks using molecular dynamics (MD) simulations (Zhu et al., 2016). Beyond the conventional water-octanol partition method, a recent investigation showed a direct measurement of nanoparticle surface hydrophobicity from the comparison of nanomaterials binding affinity to surface-modified collectors of silicon wafers of varying hydrophobicity (Valsesia et al., 2018).

However, an experimental study showed that the hydrophobicity of humic substances is accompanied by lower C/H or higher C/O atomic ratios and lower polarity (Mei et al., 2016). The higher degree of humic substances hydrophobicity is also accompanied by higher aromatic content or aromaticity (Maryganova et al., 2010). Maryganova et al. (2010) also showed that the degree of hydrophobicity (HB/HI), a ratio of the percentage of hydrophobic carbon to the percentage of hydrophilic carbon (HB/HI) is higher for the soil humic acid which contains a relatively higher aromatic carbon. Hyuang and Kim (2008) showed that the adsorption capacity of natural organic matter (NOM) to multiwalled carbon nanotubes (MWNT) was strongly dependent on the aromatic content of NOM.

From the sections as mentioned above of the hydrophobicity, we can say that the aromaticity or aromatic carbon content is a measure of the humic substances hydrophobicity.

So, we in this investigation used the term hydrophobicity interchangeably to aromaticity. In this investigation, the more the aromatic carbon content is, the more the hydrophobicity of humic substances is in the following chapters. We used three different humic substances, namely Suwannee river fulvic acid (SRFA), Suwannee river humic acid (SRHA), and Leonardite humic acid (LHA) in this thesis. The increasing trend of hydrophobicity of these three humic substances is SRFA< SRHA < LHA. The total and aromatic carbon content and the amount of carboxylic and phenolic groups are presented in table 1.2.

Table 1.2. Selected composition of the samples of three humic substances used in this thesis reported by IHSS (Reuse from Hakim and Kobayashi (2018), Colloids Surfaces A: Physicochem. Eng. Asp. 540:1-10).

IHSS samples	Carbon content % (w/w)	Carboxylic groups (meq/g-C)	Phenolic groups (meq/g-C)	Aromatic carbon (peak area percentages) (165-110 ppm)
SRFA II (Suwannee river fulvic acid)	52.34	11.17	2.84	22
SRHA II (Suwannee river humic acid)	52.63	9.13	3.72	31
LHA (Leonardite humic acid)	63.81	7. 46	2.31	58

1.3 Outline of this thesis

This thesis consists of 6 chapters in a consequent manner of discussion to explore the goal or objectives of this research. We, in this chapter (chapter 1), discuss the general rules and ways of colloidal particles charging and aggregation, and their behavior in natural environmental condition. HSs are the naturally originated negatively charged colloids of a few nm in size.

In the second chapter, we will describe the theoretical and experimental results of charge reversal and intrinsic energy of adsorption of model synthetic colloidal latex particle. We used these particles because they can be well characterized. We in this chapter will describe the charging character of hydrophobic polystyrene latex particle (PSL) in the presence of monovalent hydrophobic counterion. In this chapter, we describe the effect of hydrophobic interaction on the charge reversal of hydrophobic latex particles and the effect of surface charge density on the adsorption free energy of hydrophobic counterion on PSL particles.

Then in the third chapter, we move to the use of natural colloidal particles or humic substances (HSs), which are ubiquitous. We will use these HSs to evaluate the aggregation and charging in the presence of hydrophobic ions. We explore how hydrophobicity affects charging and aggregation. In this chapter, we will also evaluate the fractal character of the aggregates formed due to hydrophobic interaction.

In the fourth and fifth chapters, we will use the HSs again to find out the aggregation, charging, and aggregate strength in different environmental condition, which will help us to predict how the hydrophobicity, ionic condition, and solution chemistry affect the charging behavior and aggregate properties. We will also get ideas about the forces acting on the aggregation, mechanism of aggregation, and forces among particles in aggregate. We

consider how these forces affect the strength of aggregates, and the effect of some specific factor such as the pH, cation specificity, HSs hydrophobicity, solution pH and ionic strength on this forces and aggregate strength. Finally, in chapter 6, we will summarize our total chapter as a conclusion.

Chapter 2

Effect of charge density on latex particle charge reversal and the energy of adsorption for hydrophobic counter ion

2.1 Introduction

In the previous chapter, we discussed the charging of colloidal particles and charge reversal by an overcompensation of counterions. The charging (positive and/or negative), which is the basic colloidal property, depends on the solution chemistry. This surface charge of colloidal particles affects the interaction between particles and thus determines the aggregation-dispersion of colloidal suspensions. Theoretically, the aggregation of colloidal particles usually happens at a charge neutralization condition. The neutralization of particles charges is induced by counter ion and/or ionic substances adsorption present in the suspension such as polyelectrolytes (Adachi et al., 2015; Szilágyi et al., 2014; Tan et al., 2014), clays (Kobayashi et al., 2013), multivalent ions (Jiménez et al., 2012; Nishiya et al., 2016), and surfactants (Somasundaran et al., 1964; Pham et al., 2015). The adsorption of these substances and ions to the bare colloidal particles causes charge reversal. This kind of charge reversal or overcharging could be evaluated from the reverse migration of charged particles expressed as electrophoretic mobility (Hakim et al., 2016).

Overcharging of colloidal particles usually happens due to the overcompensation of counter-ions adjacent to the surface of the oppositely charged particle. Some mechanisms such as ion-ion correlation, specific ion binding, hydrophobic interaction and some other phenomena (Jiménez et al., 2012; Nishiya et al., 2016; Somasundaran et al., 1964; Lyklema, 2006) are responsible for the overcompensation of the colloidal surface by counter-ions. Different studies clearly demonstrate the effect of hydrophobicity and hydrophilicity from the measured electrophoretic mobility of colloidal particles in the presences of some big hydrophobic counterions (Calero & Faraudo, 2011; Martín-Molina et al., 2009; Perez-Fuentes et al., 2015). A simple theoretical analysis by the Stern layer adsorptions model showed that the chemical and electrostatic energy are responsible for the charge reversal. From this evaluation, the iso-electric point (IEP) is also determined by the intrinsic energy

of adsorption and the surface charge density (Somasundaran et al., 1964; Calero & Faraudo, 2011). Hydrophobic counter ions were used on hydrophobic and hydrophilic surfaces to evaluate the energy of adsorptions in some previous literatures (Somasundaran et al., 1964; Calero & Faraudo, 2011; Martín-Molina et al., 2009). Martín-Molina et al. (2009) demonstrated a value of the energy of adsorptions which is comparable to the half of the energy of transfer of hydrophobic ions from water to non-aqueous solvent. And another study demonstrated that the proportionality of IEP to the surface charge density using molecular dynamics simulations (Calero and Faraudo, 2011). But there are lacking on the systematic experimental data of the effect of surface charge density on ethe nergy of adsorptions and on IEP. From this view point, we focus our investigation to explore the relation of charge density of hydrophobic model polystyrene colloid particles and intrinsic and/or chemical energy of adsorptions and the IEP in the presence of big hydrophobic counter ion.

This investigation will demonstrate the relationship between theoretical modeling and experimental data of IEP of hydrophobic polystyrene sulfate latex colloids in the presence of hydrophobic tetraphenylphosphonium cations (TPP^+). The results will visualize the intrinsic/chemical energy of adsorption of TPP^+ to latex particles of different surface charge density depicting the IEP and charge reversal. We, in this investigation, used the polystyrene sulfate latex particles as a hydrophobic colloid, to evaluate the adsorption energy of big hydrophobic ions. The polystyrene latex particles are nowadays considering as micro and nano plastic particles pollutants in the environment.

2.2 Experimental

2.2.1 Materials

Three IDC latex spheres (polystyrene sulfate latex, PSL) (Thermo-Fischer) were used. Their manufacturer supplied parameters are listed in Table 2.1. All the three latex spheres were dialyzed in a Visking tube pre-cleaned in boiled $NaHCO_3$ (Kanto Chemical Co., Inc.) and EDTA (Sigma-Aldrich) solution, against pure water, was used. Until 2 μS/cm of electrical conductivity measured using electric conductivity meter (CM-30GTOA-DKK), and all the sulfate latex spheres were dialyzed. A UV-Vis spectrophotometer (UV-1650PC, Shimadzu) was used for the standardization of the latex particles.

The simple KCl salt (JIS special grade, Wako Pure Chemical Industries) and hydrophobic tetraphenylphosphonium chloride (TPPCl) (EP grade, Tokyo Chemical Industry Co.) was used in this experiment. The solutions were filtered (DISMIC 25HP 0.2 μm, ADVANTEC) and degassed under reduced pressure (GCD-051X, ULVAC). To avoid the dissolving effects of CO_2, the pH of the suspension was maintained at pH 4 with 0.1 mM HCl (JIS special grade, Wako Pure Chemical Industries).

2.2.2 Experimental procedure

We used the Zetasizer Nano ZS apparatus (Malvern Instruments) to measure the electrophoretic mobility of latex particles as a function of salt concentration. In this investigation the concentration of TPPCl, KCl, and sulfate latex particles were 0.0001-100 mM (TPPCl), 0.1-100 mM (KCl), and 5 mg/L, respectively. The measurement was performed at a temperature of 20ºC and pH 4. The pH of the suspension was checked by using a combination electrode (ELP-035, TOA-DKK) and maintained at pH 4. To observe the effect of hydrophobicity, the electrophoretic mobility of three sulfate latex spheres were measured in KCl and TPPCl salts separately.

2.2.3 Theoretical modeling to evaluate the electrokinetic charge density, zeta potential, and adsorption energy

2.2.3.1 Surface charge- surface potential relationship

We compared the electrophoretic mobilities from an experiment with theoretical values. From the Poisson-Boltzmann (PB) equation and standard electrokinetic theories, we calculate the theoretical electrophoretic mobility. The Gouy-Chapman model was used for the evaluation of surface potential ψ_0 from the surface charge density σ_0 in KCl solution using the Gouy-Chapman model. That is, we use Eq. (1)

$$\sigma_0 = \frac{2k_B T \varepsilon \varepsilon_0 \kappa}{e} \sinh\left(\frac{e\psi_0}{2k_B T}\right) \quad (1)$$

$$\frac{1}{\kappa} = \left(\frac{\varepsilon \varepsilon_0 k_B T}{2n_0 e^2}\right)^{\frac{1}{2}} \quad (2)$$

$1/\kappa$ is the Debye length in a solution with the concentration (number density) of electrolyte n_0. The parameters in the above equations ε_r, ε_0, k_B, T, and e are the relative permittivity of liquid, the vacuum permittivity, the Boltzmann constant, the absolute temperature, and the elementary charge, respectively. 1/κ is considered as the thickness of the diffuse double layer (Fig. 2.1). We assume $\psi_0 = \zeta$, where ζ is the zeta potential, in KCl solution. This assumption was verified by experiments (Chassagne & Ibanez, 2013; Kobayashi, 2008). In some cases, however, the reduction of charge or shift of slipping plane is needed (Kobayashi, 2013; Chassagne & Ibanez, 2013; Kobayashi, 2008). As a result, electrophoretic mobility in KCl solution is calculated from the reduced surface charge density.

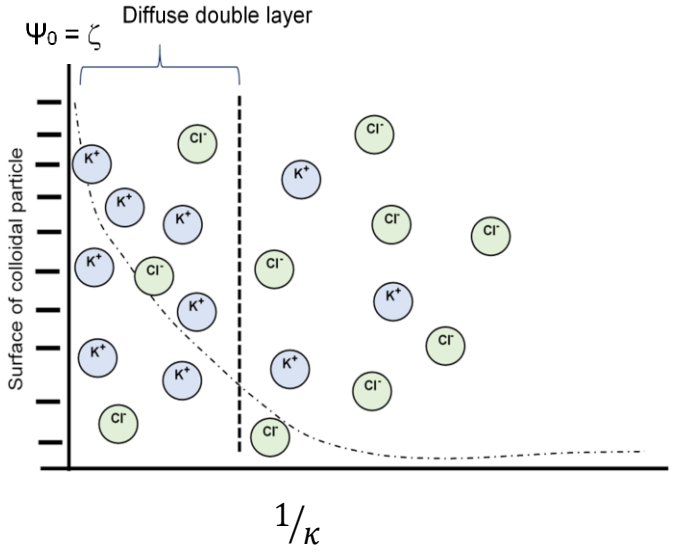

Figure 2.1. The potential distribution in the Gouy-Chapman model and the diffuse double layer.

In case of the strong adsorption of TPP^+ ion on the surfaces of the polystyrene latex, we can introduce the Stern layer as the following Eq. (3) followed by Somasundaran et al. (1964) and Martín-Molina et al. (2009) (Fig. 2.2)

$$\Gamma_S = 2r_s C_s \exp\left(-\frac{e\psi_d - \Phi}{k_B T}\right) \quad (3)$$

where the Γ_s represent the adsorbed amount of TPP ion in the Stern layer, r_s is the radius of adsorbed TPP^+ ion, here we use $2r_s$= 0.94 nm (Martín-Molina et al. 2009). C_s is the bulk concentration of TPP^+ ion, ψ_d is the diffuse layer potential, Φ is the chemical/intrinsic adsorption energy per TPP ion.

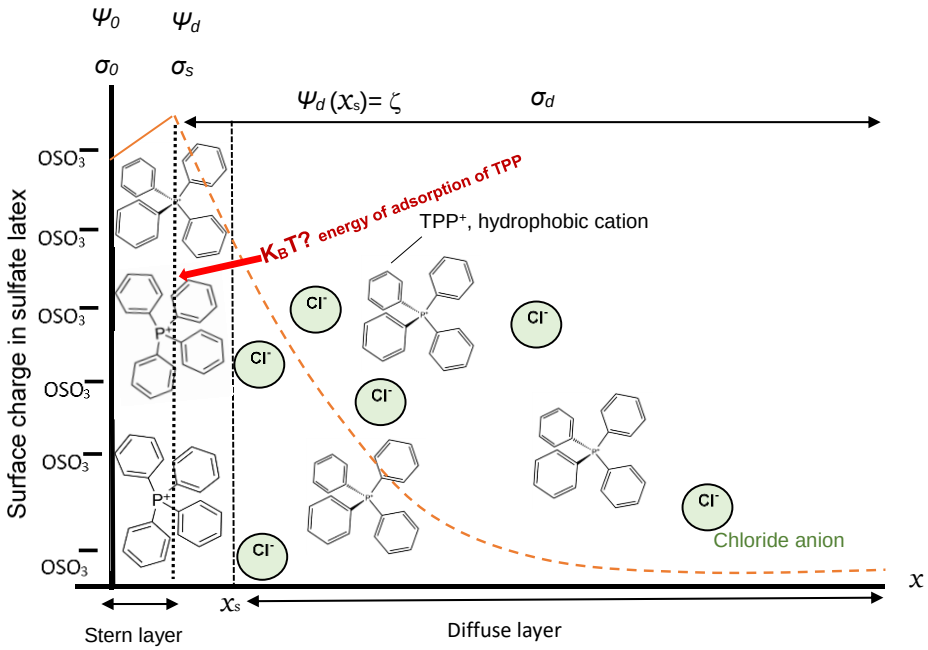

Figure 2.2. Schematic illustration of the Stern layer adsorptions of TPP^+ ion.

So, the Stern layer charge density σ_s is expressed as follows

$$\sigma_s = eN_A\Gamma_s \tag{4}$$

where N_A is the Avogadro number.

The charge in the diffuse layer σ_d is related to the potential ψ_d by following the Gouy-Chapman theory (Jiménez et al., 2012).

$$\sigma_d = -\frac{2k_BT\varepsilon\varepsilon_0\kappa}{e}\sinh\left(\frac{e\psi_d}{2k_BT}\right) \tag{5}$$

The charge neutrality means

$$\sigma_0 + \sigma_s + \sigma_d = 0 \tag{6}$$

Finally, the zeta potential ζ is extracted as follows (Borkovec et al., 2000)

$$\zeta = \psi(x_s) = \frac{4k_BT}{e}\operatorname{arctanh}\left[\tanh\left(\frac{e\psi_d}{4k_BT}\right)\exp(-\kappa x_s)\right] \tag{7}$$

The x_s in the above equation indicates the distance to the slipping plane. From Eqs. (3)-(7), in the presence of TPP^+, the zeta potential is evaluated.

At the iso-electric point, $\psi_d = 0$, a relation could be established between the adsorption energy per ion Φ and the charge reversal concentration C^I_s followed by Calero & Faraudo (2011), Martín-Molina et al. (2009) and Besteman et al. (2005). Which is,

$$C_s^I = \frac{\sigma_0}{e2r_s}\exp\left(-\Phi/k_BT\right) \tag{8}$$

2.2.3.2 Electrophoretic mobility

An approximate formula called Henry's equation is used to convert zeta potential to electrophoretic mobility. Henry's equation applicable for low zeta potential ζ for a sphere with a radius a

$$\mu = \frac{\varepsilon_r\varepsilon_0}{\eta}\zeta f(\kappa a) \tag{9}$$

where $f(\kappa a)$ is called Henry's function and the viscosity of medium is η. The approximate expression for Henry's function by Ohshima is (Ohshima, 2006)

$$f(\kappa a) = \frac{2}{3}\left[1 + \frac{1}{2\left(1 + \frac{2.5}{\kappa a\{1 + 2\exp(-\kappa a)\}}\right)^3}\right] \tag{10}$$

The Smoluchowski equation is found when $f = 1$. A spherically symmetric potential distribution in the double layer during the electrophoresis is assumed from the Eqs. (9) and (10). But at high potential, the double layer is deformed. This is called the relaxation effect of the double layer and is not considered in Eqs. (9) and (10). Considering the relaxation effect, the mobility of a sphere of radius a can be calculated by using O'Brien and White theory (O'Brien & Hunter, 1981) using a computer program.

The Ohshima's analytical equation for the mobility of a sphere can be used with the large zeta potential (Ohshima, 2006; Ohshima et al., 1983; Ohshima, 2005). The previous literature considered the relaxation effect is necessary to describe the electrophoretic mobility of silica, latex, and lysozyme (Kobayashi et al., 2013; Kobayashi, 2008; Kobayashi et al., 2005; Sugimoto et al., 2014; Yamaguchi & Kobayashi, 2016). The electrophoretic mobility μ depends on the ionic drag coefficient of the *i-th* ion species λ_i, when the relaxation effect considered

$$\lambda_i = \frac{N_A e^2 |z_i|}{\Lambda_i^0} \tag{11}$$

where Λ_i^0 is the limiting equivalent conductance of *i-th* ion specie and z_i is the valence of the *i-th* ion specie. The m_i is the scaled drag coefficient of *i-th* ion specie, that is

$$m_i = \frac{2\varepsilon_r \varepsilon_0 k_B T}{3\eta z_i^2 e^2} \lambda_i \tag{12}$$

In the *z-z* symmetrical electrolyte $z=z_1=-z_2$ solution, the approximate mobility μ applicable to an order of $1/\kappa a$ is given by the following semi-empirical mobility formula.

$$\begin{aligned} \mu = \operatorname{sgn}(\zeta) \frac{\varepsilon_r \varepsilon_0}{\eta} \left\{ |\zeta| - \frac{2F}{1+F} \left(\frac{k_B T}{ze} \right) H \right\} \\ + \operatorname{sgn}(\zeta) \frac{2\varepsilon_r \varepsilon_0 \, k_B T}{3\eta e} \left[\frac{1}{\kappa a} \left\{ -18 \left(t + \frac{t^3}{9} \right) K \right. \right. \\ + \frac{15F}{1+F} \left(t + \frac{7t^2}{20} + \frac{t^3}{9} \right) - 6(1+3\overline{m}) \left(1 - \exp\left(-\frac{\bar{\zeta}}{2} \right) \right) G \\ + \frac{12F}{(1+F)^2} H + \frac{9\bar{\zeta}}{1+F} (\overline{m} G + m H) \\ \left. \left. - \frac{36F}{1+F} \left(\overline{m} G^2 + \frac{m}{1+F} H^2 \right) \right\} \right] \end{aligned} \tag{13}$$

where

$$\bar{\zeta} = \frac{ze|\zeta|}{k_B T} \tag{14}$$

$$F = \frac{2}{\kappa a}(1 + 3m)\left(\exp\left({}^{\bar{\zeta}}/_{2}\right) - 1\right) \tag{15}$$

$$G = \ln\left(\frac{1 + \exp\left(-{}^{\bar{\zeta}}/_{2}\right)}{2}\right) \tag{16}$$

$$H = \ln\left(\frac{1 + \exp\left({}^{\bar{\zeta}}/_{2}\right)}{2}\right) \tag{17}$$

$$K = 1 - \frac{25}{3(\kappa a + 10)}\exp\left[-\frac{\kappa a}{6(\kappa a - 6)}\bar{\zeta}\right] \tag{18}$$

$$t = \tanh\left({}^{\bar{\zeta}}/_{4}\right) \tag{19}$$

where $\bar{\zeta}$ represents the scaled zeta potential magnitude; m and $\bar{m}$ are the scaled ionic drag coefficients of counterions and co-ions, respectively. The m and $\bar{m}$ indicates the cations molar average values of TPP^+ and H^+ in the presence of TPPCl. The Eq. (13) is invalid for $\kappa a < 10$. That's why it is necessary to have an alternative expression which is applicable to

the third power of zeta potential in Henry's equation. According to Overbeek (1943), the mobility expression to the third power of zeta ζ^3 is expressed as follows (Ohshima, 2006).

$$\mu = \frac{2\varepsilon_r\varepsilon_0\zeta}{3\eta}\left[f_1(\kappa a) - \left(\frac{ze\zeta}{k_BT}\right)^2\left\{f_3(\kappa a) + \left(\frac{m+\bar{m}}{2}\right)f_4(\kappa a)\right\}\right] \tag{20}$$

The first term in the right-hand side of the above equation is $f(\kappa a)$, which is Henry's function, and equals to the Henry's equation that is $(2/3)f_1(\kappa a)$ given by Eq. (10).

So, now in a *z-z* type symmetrical electrolyte solution, the final approximate expression for the mobility of a sphere given by Ohshima (2006) is as follows

$$\mu = \frac{2\varepsilon_r\varepsilon_0\zeta}{3\eta}\left(1 + \frac{1}{2\left[1 + \frac{2.5}{\{\kappa a(1+2\exp(-\kappa a))\}}\right]^3}\right) \tag{21}$$

$$-\frac{2\varepsilon_r\varepsilon_0\zeta}{3\eta}\left(\frac{ze\zeta}{k_BT}\right)^2\left[\frac{\kappa a\{\kappa a + 1.3\exp(-0.18\kappa a) + 2.5\}}{2\{\kappa a + 1.2\exp(-7.4\kappa a) + 4.8\}^3}\right.$$

$$\left.+\left(\frac{m+\bar{m}}{2}\right)\frac{9\kappa a\{\kappa a + 5.2\exp(-3.9\kappa a) + 5.6\}}{8\{\kappa a - 1.55\exp(-0.32\kappa a) + 6.02\}^3}\right]$$

Table 2.1. Some parameters of studied particles reported from the manufacturer (Reuse with permission from Hakim et al., 2016, Colloid and Polymer Science, 294:10, 1671-1678).

Parameters	**Particle 1**	**Particle 2**	**Particle 3**
Particle diameter $(2a)$(μm)	0. 25	0.47	1.2
Surface charge density σ_0(C/m^2)	-0.006	-0.049	-0.096
Electrokinetic surface charge density σ_k(C/m^2)	-0.011	-0.037	-0.043
Density(g/cm^3)	1.055	1.055	1.055

2.3 Results and discussion

2.3.1 Electrophoretic mobility of PSL particles in KCl solution

We measured electrophoretic mobility of three PSL particles of different surface charge density in the presence of different KCl concentration (Table 2.1). The electrophoretic mobility is presented as a function of KCl concentration in Figs. 2.3 (A, B, C) for latex particles having charge density of -0.006, -0.049, and -0.096 C/m^2 (manufacturer's supplied data), respectively. The symbols in Fig. 2.3 represent the experimental data. Assuming the electrokinetic charge densities of -0.011, -0.037, and -0.043 C/m^2. We obtained the dashed and solid lines from the theoretical model, which fit well in the higher salt concentration of the experimental data. The experimental values of the magnitude of electrophoretic mobility (EPM) show the maximum around 10 mM and decrease at lower and higher KCl concentrations. This trend indicates the effect of relaxation is significant, as supported by the Ohshima model. Considering the relaxation effect for large κa using Eq. (13), We calculated the solid red lines by Ohshima's theory. The green dashed lines represent the Smoluchowski equation.

The theoretical calculation of electrophoretic mobility agrees well at the concentration range 1-100 mM, below this concentration the calculated absolute value of EPM is higher than that of experimental data. In this condition, there is a need to include some other additional effects to explain this disagreement of theory with the measured value. There is an acceptable agreement at higher salts concentrations. For the salt concentration lower than (<10mM) in KCl, however, the agreement is less satisfactory. But the disagreement increases with the increase of surface charge density at the lower concentrations (Figs. 2.3 B and 2.3 C). It is still unknown to explain this disagreement clearly.

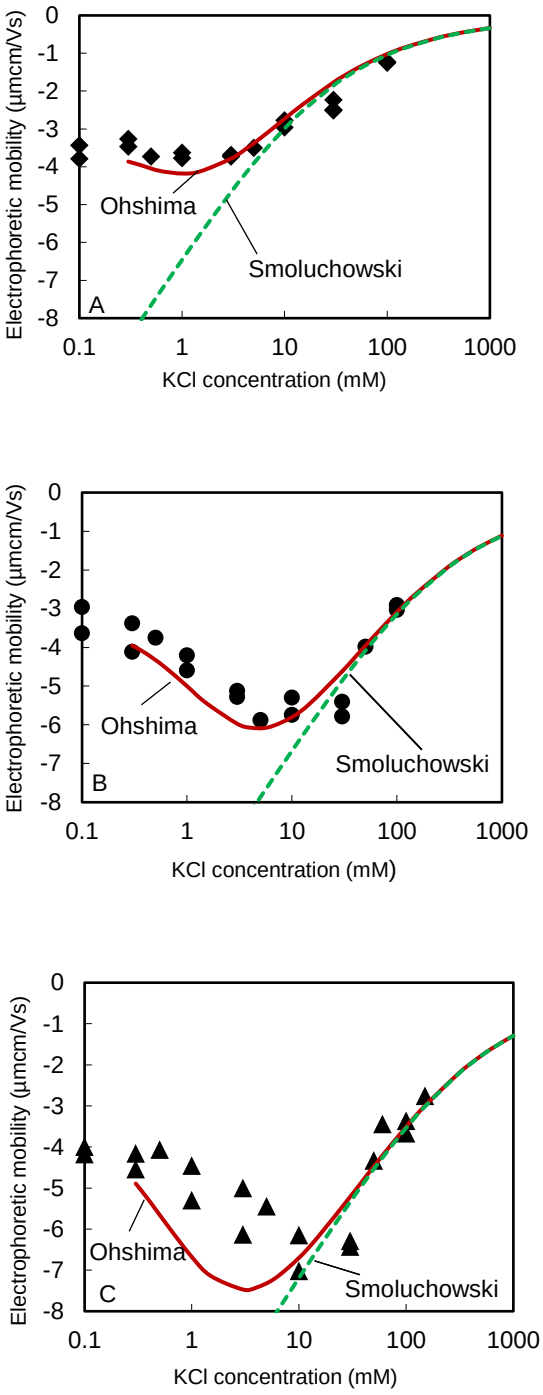

Figure 2. 3. Electrophoretic mobility of three sulfate latex sphere, 0.25 µm (A), 0.47 µm(B) and 1.2 µm (C) diameter) as a function of the concentration of KCl with HCl (10^{-4} M). Concentration of sulfate latex sphere: 5 mg/L. Symbols: Experimental data, Solid line: Theoretical model based on Eq. (13) and Dashed line: Smoluchowski equation (Reuse with permission from Hakim et al., 2016, Colloid and Polymer Science 294:10, 1671-1678)

2.3.2 Electrophoretic mobility (EPM) in the presence of hydrophobic tetraphenyl phosphonium (TPP^+) cation

The electrophoretic mobility of three hydrophobic PSL particles also measured in the presence of a different concentration of tetraphenylphosphonium chloride (TPPCl) concentration to observe the effect of hydrophobic interactions on charge reversal of polystyrene sulfate latex. We used PSL spheres with electrokinetic charge density -0.011 C/m^2, -0.037 C/m^2 and, -0.043 C/m^2 to obtain the electrophoretic mobility presented in Figs. 2.4 A, 2.4 B, and 2.4 C. At low TPPCl concentration, the EPM of sulfate latex is negative. With the increase of TPPCl concentration, the absolute value of negative mobility decreases. Subsequently, the EPM turns the negative mobility to positive values, indicating charge reversal (Figs. 2.4). The reversed electrophoretic mobility increases up to a maximum value and then decreases with increasing of the concentration of TPPCl. All the PSL spheres showed a large reversal of charges in the presence of TPP^+ ion (Figs. 2.4). The TPPCl concentrations at the point of mobility reversal or isoelectric points (IEPs) increase with the increasing surface charge density. The TPPCl concentration at the IEPs are 0.0018 mM, 0.45 mM, and 1.85 mM found from the experiments for three latex spheres of the lowest, medium, and the highest charge density, respectively. The increased amount of TPPCl concentration is needed with the increase of charge density to obtain the IEP. This tendency specifies that the increased concentration of TPP^+ ions is necessary for the neutralize of the latex spheres of higher charge density, indicates more TPP^+ adsorption with the increase of charge density.

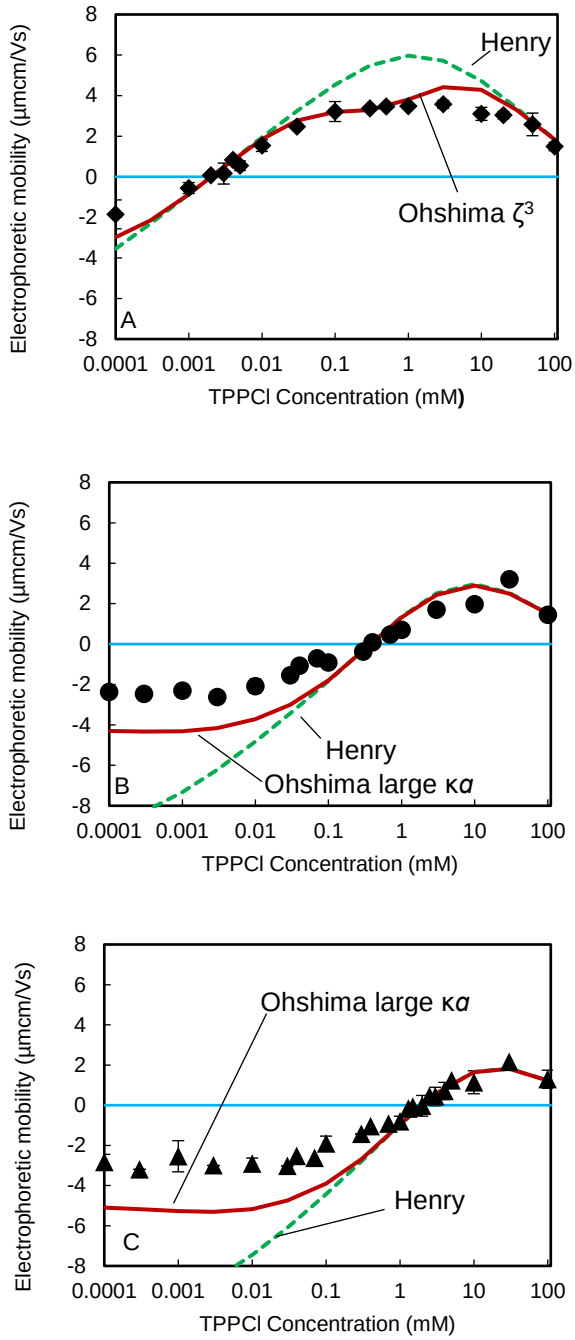

Figure 2.4. Electrophoretic mobility of three sulfate latex spheres, 0.25 µm (A), 0.47 µm (B) and 1.2 µm (C) diameter as a function of the concentration of TPPCl with HCl (10^{-4} M). Concentration of sulfate latex sphere: 5 mg/L. Symbols: Experimental data, Solid line: Theoretical model based on Eq. (21) (A), Theoretical model based on Eq. (13) (B and C) and Dashed line: Theoretical model based on Eq. (10). Error bar in experiment indicate the standard deviation of three measurements (Reuse with permission from Hakim et al., 2016, Colloid and Polymer Science 294:10, 1671-1678).

An investigation showed that the tetraphenyl arsonium chloride (Ph_4As^+Cl) reversed the charges of hydrophobic particles at a concentration higher than 1 mM (Martín-Molina et al., 2009), though another investigation showed the nature of hydrophobic and hydrophilic colloids affect the electrophoretic mobility inversion or charge reversal using the hydrophobic counter-ion (Calero & Faraudo, 2011). In their study, they found the charge reversal of hydrophobic surfaces by hydrophobic ions only. But there was the disappearance of reversal when hydrophilic colloids with organic or inorganic counter-ions only. A more recent investigation found that the effect of hydrophobic anion and cation on charge inversion and discussed the more pronounced effect of anion on charge reversal than cation (Perez-Fuentes et al., 2015). However, the interactions of hydrophobicity and charge density on charge reversal were unrevealed in their investigation. So, the present investigation designed to explore the effect of charge density on charge reversal in the presence of hydrophobic counterion TPP^+ found the increase of IEP or charge reversal point with charge density.

With the theoretical calculation using the electrokinetic charge density of -0.011 C/m^2, -0.037 C/m^2 and, -0.043 C/m^2 we found of 11 k_BT, 7 k_BT, and 5.5 k_BT of intrinsic adsorption energy, respectively (Figs. 2.4). We evaluated these adsorption energies to obtain a reasonable agreement between theoretical IEPs with experiments. The relation of electrokinetic surface charge density with the intrinsic energy of adsorption is plotted in Fig. 2.5. The energy of adsorptions is also evaluated by Eq. (8) from the iso-electric point, and the surface charge density supplied by the manufacturer (Table 2.1) (dashed line in Fig. 2.5) and plotted in the Fig. 2.5. Figure 2.5 showed that the intrinsic adsorption free energy (Φ) is decreasing with the increase of surface charge density, which means Φ is not constant.

From the molecular dynamics simulation, a previous investigation reported that the concentration of counterion at IEP is proportional to the surface charge density with

assuming Φ = 8.5 k_BT (Calero and Faraudo, 2011). This constant value of Φ showed disagreement with our study. In both values of charge density, the electrokinetic (-0.011 C/m^2) and the manufacturer (-0.006 C/m^2), we extracted the maximum free energy of adsorption Φ = 11 k_BT and 10.5 k_BT for both lowest charge density using the best fit to the experiment at Fig. 2.4 and Eq. (8), respectively. But 5.5 k_BT and 6.3 k_BT, the lowest values of the intrinsic free energy of adsorption were found for both electrokinetic (-0.043 C/m^2) and manufacturer's (-0.096 C/m^2) surface charge density, representing the highest charge density in both cases among three PSL particles. In cases of some organic cations such as Ph_4As^+, Ph_4Sb^+, Ph_4Ge^+, Ph_4C^+, and so on, the typical value of the free energy of transfer from water to non-aqueous solvent is an order of 12 k_BT (Martín-Molina et al., 2009). These values indicate a close relation to our findings of intrinsic energy of adsorption. This previous investigation (Martín-Molina et al., 2009) interestingly mentioned that a hydration free energy 6 k_BT for the organic cation (Ph_4As^+) adsorption on the hydrophobic sulfonated latex surfaces and explained that two out of the four phenyl groups were in contact or adsorbed on the latex. So, the maximum value of adsorption free energy (Φ) was 12 k_BT, which is close to our results. That is, at the surface of the lowest charge density in the latex sphere, all the four phenyl groups of TPP^+ ion were adsorbed. But the probable causes for the small decrease of the energy lower than 12 k_BT are the irregular shape of the latex sphere, surface roughness, discrete charge distribution around the layer of latex sphere, and co-ion effect near the IEP. The coions effects were discussed in a recent investigation in the presence of hydrophobic counterions (Oncsik et al., 2016). The coions effects on electrophoretic mobility and aggregation were strongly observed for the 1-butyl-3-methylimidazolium ($BMIM^+$) cation to sulfate latex particles (Oncsik et al., 2016). The strong ion-pair formation could explain this co-ions effects between TPP^+ and Cl^- or the tendency of co-ion sorption the particle surface near IEP (Oncsik et al., 2016). But it is very clear from the above

discussion that in all the cases, the free energy of adsorption decreases with the increase of surface and electrokinetic charge density.

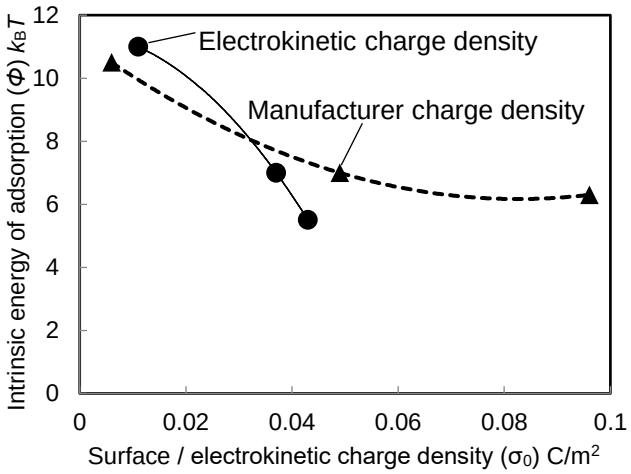

Figure 2.5. Intrinsic energy of adsorption (Φ) as a function of electrokinetic or surface charge density (σ_0). (Reuse with permission from Hakim et al., 2016, Colloid and Polymer Science 294:10, 1671-1678).

In every situation of TPP^+ adsorption of three PSL particles, we assumed a slipping plane distance 1.25 nm to the surface. But this slipping plane distance is a little bit larger than the size of TPP^+ ion, 0.94 nm. The increase of slipping plane distance from the actual TPP^+ ion size indicates some irregular adsorption phenomena due to the roughness of the latex particles' surfaces, or the phenyl groups tend to distribute unevenly on the surfaces during adsorption. Among some other possible causes for this larger slipping plane than that of TPP ion size is the dimerization of hydrophobic TPP^+ ions. In this situation, we need to investigate these phenomena at the molecular level considering some other experimental and theoretical investigation using other hydrophobic particles and hydrophobic counterions at different solution conditions.

2. 4 Conclusion

This investigation clearly shows the effect of surface charge density on the free energy of adsorption or intrinsic chemical energy of adsorptions of the monovalent hydrophobic counter ion (TPP^+) manifesting the charge reversal of polystyrene latex colloidal particles. The charge reversal concentration or the iso-electric point (IEP) is shifted towards higher concentration with the increase of charge density in the presence of TPP^+. The theoretical analysis and modeling in this study also demonstrate the dependence of intrinsic energy of adsorptions on surface charge density and found the decreasing trend of adsorptions energy with the increase of charge density. Though this investigation was designed to extract the charging and energy of adsorptions using the model PSL particle, the anomaly and difference from the pure system for adsorptions energy triggered us to use some other natural particles to confirm the aggregation and charging behavior in different solution conditions. For this reason, we designed the study steps in further by using the natural colloidal particles like natural organic matter (NOM) and humic substances to explore the adsorptions and charging along with aggregation related to more environmental problems. We will describe such phenomena in the upcoming chapters and discussions.

Chapter 3

Charging and aggregation behavior of three humic substances of different hydrophobicity in the presence of monovalent hydrophobic counter-ion.

3.1 Introduction

In our previous chapter, we discussed on the charging behavior of model PSL particles and the energy of adsorptions of hydrophobic monovalent ions on the PSL particles. It is important to explore the mechanisms of aggregation and dispersion of natural colloidal particles in natural environmental conditions. In this respect, we considered humic substances (HSs), which are one of the sources of carbons, and taking part in the transport and distributions of pollutants in soil and natural water bodies (Senesi & Loffredo, 1999; Piccolo, 2001). The binding of pollutants and contaminants and the metal ions bioavailability in the environment are strongly influenced by the presence of HSs in soil and water environments (MacCarthy, 2001; Kloster et al., 2013). Some previous investigation studied the HSs adsorptions on mineral surfaces (Weng et al., 2006) and the formation of aggregates (Maurice, et al., 1999). Some other studies also evaluated the mineral particles and nanoparticles aggregation and their charging in the presence of HSs (Baalousha, 2009; Ren et al., 2017; Domingos et al., 2009). Nevertheless, a complete understanding of the charge reversal of HSs themselves and their aggregation along with aggregate structure are still lacking.

The visible and settleable flocs of HSs are formed in the presence of lysozyme, Ca^{2+}, polymer, and surfactants (Kloster et al., 2013; Abe et al., 2011; Angelico et al., 2014). From the classical Derjaguin, Landau, Verwey, and Overbeek (DLVO) theory, the dispersion and aggregation of HSs can be described by two interactive forces, the van der Waals and electrostatic interactions. The electrostatic interaction comes from the charges of the particles. The aggregation happens at charge neutralization or iso-electric point due to the adsorptions and binding of oppositely charged ions, polymers, and surfactants. This binding and adsorption are influenced by some factors especially the pH, ternary complexes

formation, temperature, ionic strength, humic concentration, and types of humic substances, etc. (Tan et al., 2008). Some other investigations reported that the charge reversal of natural and synthetic colloids and biomaterials is also affected by the hydrophobic interaction (Tan et al., 2009; Tipping, 2002; Koopal et al., 2004; Hakim et al., 2016; Ishiguro et al., 2007; Oncsik et al., 2016).

The hydrophobic interactions (Abe et al., 2011; Angelico et al., 2014; Tan et al., 2009; Tipping, 2002; Koopal et al., 2004; Hakim et al., 2016; Ishiguro et al., 2007; Oncsik et al., 2016; Hakim and Kobayashi, 2019), depletion interactions (Jovanović et al., 2013), hydration forces (Xia et al., 2017; Alvarez-Puebla & Garrido, 2005) and hydrogen bonding (Martín-Molina et al., 2009; Calero & Faraudo, 2011) also play important role in the dispersion and aggregation of colloidal particles. In the presence of different enzymes and proteins, salts, and surfactants, and different types of HSs formed HSs aggregates showed sedimentation (Abe et al., 2011; Angelico et al., 2014; Tipping, 2002; Molina-Bolívar & Ortega-Vinuesa, 1999).

Using different hydrophobic ions such as tetraphenylphosphonium, tetraphenylboron, tetraphenylarsonium, some researches modified the interfacial property of clay colloids (Manciu & Ruckenstein, 2001; Parsons & Ninham, 2010) and such colloid were used in the lipid membranes and biological cells to detect the permeability and interaction (Duan et al., 2002; Rytwo et al., 2007). The hydrophobicity of humic substances affects adsorptions, permeability, and aggregation. Nevertheless, the charging and aggregation of HSs in the presence of such big hydrophobic ions is still vague.

In this situation, we designed the experiment to explore the charging and aggregation of HSs in the presence of monovalent hydrophobic ion, tetraphenylphosphonium (TPP^+). With TPP, we will be able to find out the mechanism of adsorptions in the presence of

hydrophobic interactions. This is because the aggregation of HSs is also influenced by some other inorganic ions, organic ions, surfactants, and polymer. The upcoming chapter will discuss the charging and aggregation behavior in the presence of these ions and surfactants and some other important factors considering the natural environmental condition and recent environmental problems.

3.2 Experimental

3.2.1 Materials

We used three different humic substances (HSs) namely Suwannee river fulvic acid (SRFA), Suwannee river humic acid (SRHA) and Leonardite humic acid (LHA) from International Humic Substances Society (IHSS) as natural organic matter (NOM). The supplied HSs were oven-dried at 65˚C before preparing the HSs suspension. After drying, the KOH solution was added to HSs solutions containing equivalent or more than the amount of carboxylic acid groups of each humic substance to prepare primary HSs stock solutions. Then the suspensions (wt. %) were stirred overnight, and subsequent stock solutions were prepared with deionized water (Elix, Millipore) to a concentration of 500 mg/L. We maintained a 50 mg/L concentration of all the HSs in every measurement of this study. These three HSs were selected according to their carbon content and aromaticity to investigate the effect of hydrophobicity in terms of carbon and aromatic contents (Hakim and Kobayashi, 2018).

The tetraphenylphosphonium (TPP^+) was used as hydrophobic counterion (EP grade, Tokyo Chemical Industry Co.). We also used the KCl as simple salts to compare the effect of charging and aggregation with TPPCl. The HCl (Wako Pure Chemical Industries) and carbonate-free KOH (prepared by following the method by Sipos et al., 2000) solutions were used to maintain the solution pH. The concentration of the salts was maintained from 10 mM-100 mM. The salts solutions were filtered (DISMIC 25HP 0.2 μm, ADVANTEC) for

all new preparation. To maintain a CO_2 free experimental condition, we performed degassing under reduced pressure (GCD-051X, ULVAC).

3.2.2 Methods

3.2.2.1 Electrophoretic mobility measurements

Electrophoretic mobilities of three HSs have measured as a functions KCl and TPPCl concentration at 20 °C using a Zetasizer Nano ZS apparatus (Malvern Instruments). The mobilities were measured as a function of pH and salt concentration of KCl (10 mM and 50 mM) and TPPCl (10 mM, 50 mM, and 100 mM). For each condition of salt concentration, the measurements were reproduced. The HSs solution was sonicated for 20 minutes before every set of experimental measurement. The suspension pH was measured for each measurement using a combination electrode (ELP-035, TOA-DKK).

3.2.2.2 Macroscopic and microscopic observation of aggregation and dispersion

The aggregates of three HSs were visually observed in the presence of TPPCl solutions at 50 mM of TPPCl in 50 mg/L of humic substances of each type as a function of pH after 24 hours. HSs of 50 mg/L in a series of 5 mL suspensions with 50 mM of TPPCl as a function of pH 3-10 was prepared by using screw-capped polystyrene bottles for 24 hours. The KOH and HCl solutions were used to maintain the pH. The macroscopic pictures of large naked eye observable aggregates were taken. The microscopic observations were also performed to confirm the structural arrangements and tentative size of aggregates at different pH. A microscope from Shimadzu (BA210E, Moticam 580INT) was used in this investigation.

3.2.2.3 Dynamic light scattering

The dynamic light scattering (DLS) technique at the backscattering detection (173° detection optics) was used for the measurement of HSs particles and/or aggregate size in TPPCl solution at 20 °C. The cleaned disposable cuvettes containing the suspensions of HSs

with TPPCl solution along with other chemicals (HC/KOH) were sonicated for 2 minutes and then DLS measurement was performed after total 5 minutes after the mixing. A 10 s run duration with a total of 5 runs were used of DLS for each measurement.

3.2.2.4 Aggregate structure analysis

To analyze the aggregate structure, the fractal dimension of HSs aggregates formed at 50 mg/L HSs in 50 mM TPPCl concentration was measured as a function of pH. A small angle light scattering technique using a SALD 2300 (SHIMADZU) was used to obtain the relation between scattered light intensity *I* and scattering angle to investigate the fractal dimension of the HSs aggregate. The difference of light in the suspension is the magnitude of the wave vectors of the incident and scattered light denoted as *Q*, which is the scattering vector and expressed as the following equation (1)

$$Q = \frac{4\pi n \sin\left(\frac{\theta}{2}\right)}{\lambda} \qquad (1)$$

In the above equation the *n* denotes as the refractive index of the solution, the scattering angle is denoted by θ and the wavelength is represented by λ of the laser light in a vacuum. The fractal dimension is determined as the relation between *I* and *Q*. That is, the power law relation of *I*, *Q* and fractal dimension D_f is expressed as (2)

$$I \propto Q^{-Df} \qquad (2)$$

From the above equation, we can plot the log-log scale relation of *I* against *Q*, which yields a straight line in the in a fractal regime following power-law relationships, and D_f was obtained from the slope of this line. The fractal dimension D_f was evaluated at pH 3 for different time intervals of the experiment. The SALD 2300 (SHIMADZU) was used to

analyze the fractal structure of HSs aggregates in a 12 mL of mixing suspension of HSs with TPPCl at stirring and no stirring conditions in every experimental condition.

Table 3. 1. Some parameter of the used HSs in this study collected from IHSS (Reuse from Hakim and Kobayashi (2018), Colloids and surfaces. A, 540, 1-10)

IHSS samples	**Carboxylic groups (meq/g-C)**	**Phenolic groups (meq/g-C)**	**Carbon content % (w/w)**	**Aromatic carbon (peak area percentages) (165-110 ppm)**
SRFA II (Suwannee river fulvic acid)	11.17	2.84	52.34	22
SRHA II (Suwannee river humic acid)	9.13	3.72	52.63	31
LHA (Leonardite humic acid)	7. 46	2.31	63.81	58

3.3 Results and Discussion

3.3.1 Electrophoretic mobility of three HSs in the presence of KCl and TPPCl

3.3.1.1 Electrophoretic mobility in KCl

Figure 3.1 shows the electrophoretic mobility of three HSs (SRFA, SRHA, and LHA) in the presence of KCl as function of pH values. The electrophoretic mobility of these HSs

at 10 mM and 50 mM shows negative values and is presented for the variations of aromaticity and/ or hydrophobicity (Table 3.1).

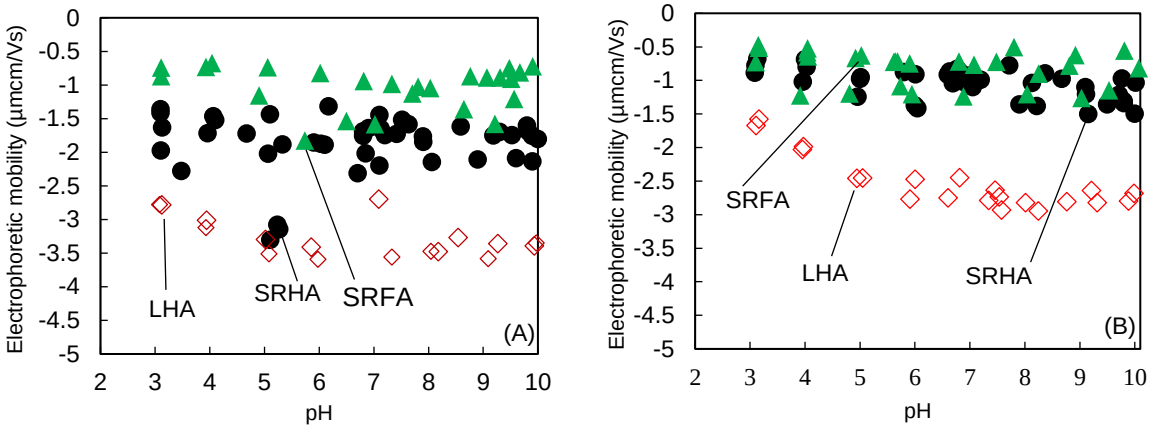

Figure 3.1. Electrophoretic mobility of three different HSs namely Suwannee river fulvic acid (SRFA), Suwannee river humic acid (SRHA) and Leonardite humic acid (LHA) at KCl 10 mM (A) and 50 mM (B) as a function of pH. Concentration of HSs is 50 mg/L. Symbols: SRFA (▲) SRHA (●), and LHA (◊). (Reuse from Hakim and Kobayashi (2018), Colloids and surfaces. A, 540, 1-10)

It is shown in the Fig.3.1 (A, B) that the absolute values of electrophoretic mobility of two HSs, the SRFA and SRHA are constant irrespective of pH values without showing any minimum or maximum of the mobility. But the mobility was negative in the all investigated pH. The less absolute value of electrophoretic mobility at 50 mM than that of 10 mM indicates the double layer screening. The negative absolute values of mobility are higher in LHA than that of SRFA and SRHA although the higher amount of negatively charged groups (carboxylic and phenolic) prevailed for SRFA and SRHA than that of LHA (Table 3.1). The probable cause of the higher absolute negative values of LHA than that of SRFA and SRHA is due to the more hydrophobic structure or aromaticity of LHA. The strong adsorptions of counterions on the HSs could be another mechanism of the net charge reduction of SRFA and SRHA in KCl solution. A previous investigation by Bonn and Fish (1993) suggest that the solution pH affect the binding of ions such as K^+, Na^+, Li^+, which

can be explained by the charge neutralization, and the base amount added in the solution affect the associated ions with HSs than that of the amount of cations. Other investigation reported binding is influenced by ion concentration, ion types, concentration and types of HSs themselves and on solution pH (MacCarthy, 2001; Kloster et al., 2013; Conte & Piccolo, 1999; D'Orazio & Senesi, 2009).

Considering the previous mechanisms, the result of our investigation found the order of K^+ ion binding affinity in the order of SRFA>SRHA>LHA. The binding is also influenced by the dissociation of COOH and/or –OH groups at different pH condition in the presence of KCl. Some predictions are mentioning the membrane-like complex structure (Maurice, 1999) and intermolecular forces originating in the supramolecular association (Ghosh, 1980; Weng et al., 2006), has the possibility of lower absolute negative electrophoretic mobility of SRFA and SRHA. But in any pH condition of 10 mM and 50 mM of KCl solution, all the HSs show negative electrophoretic mobility, showing no charge inversion or charge reversal in this investigation.

3.3.1.2 Electrophoretic mobility of HSs in the presence of TPPCl

The following Fig. 3.2 shows the electrophoretic mobility values of three HSs at 10 mM, 50 mM, and 100 mM of hydrophobic tetraphenyl phosphonium chloride (TPPCl) as a function of pH (3-10). All of three HSs (SRFA, SRHA, and LHA) shows the obvious charge inversion or positive values of electrophoretic mobilities in all the experimented concentrations of TPPCl (10 mM, 50 mM, and 100 mM) as manifested in Fig. 3.2.

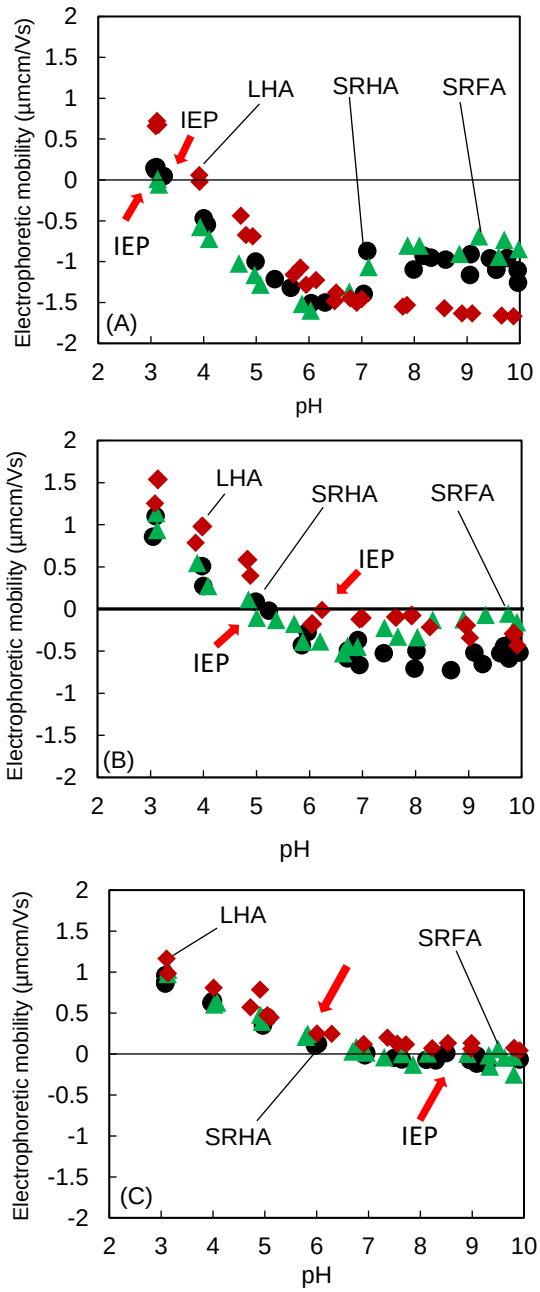

Figure 3.2. Electrophoretic mobility of Suwanne river fulvic acid (SRFA), Suwannee river humic acid (SRHA) and Leonardite humic acid (LHA) as a function of pH with tetraphenylphosphonium chloride (TPPCl) 10 mM (A), 50 mM (B), and 100 mM (C). Concentration of humic substances (SRFA, SRHA and LHA) is 50 mg/L. Concentration of HSs is 50 mg/L. Symbols: SRFA (▲) SRHA (●), and LHA (♦). The arrows indicate the iso-electric point (IEP). (Reuse from Hakim and Kobayashi (2018), Colloids and surfaces. A, 540, 1-10)

This obvious reversal of surface charge was also described and demonstrated in the previous investigation for some model and well-characterized colloidal particles induced by hydrophobic ions mentioning the effect of hydrophobic interactions and implies in this study of TPP^+ induced charge reversal of HSs (Hakim et al., 2016; Martín-Molina et al., 2009; Calero & Faraudo, 2011; Jiménez et al., 2012; Sugimoto et al., 2017). All the HSs in this research are hydrophobic though SRFA was well dissolved in water.

The charge reversal point or the iso-electric point (IEP) indicates the pH where the charge of all HSs neutralizes. This IEP or the pH of charge reversal increases with the increase of TPPCl concentration for every HSs used in this experiment (Fig. 3.2). The charge reversal point or IEP shifted toward a higher value of pH with an increase of the aromaticity or hydrophobicity (hydrophobicity: LHA>SRHA>SRFA, see Table 3.1). The IEP or charge reversal point of LHA in every TPPCl concentration has more rightward or higher pH shifting than that of SRFA and SRHA, indicating that the more hydrophobicity and/ or aromaticity of LHA influences this reversal or interaction of HSs with TPPCl.

We obtain the higher values of IEP pH around 4, 6 and 7 for LHA than that of SRFA and/or SRHA at pH around 3, 5 and 6 at 10 mM, 50 mM and 100 mM of TPPCl, respectively. The result indicates more interaction and adsorption of TPP^+ on LHA. This higher adsorption and interaction of TPP^+ ion on the LHA (most hydrophobic and/or aromatic) in this investigation is supported by a recent previous investigation of Hyuang and Kim (2008). They reported the HSs adsorption to hydrophobic carbon nanotubes is influenced by the aromatic content of HSs. Some other investigations of Hakim et al. (2016) and Sugimoto et al. (2017) reported the weakly charged colloidal surface shows strong hydrophobic interaction. These previous investigations strongly support our findings shown in Fig. 3.2. Which manifest the charge reversal at low pH is comparable with the weak charging state of the HSs.

The reversal of the electrophoretic mobility of HSs from absolute negative to positive value at all the TPPCl concentration as a function of pH could be explained by the adsorption of TPP^+ which compensate the surface charge of humic substances. Many of the previous investigations mentioned the no reversal of HSs charges or electrophoretic mobility in the presence of different mono and divalent electrolytes solutions (Kloster et al., 2013; Jovanović et al., 2013; Duval et al., 2005). This study also confirmed the same findings in the presence of KCl solution showing no reversal of charges of three HSs. In the previous chapter, we discussed the reversal of charges of model PSL particles in the presence of TPPCl and showed the relation of charges with the energy of adsorptions. This investigation firstly shows the reversal of HSs charges in the presence of big hydrophobic ion could be an initiatory approach in the electrokinetic property of NOM.

3.3.2 Macroscopic and microscopic observations of HSs aggregate formation with TPPCl

The large visual aggregates of three HSs (SRFA, SRHA, and LHA) were observed in SRFA and SRHA with 50 mM of TPPCl at pH around 3-5, and pH around 3-7 for LHA with TPPCl concentration at 50 mM (Figure 3.3). The aggregates are not only large enough but also interconnected and ramified, meaning the strong attractive force between HSs and adsorption of TPP^+ at lower pH range or at the pH for charge reversal. Some relatively smaller size aggregates were also formed at pH around 6 for SRFA and SRHA in TPPCl solution. Their formation was more obvious in case of SRHA than that of SRFA. The LHA at higher pH (7-10) shows relatively smaller aggregates. These were settled and sedimented but not large enough for interconnected and ramified. That is why the sediments are observable through the naked eye. In any cases of the HSs-TPPCl interaction, we observed the ramification and interconnection are decreased with the increase of pH. The probable causes of the dispersion of SRFA and SRHA at higher pH values (7-10) are due to the weak

hydrophobic interaction or elimination of hydrogen bond (Alvarez-Puebla and Garrido, 2005) and by the domination of electrostatic repulsion over the attraction among HSs particles themselves or with TPPCl. This naked-eye visual observation and interpretation have some limitation for quantitative evaluation due to manual handling.

These large and complex aggregates formation is discussed in the previous section with electrophoretic mobility. Hydrophobic interaction and hydrogen bonding in case of HSs interaction were reported in the previous literature (Jiménez et al., 2012). These large and visible aggregation is due to the existence of hydrophobic interactions (Sugimoto et al., 2017). The strong attractive force at charge reversal pH makes the strongly interconnected aggregates and withstand in the medium without sedimentation, annihilating the force of gravity (Baalousha et al., 2006). The large withstanding aggregates in the bottles are also because of the large coverage volume of the aggregates in the suspension of HSs-TPPCl, which has a large volume fraction occupied by the aggregates and/or HSs-TPPCl complex.

3.3.2.1 Microscopic observation of HSs aggregates in the presence of 50 mM TPPCl

Figures 3.4, 3.5, and 3.6 show the aggregation behaviors, the interconnection, and confirmation of the structure and nature of the aggregates through a microscope. In the Figs. 3.4, 3.5, and 3.6 show the structural arrangements of HSs aggregates and the tentative size. These microscopic photographs confirmed the aggregation behavior and the difference between aggregation and re-dispersion of HSs with TPPCl at different pH among the three types of HSs. In any case of the HSs aggregation, the LHA shows aggregates at all the studied pH, though the size is decreasing with pH. The hydrophobicity and/ or aromaticity trend (SRFA<SRHA<LHA) of these HSs. The larger and more interconnected aggregates of LHA in TPPCl solution is verified and supported by the more hydrophobic interaction of LHA with TPP^+ ion and/ or in the LHA-TPPCl complex. There are some smaller aggregate units along with larger interconnected aggregates at low pH. This indicates the formation of the

larger one is due to the self-assembly and/or reversible formation of aggregates. But at higher pH range, no larger aggregates unit could be observed for SRFA and SRHA, which could be due to their lower hydrophobicity. But LHA shows aggregate at higher pH range, indicating higher gathering force due to its more aromatic and/or hydrophobic structure. The aggregates hierarchical structure formed due to the repetition and rearrangements of the aggregates was discussed in the previous investigation (Kloster et al., 2013: Chilom & Rice, 2009). Moving of smaller aggregate units was observed through the microscope. This observation confirmed the Brownian motion of the aggregates and was supported by an earlier study (Kloster et al., 2013).

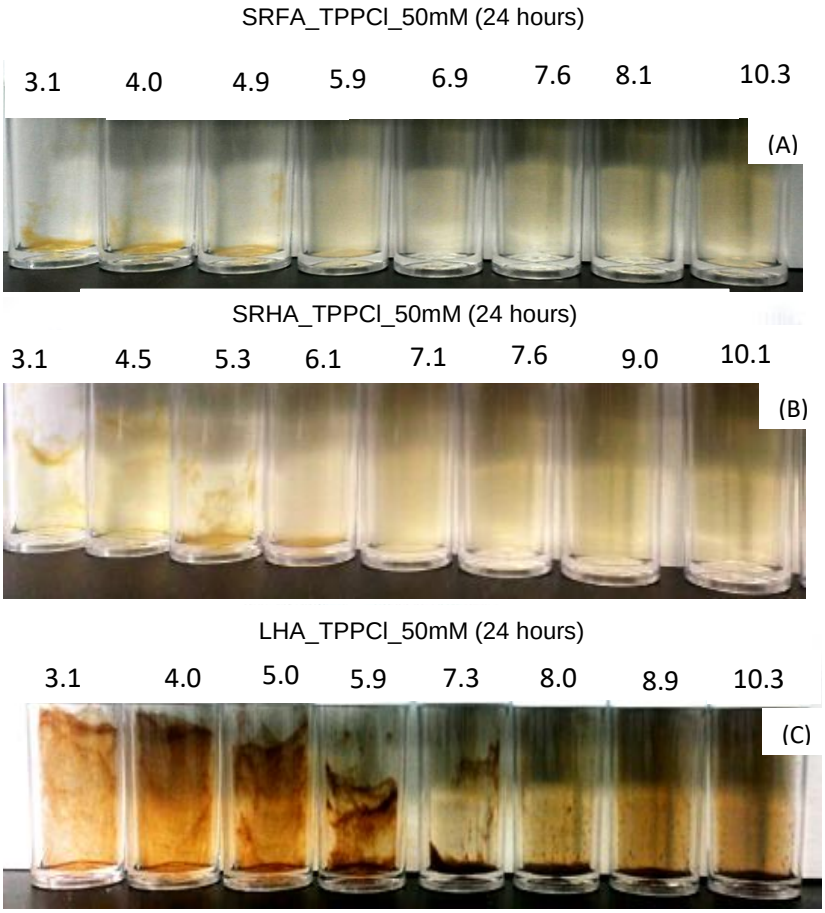

Figure 3.3. Visual observation of aggregation and re-dispersion for humic substances (SRFA, SRHA, and LHA) in tetraphenylphosphonium chloride (TPPCl) at 50 mM as a function of pH after 24 hours. Photos representing Suwannee river fulvic acid (SRFA) with TPPCl (A), Suwannee river humic acid (SRHA) with TPPCl (B), and Leonardite humic acid (LHA) TPPCl (C). Photo colour was adjusted by using GIMP 2.8.22 (Reuse from Hakim and Kobayashi (2018), Colloids and surfaces. A, 540, 1-10).

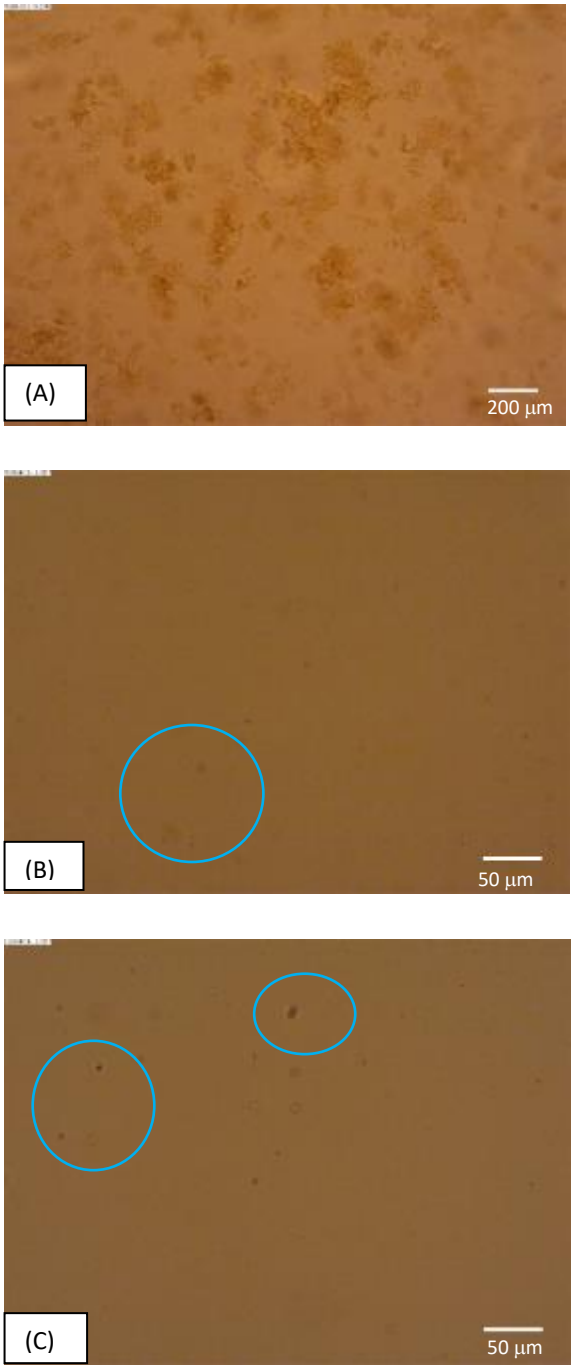

Figure 3.4. Microscopic photographs of flocs/ aggregates of Suwannee river fulvic acid (SRFA) in tetraphenylphosphonium chloride (TPPCl) 50 mM at pH 3.1 (A), pH 6.9 (B), and pH 8.9 (C). (Reuse from Hakim and Kobayashi (2018), Colloids and surfaces. A, 540, 1-10)

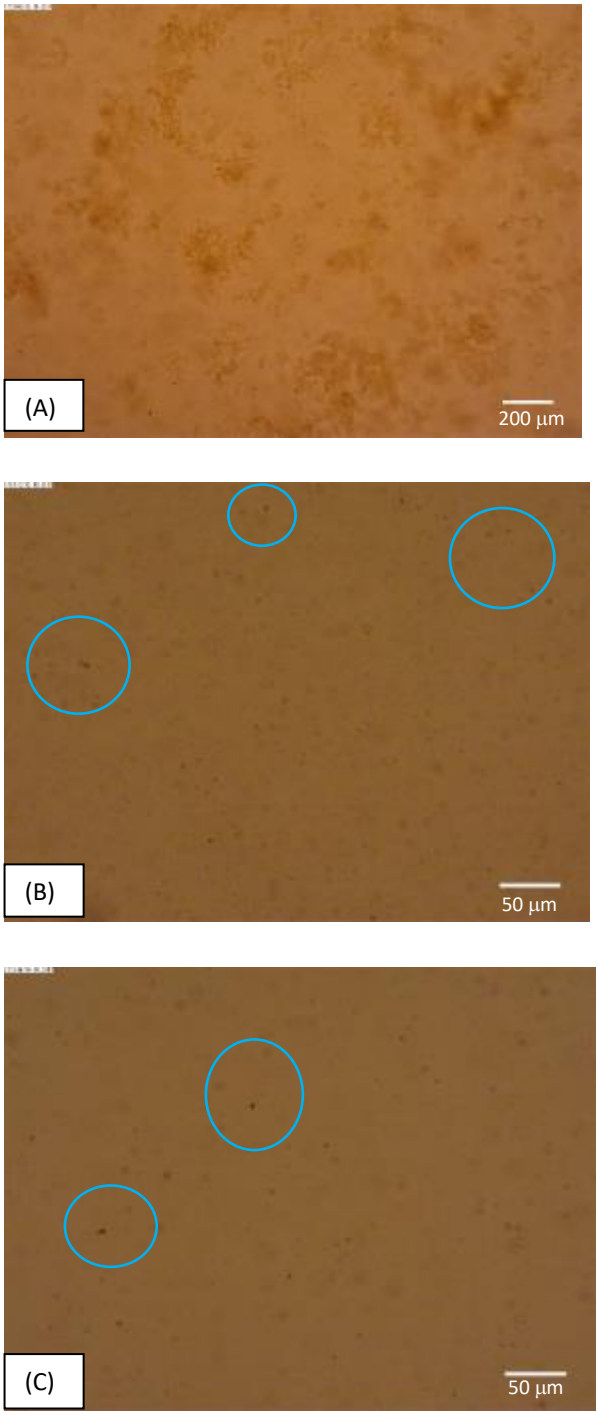

Figure 3.5. Microscopic photographs of flocs/ aggregates of Suwannee river humic acid (SRHA) in tetraphenylphosphonium chloride (TPPCl) 50 mM at pH 3.2 (A), pH 7.1 (B), and pH 8.8 (C). (Reuse from Hakim and Kobayashi (2018), Colloids and surfaces. A, 540, 1-10)

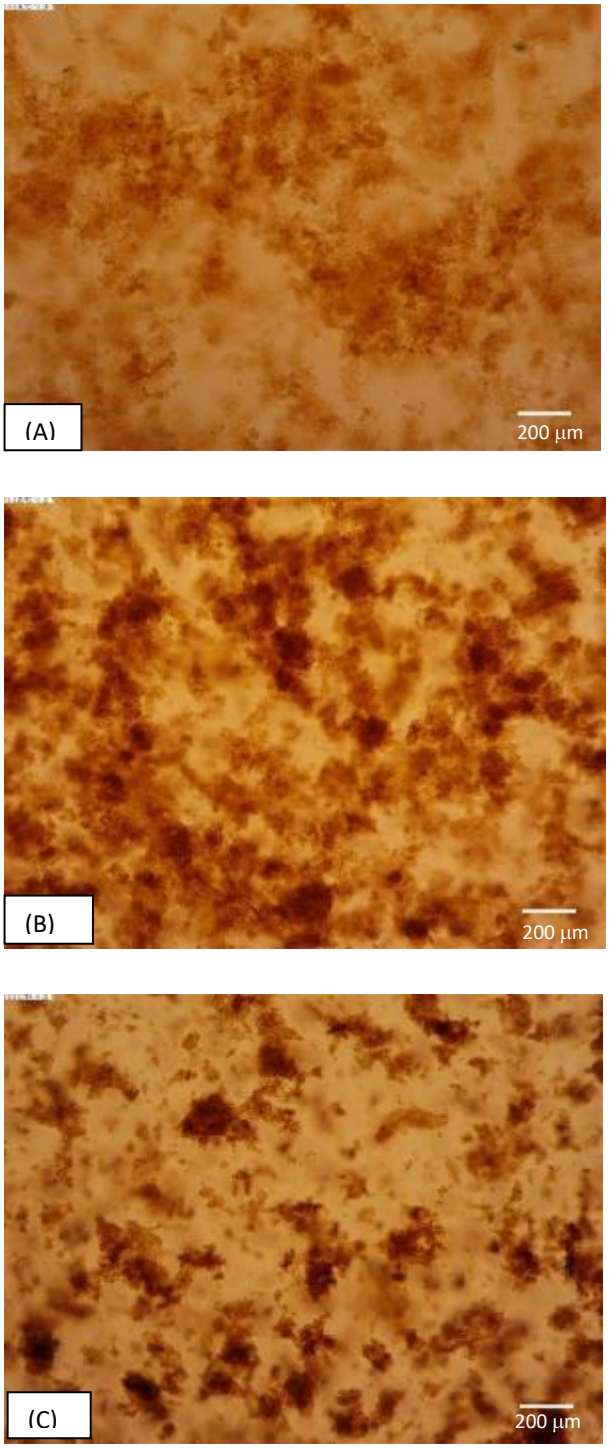

Figure 3.6. Microscopic photographs of flocs/ aggregates of Leonardite humic acid (LHA) in tetraphenylphosphonium chloride (TPPCl) 50 mM at pH 3.2 (A), pH 6.8 (B), and pH 8.9 (C). (Reuse from Hakim and Kobayashi (2018), Colloids and surfaces. A, 540, 1-10).

3.3.3 Aggregation and hydrodynamic size of aggregates by dynamic light scattering (DLS)

The dynamic light scattering (DLS) measurements of three different HSs aggregates in the presence of TPPCl solutions are presented in Fig. 3.7. The Z-average diameters for SRFA and SRHA show more than 1000 nm at the pH range around 3-4, and for LHA pH range is wider than SRFA and SRHA is around 3-5. This Z-average hydrodynamic diameter is consistent with the visual and microscopic observation indicating the formation of larger aggregates at lower pH range. The formation of colloidal aggregates usually occurs at the point of charge neutralization or around IEP, but the larger aggregates are formed at the charge reversed pH range. The probable cause of this deviation from the general rule is because of the lower charge (surface charging groups, the COOH and –OH) of all the HSs at lower pH range, trigging the more gathering to complexation by hydrophobic interaction. In the presence TPPCl, the TPP^+ ions induce to form larger aggregates of HSs triggered by the HSs hydrophobicity, and higher affinity of HSs to TPP^+ ion at the lower range of pH is caused by the escaping of HSs from surrounding water molecules. In any pH condition, the LHA shows larger aggregates in DLS measurement than that of SRFA and SRHA with the largest size of 2300 nm at pH around 3-4 for LHA-TPP complex and/or aggregates. This largest size of LHA aggregates supports the highest hydrophobicity of LHA among the three HSs used in this investigation.

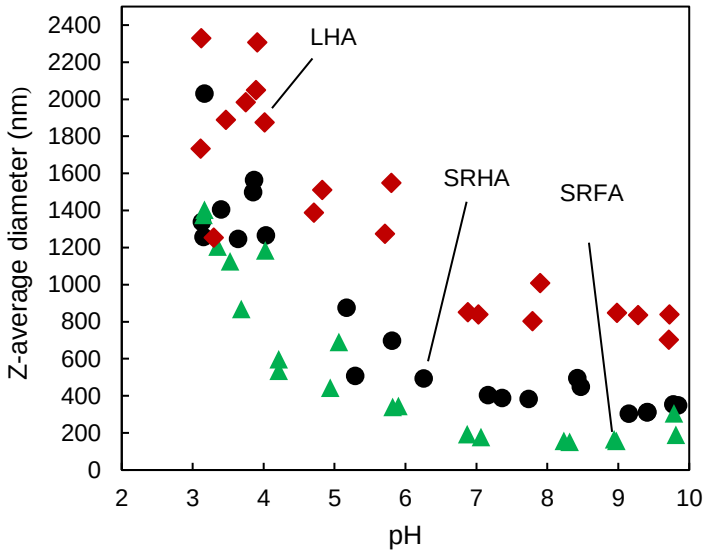

Figure 3.7. Average hydrodynamic diameter (Z-average) as a function of pH for Suwannee river fulvic acid (SRFA), Suwannee river humic acid (SRHA) and Leonardite humic acid (LHA) in 50 mM tetraphenylphosphonium chloride (TPPCl). Concentration of humic substances (SRFA, SRHA, and LHA) is 50 mg/L. Symbols: SRFA (▲), SRHA (●), and LHA (♦). (Reuse from Hakim and Kobayashi (2018), Colloids Surfaces A: Physicochem. Eng. Asp. 540:1-10)

In addition, this larger size of aggregates of HSs with TPPCl can also be explained by the formation of hydrogen bonding, and hydrophobic interaction (Jovanović et al., 2013; Ishiguro et al., 2007). Whereas the weak hydrophobic interaction and the electrostatic repulsion at higher pH range hinder the formation of the large aggregates. Some previous investigation reported aggregation of different HSs in the presence of a different concentration of hydrophilic NaCl salts at different pH and found the Z-average diameter larger than 1000 nm (Jovanović et al., 2013; Shen et al., 2016). Another study found the average hydrodynamic radius larger than 1000 nm of humic acid at different time intervals in pH around 3.1 and 7.1 for NaCl and $MgCl_2$ (Wang et al., 2013). The decreasing of size at high pH is due to the more electrostatic repulsion and the impeding to from the H-bond

(Jovanović et al., 2013). This study clearly manifests the TPP^+ induced aggregation of HSs and the order of aggregation is LHA > SRHA > SRFA.

3.3.4 Fractal dimension and aggregates structure analysis

The fractal dimensions D_f of the HSs aggregates in 50 mM TPPCl solution for different time intervals in stirring and no stirring conditions at pH 3 are presented in Fig. 3.8. The aggregates show a clear dependence of stirring condition with showing independence of time intervals. The HSs aggregates show fractal dimensions of 2-2.31 at no stirring, whereas D_f values of all HSs aggregates increase to 2.8, 2.88, and 2.87 at stirring condition (Fig. 3.8 A, B, C).

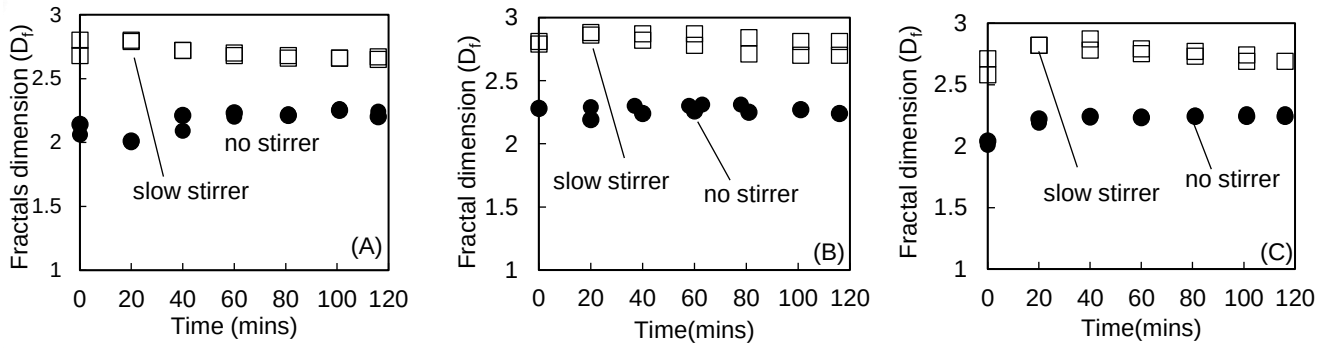

Figure 3.8. Temporal changes of fractal dimension in slow stirrer and no stirrer condition of Suwannee river fulvic acid (SRFA) flocs (A), Suwannee river humic acid (SRHA) flocs (B), and Leonardite humic acid (LHA) flocs (C) in 50 mM tetraphenylphosphonium chloride (TPPCl) at pH around 3. Concentration of humic substances (SRFA, SRHA and LHA) is 50 mg/L. Symbols: (□) slow stirrer, and (●) no stirrer. (Reuse from Hakim and Kobayashi (2018), Colloids Surfaces A: Physicochem. Eng. Asp. 540:1-10)

A previous study reported the fractal dimension D_f around 1.8 in the diffusion limited cluster-cluster aggregation, while in reaction-limited cluster-cluster aggregation with

restructuring a D_f value was around 2.1 (Gregory, 1998) for simulated flocs. These values are comparable with the findings of our study for no stirring condition. This previous finding indicates the weaker contact forces allowing the restructuring in HSs aggregates in TPPCl solution even at maximum aggregation zone at low pH condition.

Some of the previous studies evaluated the fractal dimension of aggregates in kaolin with alum (Wang et al., 2011), and humic acid with chitosan coagulants and Al species (Wang et al., 2017). A D_f value of 2.6 after breakage (Jarvis et al., 2005) for Fe precipitates flocs was reported, a modeling of viscosity for coagulated suspension showed D_f values around 2.2 - 2.6 (Kobayashi et al., 2000), whereas humic acid flocs showed a higher fractal dimension (D_f around 2.7) than clay flocs (Amjad and Khan, 2016). In this investigation, the stirring condition shows a higher fractal dimension, meaning the formation of compact aggregates structure. However, a D_f value of 2.7 was reported for the reaction limited regime under shear (Hoekstra et al. 1992) and a D_f increased to 2.9 due to the collision between primary particles and cluster in a shear flow (Torres et al., 1991). In the case of humic acid treatment for different aluminum species using chitosan coagulant higher D_f value around 2.75 was obtained (Wang et al., 2017). Also, the formation of the floc of polystyrene latex in the presence of $FeCl_3$, NaCl and $Al_2(SO_4)_3$, the highest D_f value almost 3.0 was reported (Kwaambwa et al., 2017). These previous investigations suggest that the repeated collisions among the primary HSs particles, smaller aggregate units and larger aggregates in the time of breakage and re-growth upon stirring condition produce the higher fractal dimension of TPP-induced HSs flocs and /or aggregates. This larger D_f aggregates formation could be possible due to the cluster-cluster aggregation (Wang et al., 2011) with restructuring and/or intrusion of small cluster units or broken part of larger aggregates into a new aggregate, which forms an interconnected and ramified large aggregate with higher fractal dimension.

This kind of intrusion or penetration of smaller units is possible due to the soft permeable and porous structure of HSs (Duval et al., 2005).

At high particle concentration in sheared suspension, the cluster-cluster aggregation is possible yielding a higher fractal dimension. Also, the continuous flow during shear or starring condition triggered the collision between particles and smaller aggregates, which causes the irreversible penetration of some smaller aggregates in the porous permeable structure of HSs. These continue shear flow induces the compaction of the HSs aggregates and/ or flocs (Kobayashi et al., 2002; Adachi et al., 2012).

3. 4 Conclusion

This investigation clearly indicates the charge reversal of HSs in the presence of monovalent hydrophobic counter ion TPP^{+} with the formation of large interconnected and compact aggregates at low pH. This study also revealed the aggregation is triggered by hydrophobic interaction or HSs hydrophobicity from the maximum sized aggregates of LHA among three HSs in any pH condition. The deviation from the general rule that aggregation occurs around IEP was observed. But this deviated findings partially explored the mechanism at low pH aggregation in such a hydrophobic system. The strong hydrophobic interaction at low pH influences the charge reversal and aggregation of natural colloidal particles.

Chapter 4

Strength and charging behavior of humic substances aggregate induced by the humic substances hydrophobicity and surfactant alkyl chain length

4.1 Introduction

In the surface water and groundwater, the most common dissolved organic carbons are humic substances (HSs), but it is very difficult to remove these polymeric organic acids from water environment (Nagao et al., 2003). In the earlier chapter, we discussed the aggregation of HSs and their fractal structure in the presence of big hydrophobic monovalent ion. In this chapter, we explore the strength and charging characters of HSs aggregates in the presence of two different cationic surfactants. Different techniques by using inorganic salts (Dempsey et al., 1984; Hussain et al., 2013; Song et al., 2019) have evaluated the coagulation of HSs in various environmental condition. But the coagulation and aggregation in the presence of widely used cationic surfactants concerning the strength of aggregates and charging behavior are still in vague. In the presence of organic molecules and ions, some of the previous literature reported the coagulation and removal of humic acids and natural organic matter (NOM) (Bolto et al., 1999; Matilainen et al., 2010; Sillanpää et al., 2018). It is importantly noticed in the previous investigation that the treatment and removal of HSs are influenced by the floc strength depending on shear and pH of the system in different water bodies and wastewater plants (Rong et al., 2013; Sun et al., 2011; Wang et al., 2011). The maximum strength of 0.42 Nm^{-2} (Bache et al., 1999) and 0.58 Nm^{-2} (Li et al., 2006) expressed as force per unit area due to charge neutralization (Bache et al., 1999), charge neutralization and bridging flocculation (Li et al., 2006) using alum coagulant (Bache et al., 1999) and alum coagulant with cationic polyacrylamide (PAM) were also reported in some previous study. Many investigations evaluated the flocs strength of HSs using alternate shear condition and expressed the strength as strength factors by the breakage and regrowth before and after shear (Wang et al., 2011; Wang et al., 2009; Sung et al., 2008; Yu et al., 2010).

These days two widely used cationic surfactants especially, the *n*-hexadecyl- or cetylpyridinium chloride (CPC) and *n*-dodecylpyridinium chloride (DPC) are usual in daily

commercial products and medicine. Many literatures evaluated the binding and/ or aggregation of HSs in the presence of inorganic ions (Kloster et al., 2013; Saito et al., 2005; Wang et al., 2013; Yamashita & Saito, 2015) and organic molecules (Hakim & Kobayashi, 2018; Koopal et al., 2004; Tan et al., 2008; Yee et al., 2009). But some of the investigations evaluated the aggregation of HSs, considering the charging behavior in the presence of cationic surfactants (Koopal et al., 2004; Ishiguro et al., 2007). Nevertheless, these previous studies could not be able to evaluate the numerical value of HSs aggregate strength in the presence of these surfactants.

Concerning the above discussion and to reveal the strength value of aggregate, a few nN strength value for polystyrene particle aggregates was evaluated as withstanding force against breakup. This force was comparable to the adhesion force measured by atomic force microscopy (AFM) (Kobayashi, 2004). His study revealed that the interparticle and/ or intermolecular attraction is the driving force for this strength. Using chemical force microscopy, some of the previous investigations explored that the 4.2 ± 1 nN and 28.4 ± 9.4 nN of adhesion force for -COOH/-CH_3 (carboxyl-methyl) and -CH_3/-CH_3 (methyl-methyl) tip-sample pairs interaction in water (Warszyński et al., 2003). But the effect of hydrophobic interaction on this force was also evaluated by AFM (Noy et al., 1997). It is also revealed from these previous findings that hydrophobic chain length affects the adhesion force of methyl-methyl (CH-CH_3) tip-surface pair interaction in the water. Those were 12.5 ± 4.4 nN and 60 ± 5 nN for C_{12} and C_{18} alkyl tail length, respectively (Noy et al., 1997; Sinniah et al., 1996; Vezenov et al., 1997). On the contrary, a recent study finds the hydrophobic self-assembled monolayers (SAMs) has a lower pull-off force than NH_2-terminated SAM of alginate hydrogels. The probable cause for this finding is due to the local electrostatic interactions and chemical interaction between the -COOH (carboxylic group) of alginate beads and -NH_2 (amino group) of SAM (Helfricht et al., 2017). So, the insights of colloidal

particles aggregation and forces among various organic molecules and ions in the presence of colloidal particles could be explored from these previous investigations.

In this study, we focused the aggregation and aggregate strength of HSs in the presence of two popular cationic surfactants paying attention to the HSs removal and the long distant transport of this natural organic matter (NOM) with pollutants along the waterways. Since HSs hydrophobicity (Hakim & Kobayashi, 2018; Ishiguro et al., 2007) and the pH (Sun et al., 2011; Brigante et al., 2009) affect the aggregation behaviors of HSs in different environmental condition. Therefore, we used two different HSs, Leonardite humic acid (LHA) and Suwannee river fulvic acid (SRFA) differing in their hydrophobicity and /or aromaticity (Hakim and Kobayashi, 2018) at various pH condition in the presence of two cationic surfactants. The pH, HSs hydrophobicity and different aliphatic tail length of DPC and CPC will be able to explore the deep insight of HSs aggregation and the possible mechanism of molecular adhesion of HSs with ions and molecules at various pH condition. Laminar converging flow to a glass capillary will be used in this investigation to characterize the maximum sized aggregates of HSs after breakage (Kobayashi, 2004; Kobayashi, 2005). We evaluate the strength of HSs flocs or aggregates from the maximum aggregate size after breakage.

Considering the present environmental problem this study will be able to explore the effect of HSs hydrophobicity and hydrophobic interaction on the aggregation, aggregate strength and transport of contaminants and pollutants in different water environment along with the flocs and aggregates of HSs at various microenvironmental conditions.

4.2 Materials and Methods

4.2.1 Materials

Two different humic substances from International Humic Substances Society (IHSS), the Suwannee river fulvic acid (SRFA) and Leonardite humic acid (LHA) especially differing in their hydrophobicity and/ or aromaticity, and the charge amount were used in this investigation (Table 4.1). The solution of primary stocks and subsequent secondary and experimental concentration (50 mg/L) were prepared according to the previous study (Hakim & Kobayashi, 2018) mentioned in the previous chapter 3 (Hakim and Kobayashi, 2019).

1-dodecylpyridinium chloride (DPC) and hexadecylpyridinium chloride monohydrate or cetylpyridinium chloride (CPC) from Tokyo Chemical Industry Co are the cationic surfactants used in this study. The DPC and CPC showed a critical micelle concentration (cmc) of 1.52×10^{-2} M and 6.3×10^{-4} M, respectively in the water at 25 °C (Godec and Kogej, 2007). The CMC of DPC is depended on temperature (Galan et al., 2002). Heckmann et al. (1987) reported the Krafft temperature 11.25 °C for CPC and CMC was 9×10^{-4} M (0.9mM) at 20 °C and the CMC of DPC was $1.887 \approx 1.9\times 10^{-2}$ M at 20 °C reported in another study (Van Os et al., 1993). These cationic surfactants are selected depending on their alkyl tail length to explore the effect of tail length along with HSs hydrophobicity on aggregation and aggregate strength. Carbonate free KOH solution was prepared by following the method by Sipos et al. (2000). Preparation of other salt solutions such as KOH, KCl, and HCl was described in the previous chapter 3.

4.2.2 Methods

4.2.2.1 Electrophoretic mobility measurements

A Zetasizer Nano ZS apparatus (Malvern Instruments) was used to measure the electrophoretic mobilities of two HSs (SRFA and LHA) at 0.2 mM, 1 mM, 2 mM DPC and 0.1 mM, 0.2 mM, 0.3 mM CPC in the presence 10 mM KCl solution as a function of pH at

20 °C. The 1 mM and 10 mM KCl solutions were used at 0.2 mM CPC solution and 1 mM DPC solution to evaluate the effect of KCl concentration. HCl (0.001M and 0.01 M) (JIS special grade chemicals, Wako Pure Chemical Industries) and 0.01 M KOH were used to maintain the pH of the solution. The HSs solution was sonicated once for 20 minutes before mixing all chemicals. 50 mg/L concentration of HSs (SRFA and LHA) was maintained for every measurement in this investigation. To measure the solution pH after mixing a combination electrode (ELP-035, TOA-DKK) was used. Degassing was performed for all the solution before mixing to avoid CO_2 contamination (Hakim and Kobayashi, 2019).

4.2.2.2 Macroscopic and microscopic observations of aggregation and dispersion

The visual observation was performed for the aggregation-dispersion of SRFA and LHA solutions in 5 mL prewashed screw-capped polystyrene bottles in the presence of DPC and CPC as a function of pH. This naked-eye visual observation was performed at 10 mM KCl solution in both of 1 mM DPC and 0.2 mM CPC solution as a function of pH in a series of 5 mL solutions using 50 mg/L of HSs (SRFA and LHA). The suspensions in the 5 mL polystyrene bottles were left for 24 after mixing and the bottles were turned over from upright to the normal position once for all mixing suspension of SRFA and LHA. Microscopic observations using a microscope (Shimadzu BA210E, Moticam 580INT) were performed for some selected pH conditions to confirm the effect of pH on aggregation. These microscopic observations were used to evaluate the tentative size and arrangements of aggregates at various pH condition.

4.2.2.3 Converging flow generation and the breakup of aggregates

The aggregate strength of SRFA and LHA in CPC and DPC solutions at 10 mM KCl solution were obtained from the broken aggregates in a converging flow into a glass capillary. A schematic diagram presenting the converging flow for the breakage of aggregates are shown in Fig. 4.1. Several previous investigations used the similar

experimental setup to evaluate the strength of aggregates by breakup (Sonntag & Russel, 1987; Higashitani et al., 1991; Blaser, 2000 a,b; Kobayashi, 2005).

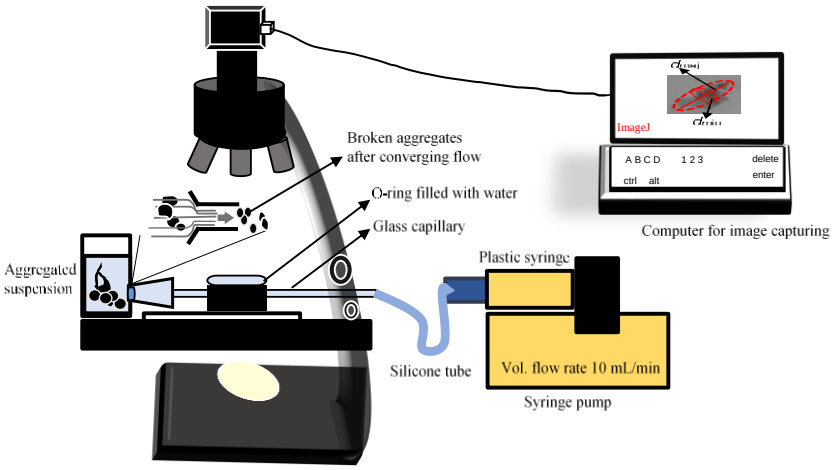

Figure 4.1. The schematic diagram for the breakage of SRFA and LHA aggregates due to laminar converging flow through a glass capillary of 0.8 mm in diameter. A 10 ml/min volumetric flow rate was used in this experiment (Reuse with modification from Hakim & Kobayashi, 2019, Colloids Surf. A: Physicochem. Eng. Aspects, Vol. 577, pp. 175-184).

A disposable polystyrene cuvette containing the HSs aggregated suspension was connected to a 0.8 mm inner diameter glass capillary which was inserted into a silicone stopper and another side of this glass capillary was inserted into a silicone tube. The SRFA and LHA aggregate suspension were pumped to the 5 mL plastic syringe using a syringe pump (Fusion 200, Chemyx) through the glass capillary at a volumetric flow rate of 10 mL/min. The aggregates of HSs were broken into smaller aggregates at the intrusion point of converging flow during the pumping. During the pumping of the aggregated suspension, a converging flow is produced at the vicinity of the entrance of capillary (Blaser, 2000a; Sonntag & Russel, 1987). The broken aggregates in the capillary after breakage were observed through a microscope and the images were captured to evaluate the maximum sized aggregates. The area of observation in the glass capillary was immersed

in water in an O-ring to reduce optical distortion. The largest aggregates represent the strength of the aggregates after breakage. So, we focused on the maximum sized aggregates to evaluate the aggregate strength in this experiment. The ImageJ software (ImageJ 1.51K) was used to calculate the lengths of major and minor axes (d_{maj} and d_{min}) of the largest aggregates using the best-fit ellipse. In a flow field, the behavior of aggregates could be approximated from the ellipsoids (Blaser, 2000 a,b). The temperature was maintained at around 20 °C in the total experimental procedure.

4.2.2.4 Calculation of aggregate strength

The aggregates of HSs will break down when the hydrodynamic rupturing force acting on the aggregates is higher than the strength of aggregates itself (Tambo & Hozumi, 1979; Kobayashi, 2005; Boller & Blaser, 1998; Kobayashi et al., 1999). According to this force balance, the hydrodynamic rupturing force F_{hyd} will exceed the strength of HSs aggregate $F_{aggregate}$ at the vicinity of the entrance of converging flow. In this case, the flow will break up the aggregate meaning that

$$F_{hyd} \geq F_{aggregate} \qquad (1)$$

The maximum size aggregates are subjected to the highest rupturing force, which induces the breakup in a certain shear/extensional flow rate. So, the aggregate strength is reflected by the largest size aggregates after breakage, where $F_{hyd} = F_{aggregate}$.

Some of the previous investigations evaluated the floc strength from the distortion of two micropipettes rupturing the flocs by direct measurement (Yeung &Pelton, 1996) or using force balance, the floc as a function of hydrodynamic force (Blaser 2000 a,b; Kobayashi et al., 1999; Kobayashi, 2004; Kobayashi, 2005; Tambo & Hozumi, 1979; Boller & Blaser, 1998). In the flow fields, the flocs and/ or aggregates are approximated from solid ellipsoids (Blaser 2000 a,b), and the extensional rate of converging flow was used to evaluate the size

of the broken flocs (Sonntag & Russel, 1987; Higashitani et al., 1991). The polymeric and/or precipitated coagulants flocs breakup and their deformation were directly observed by Higashitani et al. (1991) and Blaser (2000a). This observation evaluated that the extremely high elongation rate caused the breakage of the flocs/aggregates at the close proximity of the capillary tube entrance during the converging flow. The maximum elongation rate of flow, $A_{c,max}$, with a volumetric flow rate, Q, along the centerline of the converging flow into the capillary tube of a radius R determines the maximum floc size. That is (Blaser 2000a; Kobayashi, 2004 Kobayashi, 2005),

$$A_{c,max} = \frac{3\sqrt{3}Q}{32\pi R^3} \qquad (2)$$

An axisymmetric straining flow was deduced along the centerline of the entire flow field around an orifice, which was numerically solved (Sonntag & Russel, 1987). So, the surface area, S, of SRFA and LHA aggregates in CPC and DPC medium can be calculated from the equation given by Blaser (2002), assuming the hydrodynamic rupturing force exerted on ellipsoidal flocs or aggregates in an axisymmetric straining flow with an elongation rate, A (Blaser, 2002).

$$F_{hyd} = C_{hyd} S\mu A/2 \qquad (3)$$

The C_{hyd} in the above equation depends on the shape of the flocs.

In this experiment of flocs and/ or aggregate breakup, the maximum sized aggregate was considered, which means the maximum surface area, S_{max}, was measured after the breakage from the best-fit ellipsoids corresponding to the HSs aggregates. The maximum surface area, S_{max}, was calculated from the substitution of the major and minor lengths (d_{maj} and d_{min}) of the best fit ellipses following the equation below (Moriguchi, 1987).

$$S = 2\pi\left(a^2 + \frac{ac^2}{\sqrt{c^2 - a^2}}\arccos\frac{a}{c}\right) \qquad (4)$$

where $2a=d_{min}$, $2c=d_{maj}$. We obtained the values of C_{hyd} listed by Kobayashi (2005) as a function of d_{maj}/d_{min}. So the maximum values of $C_{hyd}S$ of the aggregates was calculated and expressed as $C_{hyd}S_{max}$, those are subjected to the maximum elongation flow $A_{c,max}$ (Kobayashi, 2005; Kobayashi, 2004). An equation was deduced from the assumption that the flocs/aggregates are subjected to higher stress in the flow through the streamlines near the wall of the glass capillary. This assumption can evaluate the flocs/aggregate strength by using the following equation (Kobayashi, 2004)

$$F_{aggregate} = (C_{hyd}S)_{max}\,\mu A_{c,max}/2 \qquad (5)$$

Table 4.1. Some of the selected parameter extracted from IHSS data (Hakim and Kobayashi, 2018; Reuse from Hakim & Kobayashi, 2019, Colloids Surf. A: Physicochem. Eng. Aspects, Vol. 577, pp. 175-184).

IHSS samples	Carboxylic groups (meq/g-C)	Phenolic groups (meq/g-C)	Aromatic carbon (peak area percentage) (165-110 ppm)	Carbon content % (w/w)	Charge amount (meq/g ≈ mmol/g) Around IEP pH			
					pH 4	pH 5	pH 6	pH 7
SRFA II (Suwannee river fulvic acid)	11.17	2.84	22	52.34	3.31	4.31	5.07	5.55
LHA (Leonardite humic acid)	7.46	2.31	58	63.81	2.08	2.97	3.78	4.39

4.3 Results and Discussion

4. 3. 1 The electrophoretic mobility of humic substances (SRFA and LHA) in the presence of CPC and DPC

4.3.1.1 Electrophoretic mobility in CPC solutions

The electrophoretic mobility of two HSs (SRFA and LHA) was measured in CPC solution in the presence of KCl solution as a function of pH. Figure 4.2 shows the electrophoretic mobility data of SRFA and LHA in 0.1 mM- 0.3 mM of CPC solutions. In every concentration of CPC for mobility measurement, 10 mM KCl solution was used. 1 mM of KCl solution was used only at 0.2 mM of CPC solution. The charge reversal of SRFA and LHA was observed at every concentration of CPC in 10 mM and 1 mM of KCl solution. Without showing any noticeable difference of charging in 1 and 10 mM of KCl solution, the IEP (iso-electric point) pH shifted towards a higher value for LHA and SRFA in any concentration of CPC. The pHs at IEP are around 5.3 and 6.4 in 0.2 mM CPC in the presence of 10 mM KCl solution for SRFA-CPC and LHA-CPC systems, respectively. The magnitude of reversed electrophoretic mobility was also higher for LHA than that of SRFA at pH around 3 in 0.2 mM and 0.3 mM of CPC solutions.

With the increase of pH, the magnitude of charge reversed electrophoretic mobility is gradually decreases to charge neutralization. This charge reversal pH range is wider with the increase of CPC concentration. This trend indicates more adsorption and binding of CPC to HSs. On the other hand, it is also demonstrated that the lower adsorption and binding of CPC with HSs from the negative absolute value of electrophoretic mobility at higher pH. Which indicates the higher surface charge of HSs is accompanied by lower hydrophobicity of hydrophobic interaction.

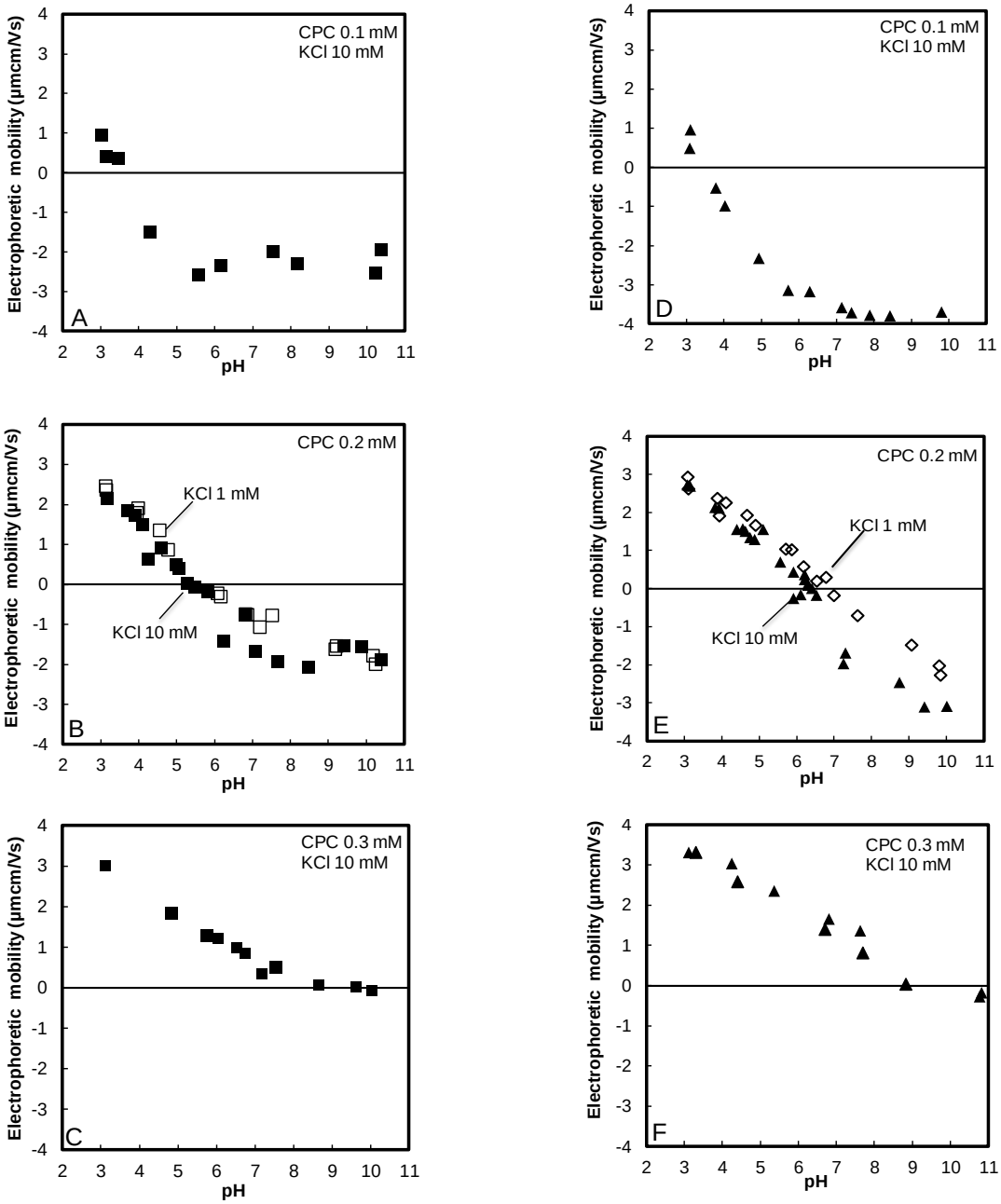

Figure 4.2. Electrophoretic mobility of Suwannee river fulvic acid (SRFA) (A, B, C) and Leonardite humic acid (LHA) (D, E. F) at 0.1 mM (A, D), 0.2 mM (B, E), and 0.3 mM (C, F) of CPC (cetylpyridinium chloride) concentration as a function of pH. Concentration of HSs is 50 mg/L (Reuse from Hakim & Kobayashi, 2019, Colloids Surf. A: Physicochem. Eng. Aspects, Vol. 577, pp. 175-184).

The shifting of IEP to higher pH value and higher absolute value for mobility in LHA indicates the more hydrophobic interaction between HSs themselves and gathering force among HSs molecules and CPC for LHA-CPC system than SRFA-CPC system.

Many previous investigations mentioned the effect of hydrophobic interactions on the charging behavior of humic substances (Hakim & Kobayashi, 2018; Koopal et al., 2004, Ishiguro et al., 2007). The LHA has more hydrophobic and/ or aromatic groups or carbon contents than that of the SRFA (Hakim & Kobayashi, 2018), indicating more hydrophobic interaction in LHA-CPC system. The insignificant effect of KCl in the electrophoretic mobility data was reported in the previous investigation described the proton binding to HSs in KCl solution (Tan et al., 2008). In these experimental findings, the dominancy of hydrophobic interaction prevails than that of double-layer screening by KCl. This phenomenon could be explained by the soft, porous and permeable structure of HSs, where there is a possibility of K^+ intrusion and entrapment by HSs (Tan et al., 2008; Duval et al., 2005). The soft and permeable structure induces the intrusion of K^+ ion inside the HSs structure and has a self-regulatory effect on the electrophoretic mobility to maintain the equilibrium condition of K^+ between the bulk and near to the surface.

4.3.1.2 Electrophoretic mobility of LHA in DPC solutions

The electrophoretic mobility data of LHA at 0.2 mM to 2 mM DPC in the presence of KCl solution is presented in the Figure 4. 3. We do not observe any charge reversal of LHA in 0.2 mM of DPC, but it shows charge reversal at a higher concentration of DPC at 1 mM and 2 mM. The insignificance of KCl concentration in the electrophoretic mobility measurement was also observed at 1 mM of DPC solution in 1 mM and 10 mM of KCl concentration like CPC for LHA and SRFA. With the increase of DPC concentration from 1 mM to 2 mM, the IEP of LHA solution shifts toward a higher pH value. The electrophoretic

mobility data (Fig. 4.3) shows that the pH at IEP shifts toward a higher pH value from pH 3.9 to pH 5.8 in 1 mM and 2 mM DPC at 10 mM KCl solution, respectively. This kind of IEP shifting to a higher pH value were also observed in previous literature in the presence of organic molecules and hydrophobic ions explaining more adsorption of these ions on humic acid (Hakim & Kobayashi, 2018; Koopal et al., 2004; Ishiguro et al., 2007).

It is clearly shown from the Figs. 4.2 and 4.3 that the magnitude of electrophoretic mobility for SRFA-CPC and LHA-CPC at charge reversed pH around 3 are higher than that of LHA- DPC system. But the LHA-CPC system shows a higher IEP pH (pH around 6.4) than that of LHA-DPC system (pH around 3.9). This result manifests the higher hydrophobic interaction in LHA-CPC system than that of LHA-DPC system. This strong hydrophobic interaction is also supported by the requirement of higher DPC concentration for charge reversal of LHA than CPC concentration. The LHA-CPC system at 0.2 mM of CPC shows a higher IEP pH than that of IEP pH around 3.9 of LHA-DPC system in 1 mM DPC at 10 mM KCl solution. This higher interaction, binding and adsorption of CPC on LHA than that of DPC indicates a more hydrophobic interaction for longer alkyl tail CPC with LHA that shorter alkyl tail of DPC with LHA (Hakim and Kobayashi, 2019).

LHA has charge amount around 2.08 meq/g at pH around 4. This low amount charge than that of 1 mM DPC concentration indicates the possibility of unbound or free DPC molecules in the bulk when the IEP is induced by charge neutralization. The higher solubility of DPC in water than that of CPC induces the lower magnitude of electrophoretic mobility in the charge reversed condition at 1 mM of DPC. This condition could be explained by the weak attraction of DPC to LHA because of shorter alkyl tail length and higher solubility of DPC. Cases and Villieras (2005) support these findings.

At pH around 6, the total CPC and DPC concentrations to CMCs of CPC and DPC ($C_{CPC,\ DPC}/CMC_{CPC,\ DPC}$) and total amounts of CPC and DPC to the charge amounts of HSs ($C_{CPC,\ DPC}$/charge of HSs) are presented as normalized ratios in Figure 4. 4. No notable difference of the ratios of $C_{CPC,\ DPC}/CMC_{CPC,\ DPC}$ and $C_{CPC,\ DPC}$/charge of HSs were observed for SRFA and LHA in CPC (Figure 4.4 A, B). Usually, the bare charge amount of SRFA and LHA differ at pH around 6. But the normalization of concentration to CMC shows no noticeable effect. This fact indicates the greater interaction of CPC with HSs, this greater interaction is accompanied by the higher hydrophobicity or least solubility of CPC than DPC (Hakim and Kobayashi, 2018).

4.3.2 Aggregation-dispersion of Suwannee river fulvic acid (SRFA) and Leonardite humic acid (LHA) in CPC and DPC solutions

Naked eye visual observation and microscopic observation of SRFA and LHA aggregates were conducted at CPC and DPC system in the presence of KCl solution. This investigation was carried out to confirm the approximate size and arrangements of HSs aggregates in SRFA-CPC, LHA-CPC, and LHA-DPC systems at various pH condition (3-10) in 5 mL polystyrene plastic bottles. In Fig. 4.5 the visual observation of aggregates in SRFA-CPC and LHA-CPC systems shows that the aggregation is more pronounced around IEP pH.

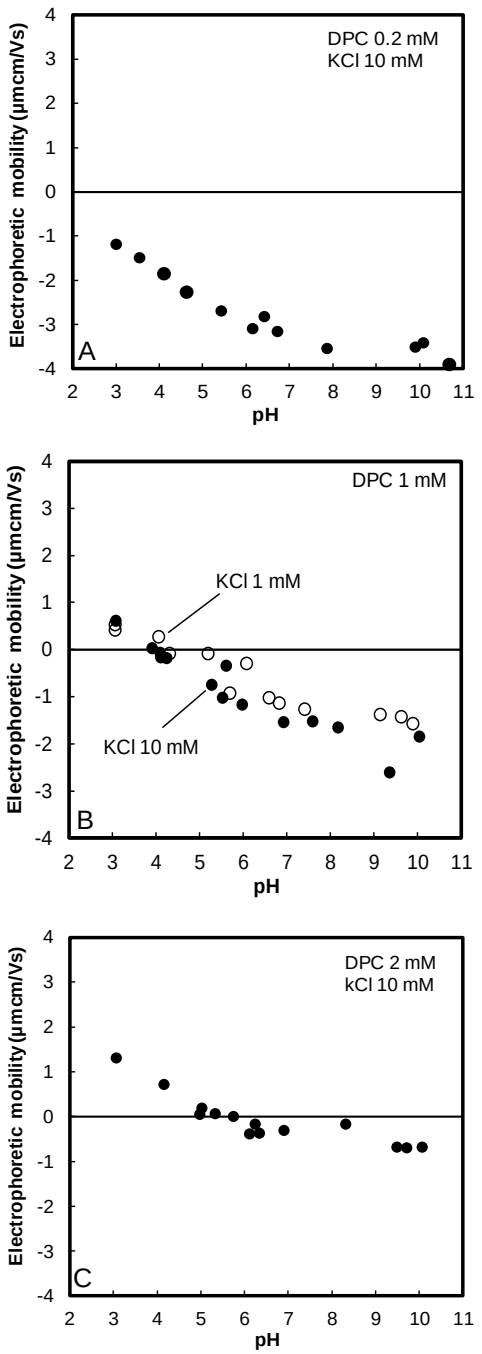

Figure 4. 3. Electrophoretic mobility of Leonardite humic acid (LHA) at 0.2 mM (A), 1 mM (B), and 2 mM (C) DPC (dodecylpyridinium chloride) as a function of pH. Concentration of LHA is 50 mg/L (Reuse from Hakim & Kobayashi, 2019, Colloids Surf. A: Physicochem. Eng. Aspects, Vol. 577, pp. 175-184).

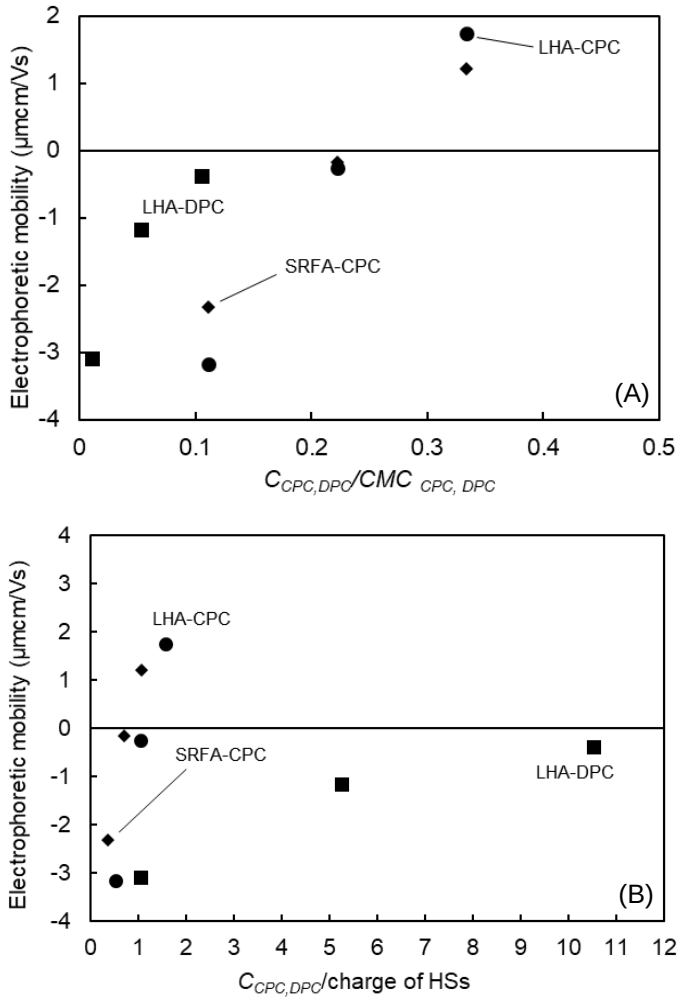

Figure 4. 4. Normalized ratios of CPC and DPC concentration to CMC at 20°C (A) and CPC, DPC concentration to SRFA and LHA charge amount (B). The charge amount calculated at pH 6. The electrophoretic mobility data are around pH 6 (5.8-6.3). The CMC of CPC is 9×10^{-4} M (Heckmann et al. 1987) and DPC is $1.887 \approx 1.9\times10^{-2}$ M (Van Os et al. 1993). The KCl concentration is 10 mM. (Reuse from Hakim & Kobayashi, 2019, Colloids Surf. A: Physicochem. Eng. Aspects, Vol. 577, pp. 175-1845

The LHA-CPC system shows a wider range of aggregation pH than SRFA-CPC system. It was also confirmed that the aggregates in LHA-CPC system are more interconnected and darker than SRFA-CPC aggregates (Fig. 4. 5). The SRFA-CPC and LHA-CPC aggregates in KCl media were also observed through the microscope at some designed pH condition. This microscopic observation confirmed the closer look of aggregate structural arrangement and the interconnection, which revealed the effect of aromaticity and/or hydrophobicity on the aggregation behavior of two different HSs at various pH condition. It is also clearly observed from the microscopic pictures that in both systems of SRFA-CPC and LHA-CPC, the more pronounced, larger and interconnected aggregates form in case of LHA-CPC system than SRFA-CPC system (Figs. 4.5 and 4.6). Thus, the larger aggregates are formed due to the charge neutralization of humic substances by cationic surfactants. In addition, the more pronounced and wider pH range of LHA aggregation around IEP indicates more hydrophobic moieties of humic substances determine the higher degree of HSs aggregation.

SRFA in the presence of cationic surfactants formed vesicles type aggregates (Chaaban et al., 2016). This weak aggregation and poorly formed aggregate structure are also supported by our investigation beyond the IEP (Figure 4. 6 A, C, and D, F).

The visual macroscopic pictures of aggregation-dispersion in LHA-DPC system are presented in Fig. 4.5. This picture shows that the aggregation range for LHA-DPC system increases with the increase of DPC concentration. Figure 4.5 shows that at lower pH range the LHA-DPC system at 0.2 mM DPC in 10 mM KCl solution shows aggregation. This low pH aggregation is shifted to a more wider pH range of aggregation up to pH around 7 at higher concentration of DPC (1 mM) at 10 mM KCl solution (Fig. 4.5). This visual observation of aggregation- dispersion is supported by microscopic pictures of aggregates at the different condition of pH (Fig. 4.7). The larger aggregates at low pH indicate more hydrophobic interaction prevails at low charging state of HSs at lower pH (Hakim &

Kobayashi, 2018). The aggregation at lower pH range can also be explained by higher hydrophobicity and/ or aromaticity accompanied with a lower charge state of HSs at low pH (Table 4.1). This higher hydrophobicity can induce strong hydrophobic interaction along with some patch attraction and hydrogen bonding (Jovanović et al., 2013). In the HSs molecules, there is a possibility of intermolecular hydrogen bonding due to the carboxyl hydrogen at low pH (Jovanović et al., 2013). The heterogeneity of HSs charge distribution could be one of the mechanisms for the charge-patch attraction, which trigger the aggregation at low pH. This charge-patch attraction for colloidal aggregation was also mentioned in the previous investigation (Bouyer et al., 2001; Illés and Tombácz, 2006).

The DPC concentration influences the aggregation pH range in the microscopic and visual observation (Figure 4.5 and Figure 4.7). A wider pH range for aggregation is observed with the increase of DPC concentration (Figure 4.5) and the network like structure is formed. This network like aggregates structure formation is supported by the humic substances and colloidal particle interactions with cationic detergents (Thieme and Niemeyer, 2008). In this previous investigation at lower cationic detergents concentration, the sphere-shaped particles were observed, which disappeared at higher concentration. This type of aggregation is demonstrated in our investigation at the lower concentration of DPC at higher pH range (Figure 4.7 B and C).

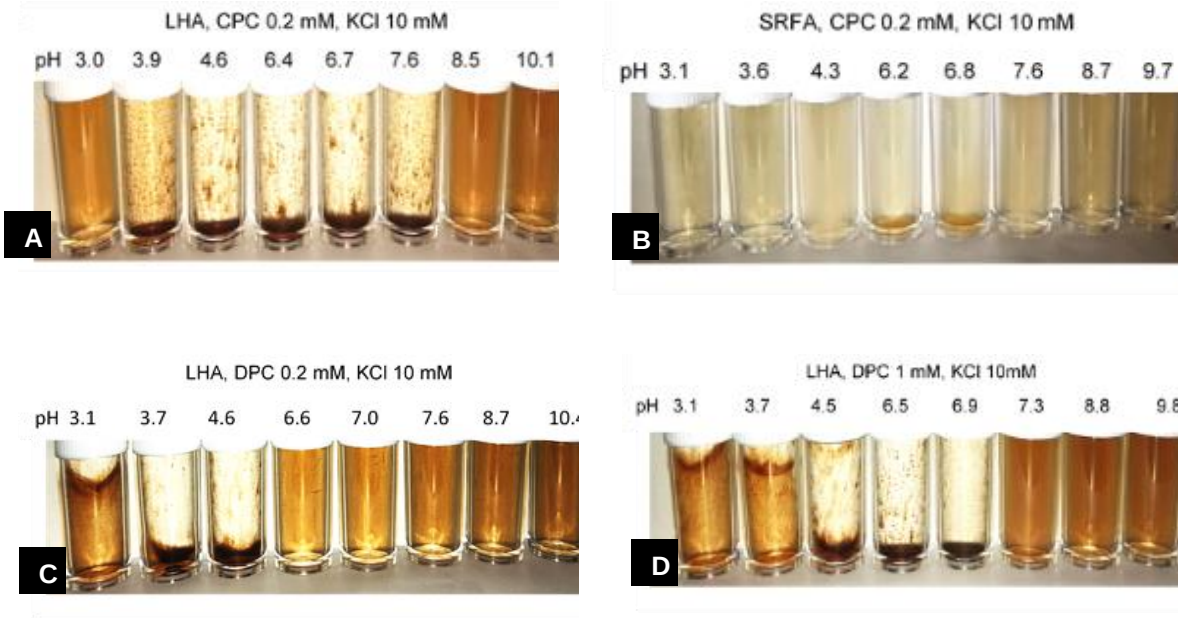

Figure 4.5. Aggregation dispersion of Leonardite humic acid (LHA) and Suwannee river fulvic acid 50 mg/L in 0.2 mM CPC (cetylpyridinium chloride) at 10 mM KCl solution (A and B), and Leonardite humic acid (LHA) 50 mg/L at 0.2 mM and 1 mM DPC (dodecylpyridinium chloride) at 10 mM KCl solution (C, D), respectively. Brightness and contrast of the images were corrected to visualize the aggregates clearly. Photos were captured after 24 hours and the color was also adjusted by using GIMP 2.8.22 (Reuse from Hakim & Kobayashi, 2019, Colloids Surf. A: Physicochem. Eng. Aspects, Vol. 577, pp. 175-184).

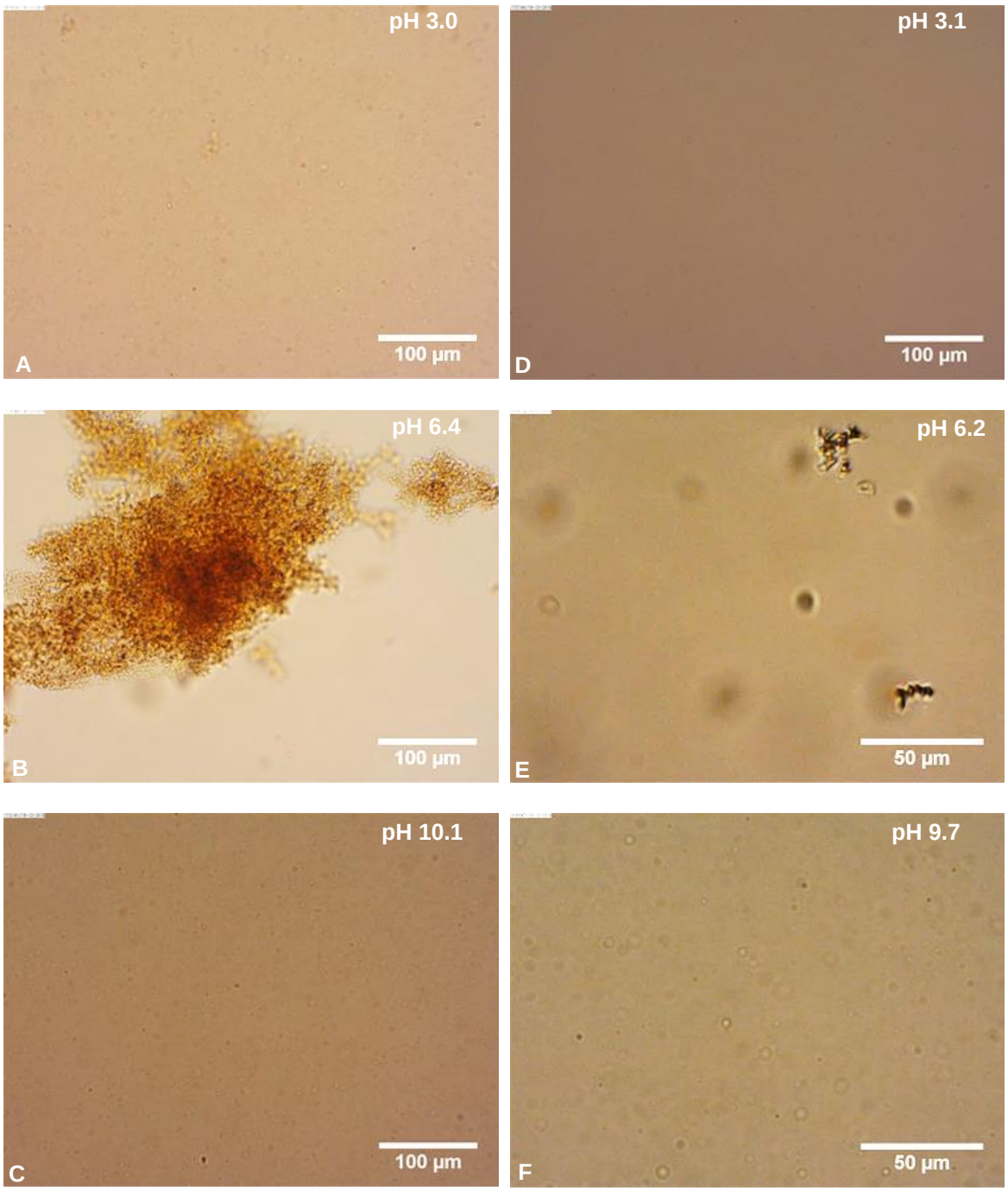

Figure 4.6. Microscopic images of Leonardite humic acid (LHA) in 0.2 mM CPC and KCl 10 mM solution at pH 3 (A), 6.4 (B) and 10.1 (C) and Suwannee river fulvic acid (SRFA) in 0.2 mM CPC and 10 mM KCl solution at pH 3.1, 6.2, and 9.7 (D, E, and F). Concentration of LHA and SRFA is 50 mg/L. Brightness and contrast were corrected. (Reuse from Hakim and Kobayashi, 2019, Colloids Surf. A: Physicochem. Eng. Aspects).

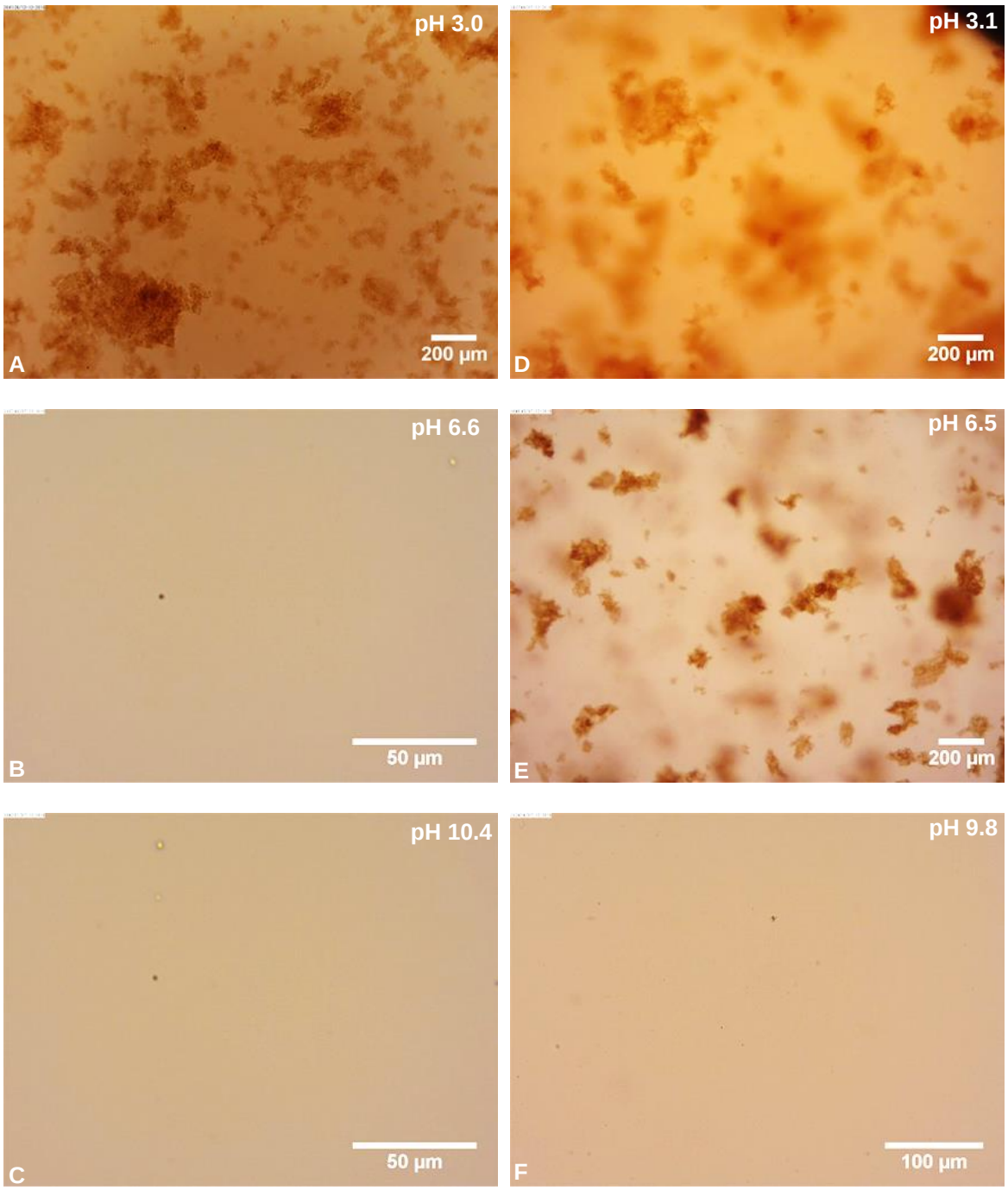

Figure 4.7. Microscopic images of Leonardite humic acid (LHA) in 0.2 mM DPC and KCl 10 mM solution at pH 3, 6.6 and 10.4 (A, B, and C) and 1 mM DPC at 10 mM KCl solution at pH 3.1, 6.5, and 9.8 (D, E, and F). Concentration of LHA is 50 mg/L. Brightness and contrast were corrected. (Reuse from Hakim and Kobayashi, 2019, Colloids Surf. A: Physicochem. Eng. Aspects).

4.3.3 Suwannee river fulvic acid (SRFA) and Leonardite humic acid (LHA) aggregate strength in CPC and DPC solutions

The strengths of SRFA and LHA aggregates in CPC and DPC in the presence of 10 mM KCl solution are shown in Fig. 4.8. The effect of hydrophobicity of HSs can be evaluated from the strength value of SRFA and LHA aggregates in CPC solution (Figure 4.8 A, C). The effect of alkyl tail length of two cationic surfactants, CPC and DPC, could be inferred from the comparison of strength value in Fig 4.8. A, B, and C.

In any case of SRFA-CPC and LHA-CPC systems, the maximum aggregate strength is around the IEP. The maximum aggregate strength of SRFA-CPC system is around 5.2 nN, which is lower than the aggregate strength of LHA-CPC system of around 27.6 nN at pH around 6.2. In addition, the LHA-DPC system also shows a maximum aggregate strength around 19.1 nN at around pH 3.7, which is near IEP pH 3.9. All the systems show maximum aggregate strength around IEP pH, though the order of maximum strength is LHA-CPC > LHA-DPC > SRFA-CPC. This maximum aggregate strength around IEP pH indicates the charge neutralization and/ or electrostatic attraction playing a key role for aggregation of these HSs in any case. The higher value of LHA-CPC system aggregate strength than that of SRFA-CPC system indicates more hydrophobic interaction or more gathering of hydrophobic moieties of LHA with CPC than SRFA with CPC. On the other hand, the higher strength of LHA aggregates in 0.2 mM DPC and 10 mM KCl than that of SRFA-CPC system. These results indicate the higher hydrophobicity of LHA induces stronger aggregates due to the higher aromaticity and carbon content of LHA than that of SRFA (Table 4.1). Some previous study also observed the effect of different HSs hydrophobicity and/ or aromaticity on the charging and aggregation (Hakim & Kobayashi, 2018; Hakim and Kobayashi, 2019) of three different HSs by using a monovalent hydrophobic ion.

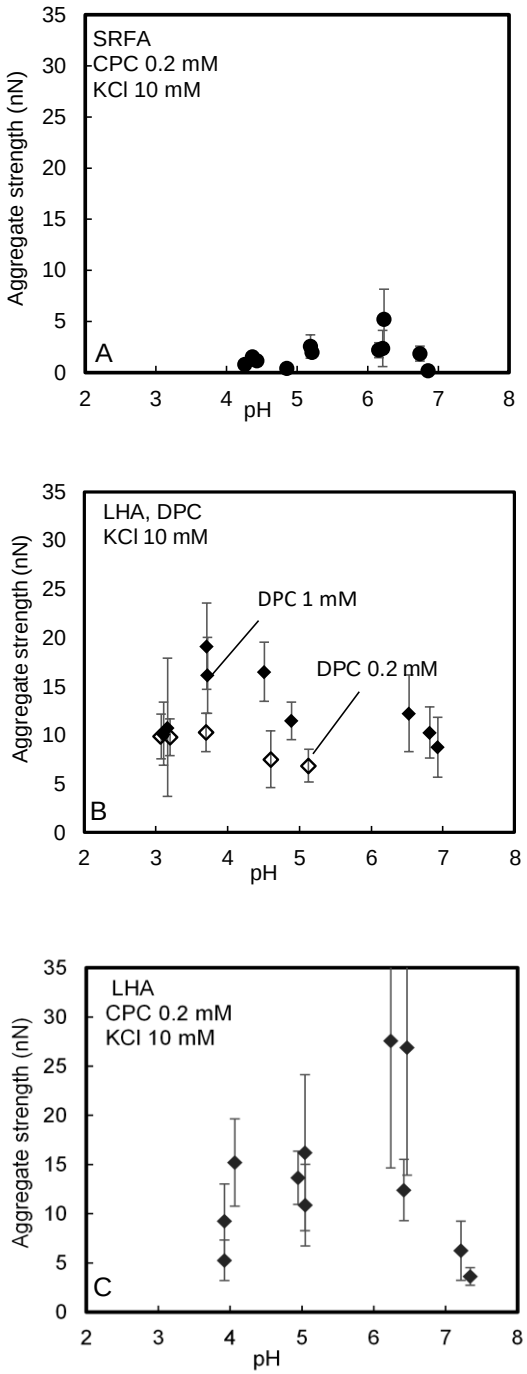

Figure 4.8. Aggregate strength of SRFA in 0.2 mM CPC at 10 mM KCl solution (A), LHA in 0.2 mM DPC and 1 mM DPC at 10 mM KCl solution (B) and LHA in 0.2 mM CPC at 10 mM KCl solution (C) as a function of pH. Concentration of LHA and SRFA are 50 mg/L. (Reuse from Hakim & Kobayashi, 2019, Colloids Surf. A: Physicochem. Eng. Aspects, Vol. 577, pp. 175-184).

However, some other investigations of humic acid-protein complexation (Tan et al., 2008), and HSs with cationic surfactants (Koopal et al., 2004; Ishiguro et al., 2007; Hakim & Kobayashi, 2019) described the importance of hydrophobic and electrostatic interactions on the charging behavior and aggregation of HSs. Beyond the value of maximum aggregate strength around IEP, the strength was comparatively higher in the range of charge reversed range of pH than that of the negative electrophoretic mobility. The possible mechanism for this higher strength value at the charge reversal pH range is because of hydrophobic interaction along with electrostatic and charge patch attraction.

The result in the above sections explores the impact of HSs hydrophobicity and the alkyl tail length of cationic surfactant on the charging, aggregation behavior, and strength of humic substances aggregate. Nevertheless, it was importantly noticed that the hydrophobicity and/or aromaticity has a strong effect on the adsorption of natural organic matters (NOM) in hydrophobic carbon nanotubes (Hyung & Kim, 2008). The effect of HSs hydrophobicity on the aggregation behavior of three different HSs was also evaluated by Hakim & Kobayashi (2018). The higher aggregate strength in LHA-CPC system shows the distinct effect of hydrophobic interactions on the aggregation and strength behavior in this investigation. The higher hydrophobicity accompanied with the lower charge were mentioned in the previous literature (Hakim et al., 2016; Sugimoto et al., 2017), which means the strong hydrophobic interaction prevails with the weak charging state of colloidal particles. 4 nN of maximum strength was reported by Kobayashi (2005) for natural soil flocs and this strength was explained due to the hetero-coagulation caused by attractive electric double layer interactions (Ryde & Matijevic,1994; Yu & Borkovec, 2002). The LHA aggregates in CPC in this investigation shows around 6.9 times (27.6 nN) higher strength than the previous investigation by Kobayashi (2005). The possible cause of this higher strength could be explained by the strong attractive interaction of hydrophobic surfaces of

HSs. The effect of HSs hydrophobicity and the dominance of hydrophobic effects for the charging and aggregation of HSs was manifested in the previous study by Hakim and Kobayashi (2018). In their investigation, they explained how the hydrophobicity of HSs affect the size of the aggregate, and they clearly manifested the increased aggregate size of LHA than other HSs by DLS, visual, and microscopic observations.

Meanwhile, the strong adsorption of big hydrophobic ion on sulfate and carboxylic latex particles and reversal of surface charge was mentioned and explained by some author in previous investigations (Hakim et al., 2016; Sugimoto et al., 2017). Considering these previous investigations, the higher aggregate strength for LHA-CPC system could be explained and reasonable to describe by charge neutralization and/or hydrophobic interaction. In the different chemical systems, the adhesive forces and strength of flocs/aggregates are summarized in Table 4.2. In table 4.2, the range of the forces or strengths are from 0.3-60 nN; these values are comparable with our findings of this investigation.

Table 4.2. Force or aggregate/ floc strength demonstrated in previous literature. (Reuse from Hakim & Kobayashi, 2019, Colloids Surf. A: Physicochem. Eng. Aspects, Vol. 577, pp. 175-184).

Forces and/ or strength value	System of investigation	Presented in the literature
12.5 ± 4.4 nN	Methyl-methyl (CH_3-CH_3) tip-surface pair interaction in water for thiol C_{12}	Sinniah et al., 1996; Noy et al., 1997
60 ± 5 nN	Methyl-methyl (CH_3-CH_3) tip-surface pair interaction in water for thiol C_{18}	Vezenov et al., 1997; Noy et al., 1997
28.4 ± 9.4 nN	-CH_3/-CH_3 (methyl-methyl) tip-sample pair in water	Warszyński et al., 2003
4.2 ± 1 nN	-COOH/-CH_3 (carboxyl-methyl) tip-sample pairs in water	Warszyński et al., 2003
2 nN	Polystyrene latex flocs	Kobayashi, 2004
0.3 nN, 0.7 nN and 4 nN	Natural soil flocs (Na-, Ca-, and H-coagulated flocs)	Kobayashi, 2005
0.65−31 nN	Alginate hydrogels on −OH, −COOH, −CH_3, or −NH_2-terminated self-assembled monolayer or protein films	Helfricht et al., 2017
5.8 nN and 2.4 nN	The maximum aggregate strength of Leonardite humic acid in $CaCl_2$ and $MgCl_2$ solution	Hakim et al., 2019

Some other studies on humic substances (Ishiguro et al., 2007) and poly (L- glutamic acid) (Godec & Kogej, 2007) also confirm the more hydrophobic interaction and binding of longer tail cationic surfactant (CPC > DPC). The higher value of adhesion force for C_{18} than that of C_{12} of thiol monolayer in methyl-methyl (CH_3-CH_3) tip-surface pair interaction was also confirmed by using AFM, where the adhesion force was 60 ± 5 nN and 12.5 ± 4.4 nN, respectively (Noy et al., 1997; Sinnaih et al., 1996; Vezenov et al., 1996). The effect of hydrophobic side groups size on the binding of surfactant ion was manifested by the Gibbs energy of binding (Shimizu et al., 1986; Shimizu & Kwak, 1994). All the previous studies and experimental findings discussed in the earlier section strongly support the outcome of our experiment and help us to conclude the strong attractive hydrophobic interaction in case of most hydrophobic HSs and a longer tail length of cationic surfactant, CPC (Hakim & Kobayashi, 2019)

4.4 Conclusion

The aggregation, charging behavior of aggregated suspension and the strength of two different humic substances (SRFA and LHA) in the presence of two cationic surfactants of different alkyl tail length has been clearly evaluated in this study. The charge reversal of SRFA and LHA was observed in all experimental condition except the 0.2 mM DPC concentration. In any case of pH condition, the LHA aggregates show higher strength than that of SRFA aggregates, but it is also obvious that the strength of LHA in CPC is higher than LHA in DPC at around IEP. This higher strength of LHA than SRFA aggregates could be explained by the high aromatic and /or hydrophobic content of LHA than that of SRFA. The discussion is supported by the findings of the third chapter of this thesis. This charge reversal of the HSs is also validating the findings of the charge reversal and adsorption of hydrophobic ion on HSs in the third chapter.

A significant ($p < 0.05$) difference is confirmed between the strength values of maximum and around the maximum of LHA and SRFA in CPC. Additionally, the effect of DPC concentration on the LHA aggregate strength was significant at $p < 0.001$. We found the effect of alkyl tail length of cationic surfactant on the aggregate strength of LHA in CPC and DPC system. The maximum aggregate strengths of LHA in CPC and DPC were around 27.6 nN and 19.1 nN, respectively, and those values are found around IEP pH. The facts indicate charge neutralization induces strong electrostatic attractive force along with hydrophobic interaction of LHA particles with longer tail CPC.

Finally, we observed the effect of tail length on the shifting of IEP pH. Thus, the shifting of IEP towards a higher pH value was observed by the increase of surfactant tail length and hydrophobicity of HSs. The findings of this experimental study are partly able to explore the forces acting in a complex system of colloidal mixture beyond the classical DLVO by placing the effect of hydrophobicity and hydrophobic interaction in such a complex system of study. We strongly believe that the charging and aggregation behavior and the numerical value of aggregate strength will be helpful to investigate and evaluate the transport and aggregation – dispersion of hydrophobic and big organic molecules in the natural waterways or simulated flow field. Considering the other environmental problems and the importance of hydrophilic inorganic ions in natural environmental condition, we will describe the aggregation, charging and strength behavior of NOM in the presence of two important cations Ca^{2+} and Mg^{2+} in the upcoming chapter.

Chapter 5

Effects of Ca^{2+} and Mg^{2+} ions on the strength of Leonardite humic acid aggregate in different pH condition

5.1 Introduction

Humic substances (HSs) are organic macromolecules and have charging characters (Jones & Bryan, 1998; Myneni et al., 1999; Swift, 1999). These natural organic matters (NOMs) are ubiquitous in the natural environment (Gaffney et al., 1996). The important properties and the transport behavior of HSs aggregate and its role in the environment are discussed in the previous chapters 3 and 4. The previous chapter discussed the charging and aggregation of HSs in the presence of hydrophobic organic molecules and two widely used cationic surfactants. This chapter describes the charging and aggregation of humic substance in soil and water environments considering important inorganic hydrophilic cations. HSs play multifunctional roles for the aggregation, transport, and distribution of macro and micronutrients from soil water to plants along with the distribution and binding of some other contaminants and pollutants (Luo & Gu, 2009; Wang & Mulligan, 2009). The aggregation-dispersion, binding, sorption, and transport of HSs depends on several environmental factors such as solution pH (Bonn & Fish, 1993; Benedetti et al., 1995; Saar et al., 1979), temperature (Bryan et al., 2000; Shaffer & Wandruszka, 2015), ionic strength (Fitch et al., 1986; Tipping & Hurley, 1992; Higgo et al., 1993; Zachara et al., 1994) concentration of HSs themselves (Saar et al., 1979), and other parameters of the environment.

The transport and distribution of HSs along with pollutants, is an important function of HSs depending on particles size. Therefore, the size of HSs particles and/ or aggregates is a matter of concern in the case of pollutants and nutrients transport in soil and water environment (Luo & Gu, 2009; Chen et al., 2012; Bian et al., 2011; Mccarthy & Zachara, 1989; Deb & Shukla, 2011; Weng et al., 2002). The size of HSs is related to its aggregation behaviors, which is influenced by Na^{+}, K^{+}, Cs^{+}, Ag^{+}, Ca^{2+}, Mg^{2+}, Cu^{2+}, Cd^{2+}, Al^{3+}, Eu^{3+}, Sr^{2+}, Fe^{2+}, Fe^{3+} etc. (Sharpless & McGown, 1999; Wang et al., 2013; Kloster et al., 2013;

Balnois et al., 1999; Brigante et al., 2009; Schmitt et al., 1996; Wall & Choppin, 2003; Bryan et al., 2001; Tan et al., 2018). Therefore, HSs transport is influenced by the degree of HSs aggregation.

Some of the previous investigations reported the effect of divalent cations, their concentration and pH on the aggregation and ion-binding to HSs or NOM (Wang et al., 2013; Kloster et al., 2013; Kalinichev et al., 2011; Bryan et al., 1997). Hydrophobicity of HSs and the stronger interaction with organic ions also play an important role in the aggregation of HSs (Hakim & Kobayashi, 2018; Tan et al., 2008; Tan et al., 2009; Ishiguro et al., 2007; Koopal et al., 2004). Some of the previous literature reported pronounced aggregation of HSs at low pH regardless of the ionic valance (Wang et al., 2013; Tan et al., 2018; Alvarez-Puebla & Garrido, 2004). But several investigations reported that HSs has a comparatively higher degree of aggregation at higher pH values than that of low pH (Kloster et al., 2013; Palmer & Wandruszka, 2001). In this situation, considering the dilemma of aggregation depending on the ionic valence, ionic specificity, and pH, we consider that aggregation of HSs is still unclear.

So, the discussion in the previous sections and chapters trigger us to consider the strength of HSs aggregate because the aggregate strength is an important parameter to be evaluated in the presence of ionic specificity and variability of solution pH. The strength of aggregates comes from the forces among primary particles of the HSs in the aggregate and the higher aggregate strength represent its withstanding capacity in the flow field especially in the natural transport system or artificial waterways.

Therefore, the divalent cationic specificity, pH, and the concentration of cations on the aggregation and the strength of aggregate have been explored. This investigation will be able to explore the ion specificity on the aggregation of HSs and strength of HSs aggregate.

This study will be able to partly unveil the mechanism of HSs aggregates strength in the presence of specific divalent ions at different solution pH.

5.2 Materials and Methods

5.2.1 Materials

In this chapter, we used standard Leonardite humic acid (LHA) from the International Humic Substances Society (IHSS). The preparation of primary and secondary stocks solution was described in the previous chapter 3 and 4 following the methods described in Hakim & Kobayashi (2018). The salts solutions of $CaCl_2.2H_2O$ and $MgCl_2.6H_2O$ (JIS special grade, Wako Pure Chemical Industries) were used to examine the effect of divalent cation types. The concentration of salt was 2 mM to 30 mM in ionic strength. In this study, the concentration of $CaCl_2$ and $MgCl_2$ will be expressed in ionic strength (I). The CO_2 free KOH solution preparation was prepared following the previous chapters 3 and 4 following the method of Sipos et al. (2000).

5.2.2 Methods

5.2.2.1 Electrophoretic mobility measurements

A Zetasizer Nano ZS apparatus (Malvern Instruments) was used to measure electrophoretic mobilities of LHA in the presence of both $CaCl_2$ and $MgCl_2$ at 20 °C. The electrophoretic mobility was measured at 2 mM, 10 mM, 30 mM of $CaCl_2$ and $MgCl_2$ ionic strength as a function of pH 3-10. The solution pH was maintained using HCl (JIS special grade chemicals, Wako Pure Chemical Industries) and KOH solution. In the whole experimental study of this research, the LHA concentration was maintained at 50 mg/L. A combination electrode (ELP-035, TOA-DKK) was used to measure the pH of the solution.

5.2.2.2 Macroscopic and microscopic observations of aggregation and dispersion

A 50 mg/L of LHA solution in different ionic strength from 2 mM -30 mM of $CaCl_2$ and $MgCl_2$ were used as a function of pH for the visual and microscopic observation of aggregation-dispersion. 5 mL of LHA suspension at the ionic strength 2-30 mM of $CaCl_2$ and $MgCl_2$ solution as a function of pH was placed in a series of 5 mL of polystyrene plastic bottle. The naked eye visual observation was done with the microscopic observation (Shimadzu BA210E, Moticam 580INT) after 24 hours of the experimental setup.

5.2.2.3 Converging flow generation and the breakup of aggregates

The LHA aggregate strength was evaluated from the breakage of aggregates in a converging flow into a glass capillary. The aggregates were taken after 24 hours of the LHA in $CaCl_2$ and $MgCl_2$ suspensions from the polystyrene plastic bottles at different pH condition. The experimental setup is presented in an illustration in Fig. 4.1. This similar experimental setup was used by Sonntag & Russel (1987), Higashitani et al. (1991), Blaser (2000 a,b), Kobayashi (2005) and Kobayashi (2004) to evaluate the strength of flocs by the breakup.

The galas capillary (0.8 mm diameter), the volumetric flow rate (10 mL/min), and flow condition using the syringe pump (Fusion 200, Chemyx) were thoroughly described in the previous chapter 4. In this experiment, we used a similar procedure following chapter 4. Nevertheless, two different inorganic divalent cations at different solution pH were used to evaluate the ionic specificity and the effect of solution pH on the aggregate strength of LHA aggregate. 20 °C room temperature was maintained in the total experimental measurements.

5.2.2.4 Calculation of aggregate strength force

Usually, the LHA aggregate in the flow field will be broken down when the hydrodynamic rupturing force acting on the aggregates in the flow field overcome the strength of the aggregate. During the entrance of the LHA aggregates into the glass capillary

the hydrodynamic rupturing force F_{hyd}, exceeds the strength of LHA aggregate $F_{aggregate}$. Thus, the breakup happens. That is aggregate breakup occurs when

$$F_{hyd} \geq F_{aggregate} \quad (1)$$

The larger aggregates at a certain shear rate of flow are subjected to higher rupturing force. Therefore, after the breakage, the maximum sized aggregates reflect the strength of aggregates where $F_{hyd} = F_{aggregate}$. (2)

The flocs/aggregates of maximum size with the maximum surface area at the maximum elongation rate of flow are subjected to higher stress. Based on the assumptions, an equation was deduced by Kobayashi (2004) to evaluate the flocs/aggregate strength. The theoretical background and explanation were discussed in earlier chapter 4 of this thesis.

$$F_{aggregate} = (C_{hyd}S)_{max}\,\mu A_{c,max} / 2 \quad (3)$$

where $(C_{hyd}S)_{max,}$ represents the maximum values of $C_{hyd}S$ of maximum sized aggregates of the maximum surface area subjected to a maximum elongation rate of flow $A_{c,max}$.

5.3 Results and Discussion

5.3.1 Electrophoretic mobility of Leonardite humic acid in $CaCl_2$ and $MgCl_2$ solutions

Figure 5.1 shows the electrophoretic mobility of Leonardite humic acid (LHA) at 5 mM, 10 mM, and 30 mM of $CaCl_2$ and $MgCl_2$ as a function of pH. The electrophoretic mobility of LHA at all pH and ionic strength is negative values. This negative mobility of three different humic substance is discussed in the presence of KCl in previous chapter 3. The absolute value of mobility in the presence of KCl was higher than the absolute value in $CaCl_2$ and $MgCl_2$ solution. The behavior indicates the more screening of double layer due to the increase of ionic valence from K^+ to Ca^{2+} and Mg^{2+}. Carboxylate latex also showed

similar trends though the mobility was constant at high pH (Nishiya et al., 2016). In Figure 5.1 A and B, we also use the Smoluchowski equation and Hückel equation to convert zeta potential, ζ into electrophoretic mobility, μ. We consider the zeta potential, ζ as diffuse-layer potential Ψ(d) calculated by using the Visual MINTEQ. In the calculation of diffuse-layer potential Ψ(d), we used the parameters that were fixed for typical humic acid (spherical radius 1.8 nm). For this calculation in Visual MINTEQ, we considered the Stockholm Humic Model (SHM) and the parameters are considered from this SHM model (Gustafsson, 2001; Molina, 2014). We also used the dissolved organic carbon concentration 31.5 mg/L, which represents around 50 mg/L of LHA, since LHA has 63.81 (wt%) of carbon (C). The theoretical values at 30 mM of $CaCl_2$ and $MgCl_2$ solution show overestimation than the experimental values. This overestimation could be due to the consideration of the parameters fixed for a typical soil humic acid in Visual MINTEQ, but in our experiment, we used the LHA (Leonardite humic acid). This HSs differ in size, site density, chargeable groups, and hydrophobicity from the typical soil humic acid. But the trend of binding and electrophoretic mobility values shows a similar trend for theoretical and experimental values at 30 Mm of ionic strength (Fig. 5.1 A). The increases of $CaCl_2$ and $MgCl_2$ concentration there is a decreasing absolute negative value of mobility, which is due to the binding of the divalent cation with $–COO^-$ groups of LHA. In the presence of Ca^{2+} (Klostert et al., 2013, Kinniburgh et al., 1999; Milne et al., 2003; Majzik & Tombácz, 2007) and Mg^{2+}(Wang et al., 2013), the humic substances show no charge reversal in any case of specific or nonspecific binding explained by theoretical modelling and experimental studies. It was also confirmed that no notable change is observed at high pH. This same trend of constant charging behavior was previously investigated by measuring zeta potential in the presence of Ca at high pH (Kloster et al., 2013 & Attard et al. 2000). In Fig. 5.1 A, B, and C, no notable variation is shown for any experimental condition of $CaCl_2$ and $MgCl_2$, though at 5 mM ionic strength the absolute

mobility in the presence of $CaCl_2$ is lower than $MgCl_2$ solution (Fig. 5.1 C). The results mean that more binding of Ca^{2+} ion to LHA than Mg^{2+} ion. At this low ionic strength, the higher binding affinity is also demonstrated by the aggregation of $CaCl_2$ at 5 mM compared to no aggregation by $MgCl_2$ solution in Figure 5.2 A, B.

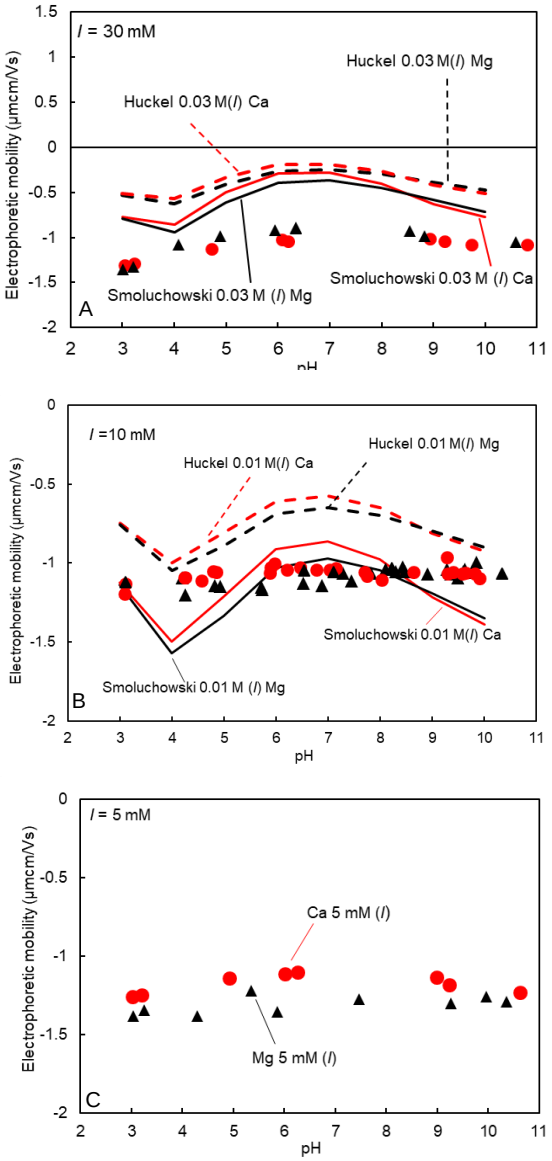

Figure 5.1 Electrophoretic mobility of Leonardite humic acid (LHA) at 30 mM (A), 10 mM (B), and 5 mM (C) of $CaCl_2$ (●) and $MgCl_2$ (▲) as a function of pH. The solid lines: Smoluchowski equation and dashed line: Huckel equation. Concentration of LHA is 50 mg/L. (Reuse from Hakim et al., 2019, ACS Omega, 4 (5), 8559-8567).

5.3.2 Observation of aggregation of Leonardite humic acid in $CaCl_2$ and $MgCl_2$ solutions

The naked eye visual and microscopic observations of Leonardite humic acid (LHA) aggregates in $CaCl_2$ and $MgCl_2$ solutions at different ionic strength as a function of pH were performed. Figure 5.2 A shows no aggregates of LHA through naked eye at 5 mM of $MgCl_2$ solution (Fig. 5.2 A) in any pH condition, while LHA aggregates were observed after 24 hours at all pH range for $CaCl_2$ 10 mM and 30 mM and 30 mM of $MgCl_2$ (Fig. 5.2 D and Fig. 5.2 D, E, F). Furthermore, LHA in $CaCl_2$ shows faster aggregation than $MgCl_2$ solution in every case of the experimental ionic strength (Fig 5. 3). The temporal changes of visual aggregation confirm this condition and the aggregates arose at higher pH value than lower pH at an earlier time after preparing the LHA suspension in $CaCl_2$ or $MgCl_2$ solution (Fig. 5.3).

Large visual macroscopic aggregates were observed for 5 mM of $CaCl_2$ solution at pH ranges around 7-10 (5.2 B), though it also shows microscopic aggregates at the lower range of pH (Fig. 5. 2 B and Fig. 5.4 C). This indicates that the Ca-induced aggregation of HA is triggered at higher pH values than low pH. This also indicates the aggregation of LHA is induced by a higher pH range in the presence of Ca^{2+}. But in the presence of Mg^{2+}, visible aggregates were found only at pH around 3 and 10 (Fig. 5. 5 A, C). At 30 mM of $CaCl_2$ and $MgCl_2$ solution large visible macroscopic and microscopic aggregates were observed in any pH condition (Fig. 5.2 E, F, Fig. 5.6)

This high pH aggregation of HSs in $CaCl_2$ was demonstrated by Kloster et al. (2013) and Baalousha et al. (2006). The interactions of Ca^{2+} and Mg^{2+} ions are different in the presence of natural organic matter (Kalinichev & Krikpatrick,2007; Ahn et al., 2008; Abe et al., 2011) and humic acid coagulation (Wall & Choppin, 2003); and it was confirmed that the dominance of Ca over Mg for HA aggregation. These results support the findings of our

investigation. The difference in the interaction, binding, and activity of Mg^{2+} and Ca^{2+} ion could be explained by the strong hydration shell of Mg^{2+} ion than that of Ca^{2+} ion (Ahn et al., 2008). That is, the divalent bridging mechanisms for Ca^{2+} ion is stronger in closer proximity. This closer proximity of Ca^{2+} ion to LHA induces stronger aggregates more expressed in the aggregate's strength. But in this investigation, we predict that the hydrated Mg ion affects the increases of the distance to the chargeable site of humic acid and ion. Which subsequently weakens the ion-binding and the adhesion of Mg^{2+} ion to humic acid.

This low pH aggregation of LHA in the presence of Mg^{2+} ion could be the effect of the higher hydrophobicity accompanied by the lower charge at low pH (Terashima et al., 2004). This low pH aggregation of humic acid was also reported in many previous investigations (Wang et al., 2013; Tan et al., 2018). The parameters of HSs aggregation and binding such as the size, polydispersity, hydrophobicity, and surface activity vary with their source and type (Hakim & Kobayashi, 2018; Pal & Sengupta, 1985). It was also demonstrated that the coagulation of humic acid in the presence of Cs^{+}, $Sr^{2+,}$ and Eu^{3+} was consistent with the classical Schulze-Hardy rule (Tan et al., 2018). The intra- or inter-molecular bridges triggered the coagulation for Sr^{2+} and Eu^{3+} explained by molecular dynamics simulation (Tan et al., 2018).

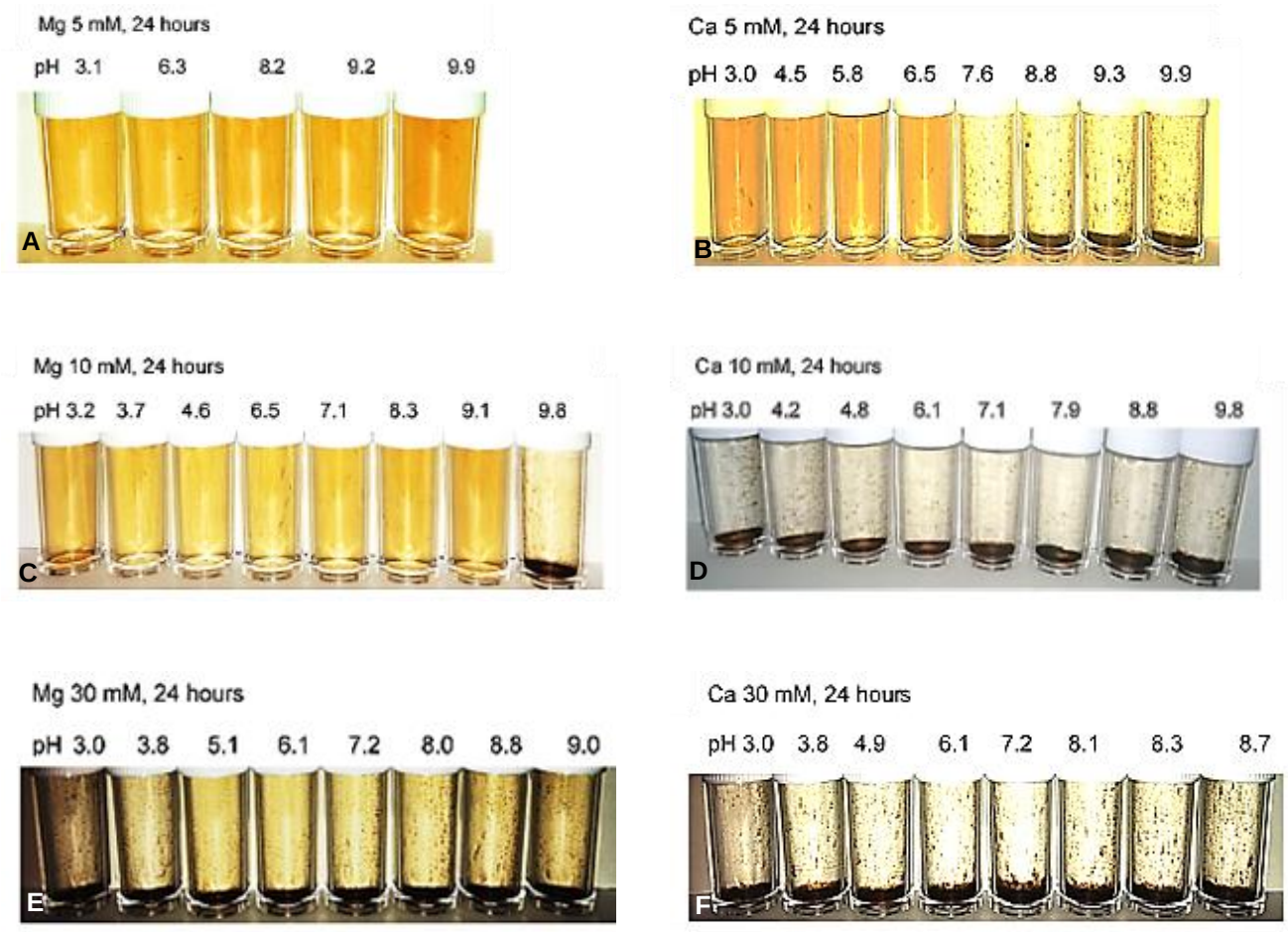

Figure 5.2. Aggregation dispersion of Leonardite humic acid (LHA) 50 mg/L in 5 mM $MgCl_2$ and $CaCl_2$ (A and B), 10 mM $MgCl_2$ and $CaCl_2$ (C and D) and 30 mM $MgCl_2$ and $CaCl_2$ (E and F). Photo color was also adjusted by using GIMP 2.8.22. (Reuse from Hakim et al., 2019, ACS Omega, 4 (5), 8559-8567)

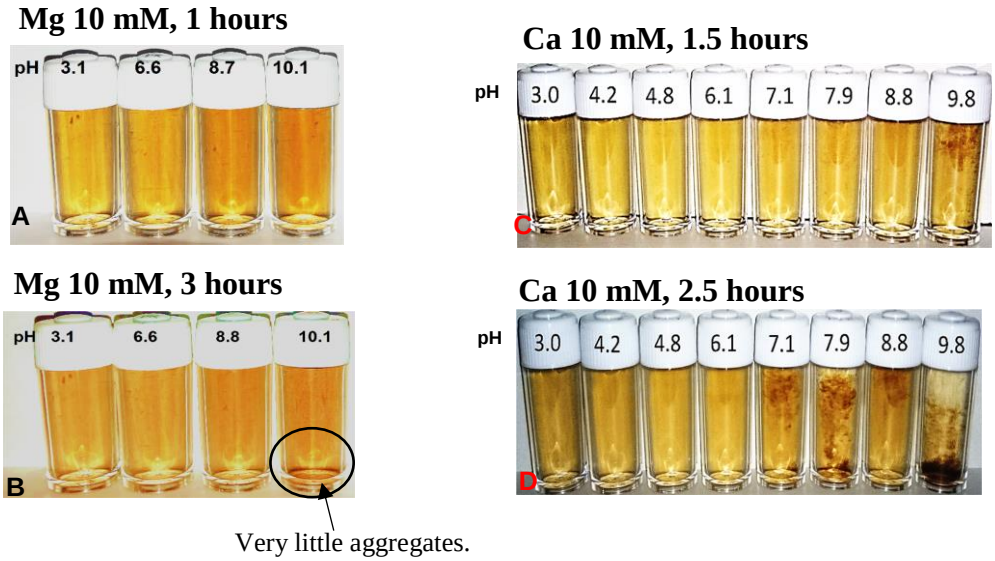

Figure 5.3. Temporal changes of aggregation dispersion of LHA in 10 mM of $MgCl_2$ and $CaCl_2$ solutions. Brightness and contrast of the images were corrected to visualize the aggregates clearly. Photo color was adjusted by using GIMP 2.8.22 (Reuse from Hakim et al., 2019, ACS Omega, 4(5), 8559-8567).

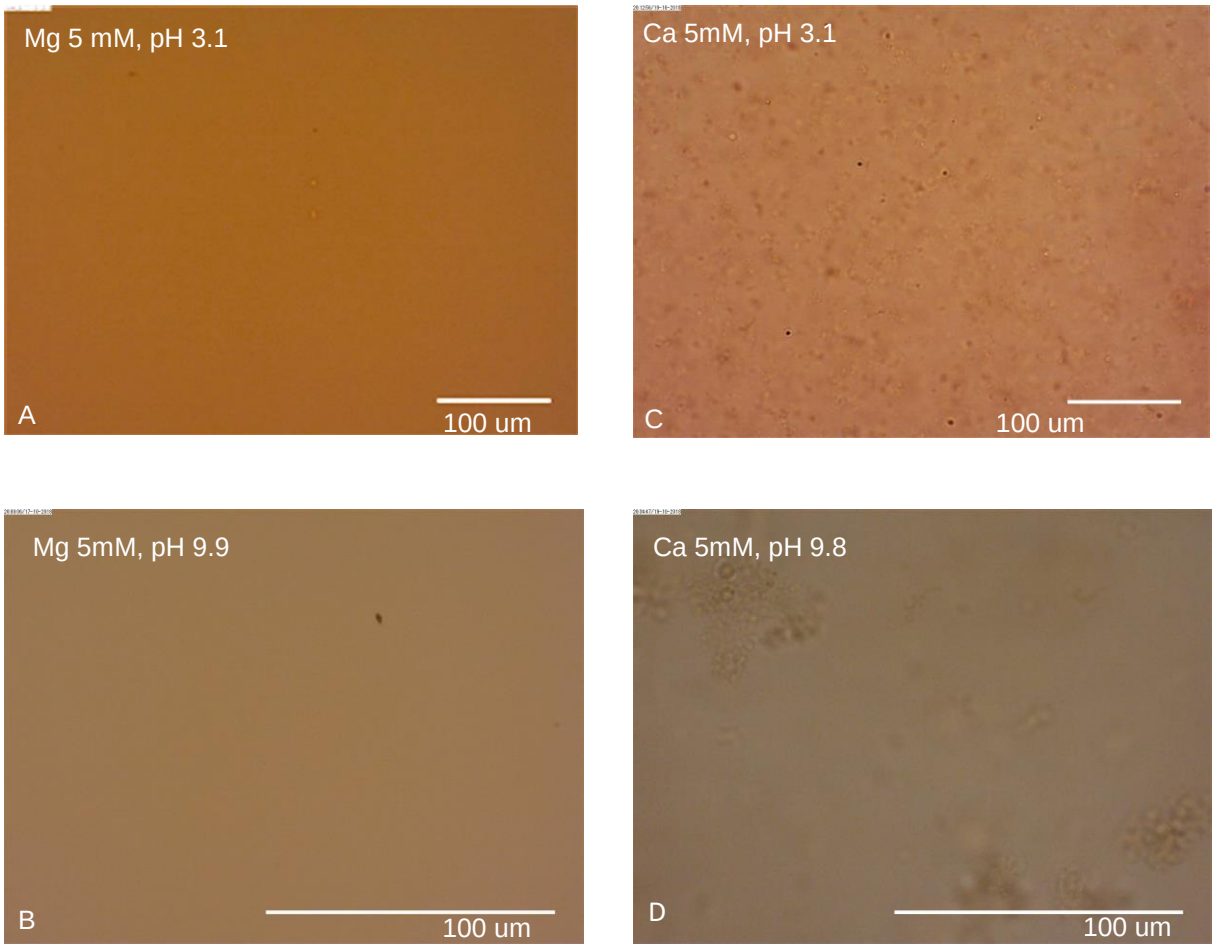

Figure 5.4. Microscopic images of Leonardite humic acid (LHA) 50 mg/L in $MgCl_2$ 5 mM (A, B) and $CaCl_2$ (C, D) 5 mM ionic strength solutions. Brightness and contrast were corrected. (Reuse from Hakim et al., 2019, ACS Omega, 4 (5), 8559-8567)

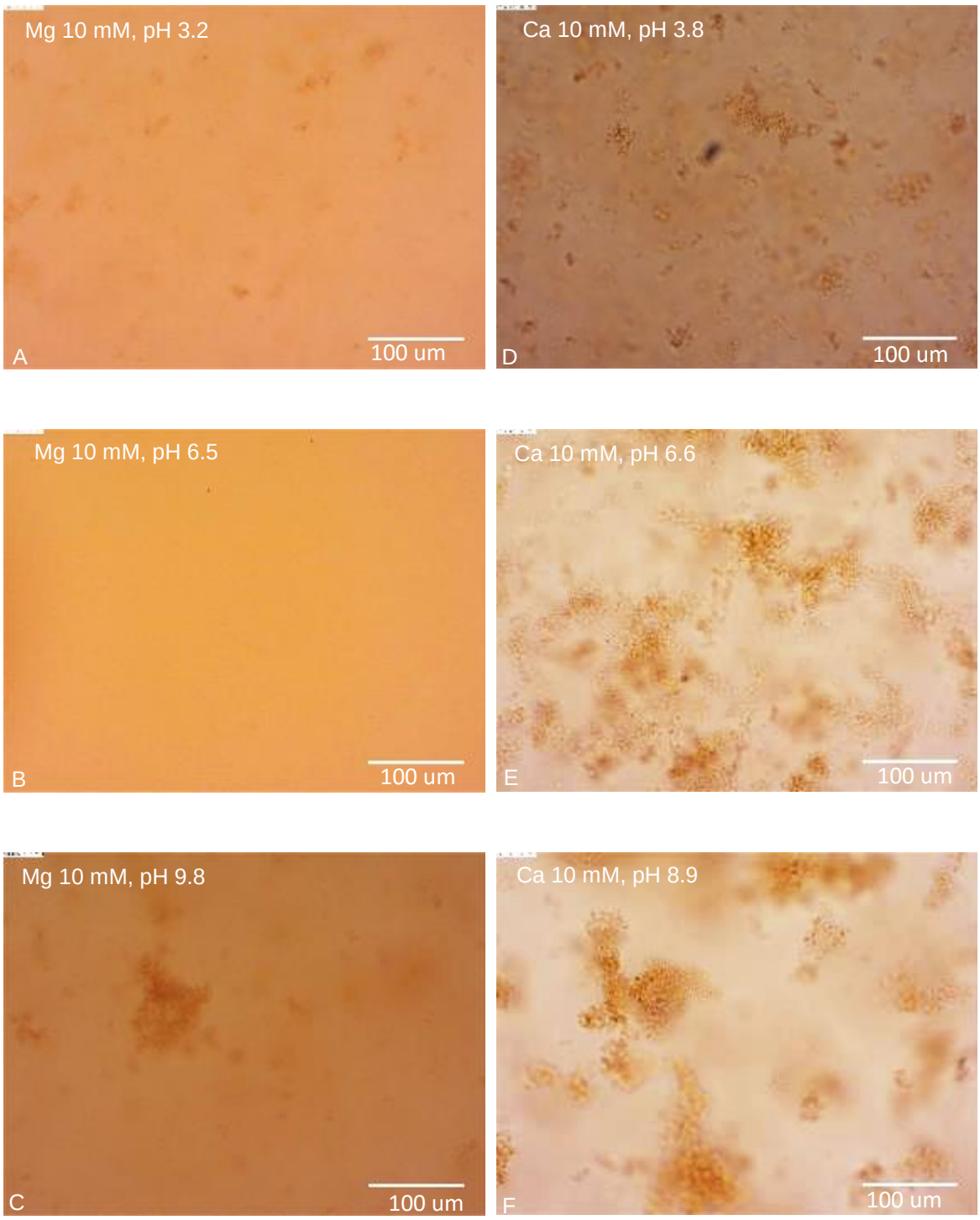

Figure 5.5. Microscopic images of Leonardite humic acid (LHA) 50 mg/L in $MgCl_2$ 10 mM (A, B, and C) and $CaCl_2$ 10 mM (D, E, and F) ionic strength solutions. Brightness and contrast were corrected. (Reuse from Hakim et al., 2019, ACS Omega, 4 (5), 8559-8567)

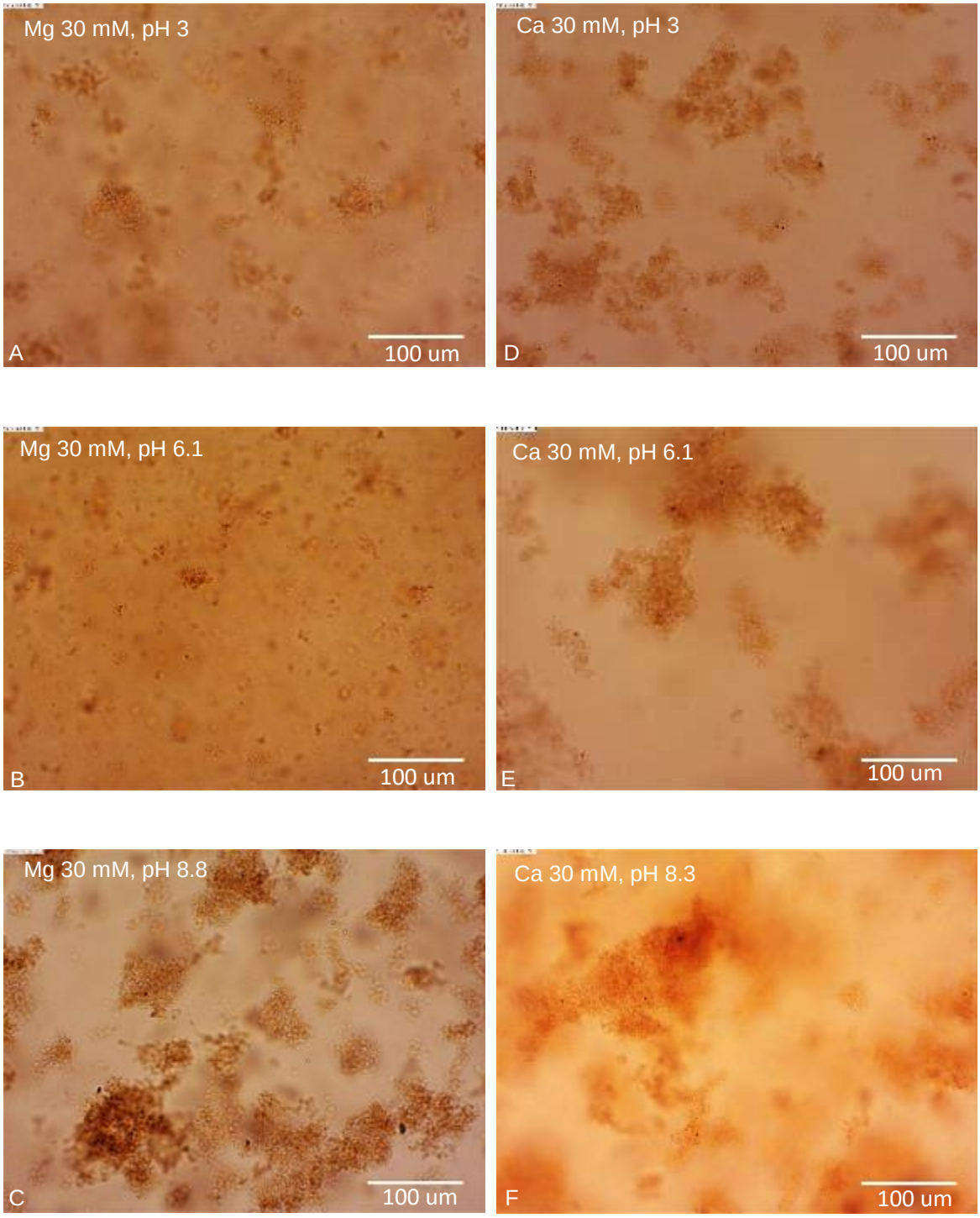

Figure 5.6. Microscopic images of Leonardite humic acid (LHA) 50 mg/L in $MgCl_2$ 30 mM (A, B, and C) and $CaCl_2$ 30 mM (D, E, and F) ionic strength solutions. Brightness and contrast were corrected. (Reuse from Hakim et al., 2019, ACS Omega, 4 (5), 8559-8567)

5. 3. 3 Aggregates strength of Leonardite humic acid in $CaCl_2$ and $MgCl_2$ solutions

Aggregates strength of Leonardite humic acid (LHA) was measured in the presence of 5 mM, 10 mM and 30 mM ionic strength of $CaCl_2$ and $MgCl_2$ (Figure 5.7 A, B, C). No macroscopic visual and microscopic aggregates of LHA was observed for $MgCl_2$ at 5 mM except some tiny particulates under a microscope (Fig. 5.2. A; Fig. 5.4 A, B). So, we considered the condition of aggregation for the capturing of maximum sized aggregates image in laminar converging flow to evaluate the strength. A previous investigation reported the withstanding force of few nN for polystyrene aggregates against breakup (Kobayashi, 2004). This force was explained as an interparticle/intermolecular force because the PSL strength is comparable with the adhesion force measured by atomic force microscopy (AFM) (Kobayashi, 2004). On the other hand, adhesion forces of 1-60 nN between different functional groups in water were also reported in some other studies (Noy et al., 1997). The adhesion forces for alginate hydrogels on –OH, -COOH, $-CH_3$, or $-NH_2$ terminated self-assembled monolayer (SAM) or protein films were reported from 0.65-31 nN (13-618 μN/m × ~50 μm), and the origin of this force was because of hydrogen bonding and local electrostatic interactions (Helfricht et al., 2017). The maximum aggregate strength of around 2 nN at pH around 9.5 is shown in Figure 5.7 A at 5 mM of $CaCl_2$ (Figure 7 A). Figure 5.7 shows the increasing trend of aggregate strength with pH in any ionic condition of $CaCl_2$ and $MgCl_2$, which could be explained by the more electrostatic attraction between negatively charged deprotonated $–COO^-$ sites of LHA through the bridging with Ca^{2+} ions and Mg^{2+} ion. Also, the strength in any pH and ionic condition shows lower values for $MgCl_2$ than that of $CaCl_2$ (Fig 5.7 A, B, and C). This is due to the strong hydration shell of Mg^{2+} ion than that of the Ca^{2+} ion explained in the previous section for aggregation. It is also confirmed that the

Ca^{2+} ion bridging with the LHA makes strong and large aggregates at higher pH values than that of lower pH values clearly depicted in the Figs. 5.2 B, 5.4 C, D and Figure 5.7 B, C.

A recent study (Nap & Szleifer, 2018) proposed the formation of calcium bridges in two opposing planner surfaces end-tethered with poly (acrylic acid) in the presence of calcium ions using molecular theory. This study theoretically confirmed that the surface-surface attractions increase with the increase of solution pH and calcium concentration (Nap & Szleifer, 2018). This theoretical finding (Nap & Szleifer, 2018) certainly verify the findings in our investigation that the strength of LHA aggregates increases with the increase of solution pH and ionic strength of $CaCl_2$ and $MgCl_2$. Nevertheless, Kobayashi (2005) summarized the higher floc strength for Ca-induced coagulation of natural soil flocs than that of Na induced coagulated flocs. This higher strength of Ca-flocs is explained by divalent Ca bridging to the surfaces or strong attraction due to ion-ion correlation. In figure 5.7 C the maximum aggregate strength around 2.4 nN in $MgCl_2$ solution, which is much lower than that of 5.8 nN aggregate strength for $CaCl_2$ solution at 30 mM ionic strength. This phenomenon of higher strength at $CaCl_2$ solution is already discussed in the earlier section. This difference can be explained by stronger hydration prevents closer contact between Mg^{2+} ions and carboxylic group of LHA and thus weakens the binding with LHA, unlike Ca^{2+} ion. In the previous investigation by Ahn et al. (2008) demonstrated the adsorptive fouling of polyethersulfone membranes by natural organic matter in the presence of common cations. In this previous study, Ahn et al. (2008) described the coordination complex between NOM carboxylate groups with Ca^{2+} and Mg^{2+} were predominantly the outer-sphere-type complexation. From the molecular modeling using MD computer simulations, they explained that there is a greater chance of Ca^{2+} interaction with carboxylate groups than Mg^{2+} due to the weaker hydration shell structure of Ca^{2+}. This phenomenon could be explained from their modeling and MD simulations, where they describe that in the second hydration

shell of Ca^{2+} and Mg^{2+} at a distance of 5.0 Å an average of 0.6 and 1.0 oxygen atom of the NOM carboxylate groups was present, respectively.

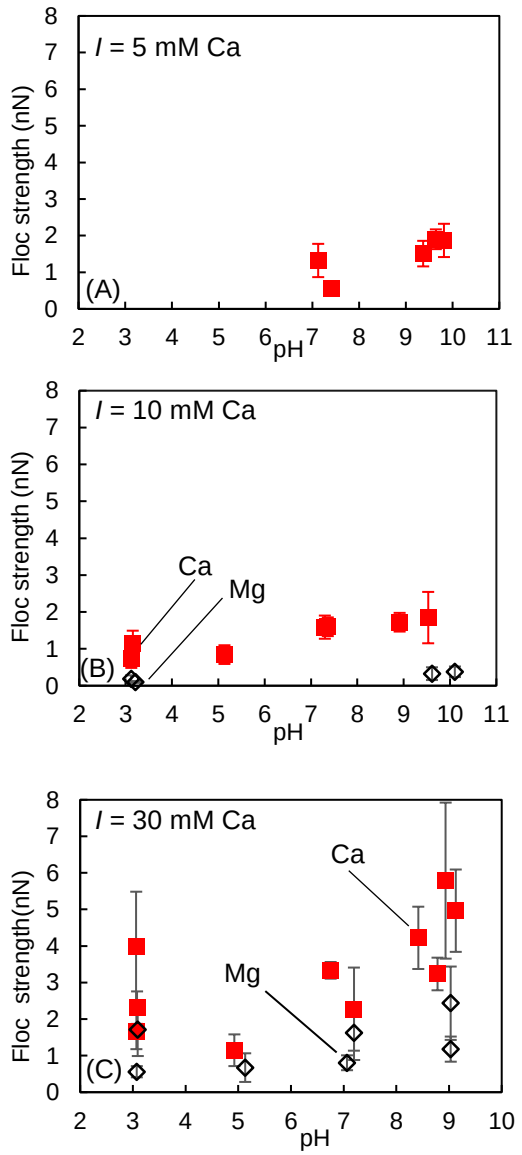

Figure 5.7. Strength of LHA aggregate at 5 mM (A), 10 mM (B), and 30 mM (C) ionic strength of $CaCl_2$ and $MgCl_2$ solutions as a function of pH. (Reuse from Hakim et al., 2019, ACS Omega, 4, 5, 8559-8567)

In this study, the influence of hydrolyzed species was not considered as a significant factor of concern, due to the lower ionic strength and pH condition. An investigation found the highest stress at pH around 12 and 13 for the yield stress of washed α-Al_2O_3 suspensions,

which was explained as the formation of Ca $(OH)_2$ and Mg $(OH)_2$ precipitates (Zhu et al., 2016). Additionally, some other studies did not pay attention to the hydrolyzed species for the divalent Ca^{2+} ion in carboxylic latex particles (Nishiya et al, 2016), whereas Sugimoto et al. (2019) confirmed the significant effect of the hydrolyzed species of La^{3+} ion on the charge reversal of sulfate latex particles.

5.4 Conclusion

In this chapter, we discussed the aggregate strength of LHA, which is a withstanding force against breakage. This force is an important factor to make large size aggregates and affects the aggregate size and subsequently influences the transport behavior of HSs and/ or natural organic matter in the soil and water environment. In this investigation, the aggregation and dispersion of humic substances are certainly influenced by the ionic strength, pH, and ion species. The previous chapter clearly explored the effect of humic substances hydrophobicity and hydrophobic interaction on the aggregation and charging behavior along with the strength of HSs aggregate. This chapter clearly focuses on the electrostatic interaction, which greatly influenced the aggregation and strength of LHA aggregates in the presence of two divalent cations Ca and Mg ions. Though the hydrophobicity of LHA at low pH has an effect on the aggregation and strength of LHA aggregates in the presence of Mg ion.

The results of this experiment will be a useful insight for the determination, prediction and the fate control of humic substances sorbed with organic or inorganic chemicals and/ or pollutants in the transport system of natural and artificial waterways. So, we believe that the method used in this experiment explored the partial mechanism of aggregation of HSs colloid or NOM, and the obtained numerical value comparable with the AFM values of aggregates strength will be a key idea of aggregate strength evaluation in the

natural water system or wastewater treatment for pollutant transport, removal and distribution.

Chapter 6

Conclusion of the thesis and future research perspective

6. 1 Conclusion

In this thesis, we have evaluated the charging behavior of a model polystyrene sulfate latex particle (PSL) and adsorption energy of hydrophobic monovalent ion (tetraphenylphosphonium ion, TPP^+). The charging, aggregation, and aggregate strength of humic substances (HSs) particles have been studied. The charging properties of all the studied colloidal substances (PSLs, and HSs) was evaluated in the presence of hydrophobic counter ions, cationic surfactants, and inorganic divalent, and monovalent salts namely TPP^+, CPC (cetylpyridinium chloride), DPC (dodecylpyridinium chloride), Ca^{2+}, Mg^{2+}, K^+ as a function of salt concentration and solution pH. Though we evaluated the charging of three different HSs in the presence of TPP^+ and K^+. But the charging and aggregation along with the strength of HSs aggregates in the presence of CPC, DPC, Ca^{2+}, and Mg^{2+} were evaluated as a function of ionic concentration and solution pH.

This investigation clearly depicts the charge reversal of PSL particles and HSs in the presence of TPP^+ ion. This charge reversal in PSL particles indicates strong adsorption due to hydrophobic interaction because we did not observe any charge reversal in the presence of hydrophilic KCl solution. The charge reversal is caused by the strong adsorption of TPP ion, which has strong adsorption energy. The magnitude of adsorption energy decreases with the increase of surface charge density of PSL particles. That is, the lowest charge density is accompanied by the highest adsorption due to the higher hydrophobic interaction between TPP^+ and PSL particles. We found the maximum adsorption energy of 11 k_BT for the lowest electrokinetic charge density (-0.011 C/m^2) of PSL particles, and this was supported by the manufacturer supplied surface charge density gave adsorption energy of 10.5 k_BT. So, this

TPP induced charge reversal and energy of adsorption, which is comparable with the transfer energy from water to non-aqueous solvent for some organic cations, triggered us to use this TPP for testing different hydrophobic HSs. This method will lead us to explore the possible mechanism for this charging, adsorption, and binding of other organic ions to hydrophobic colloidal particles.

Accordingly, in the presence of hydrophobic monovalent counterion TPP^+, the HSs showed charge reversal, and again we did not observe any charge reversal for HSs in KCl solution. This charge reversal was higher for higher hydrophobic HSs, the LHA (Leonardite humic acid). In this case, we observed pronounced charge reversal for all the three HSs of different hydrophobicity at lower pH range, where HSs usually have lower charge amount. With the increase of hydrophobicity of HSs (LHA > SRHA > SRFA), the charge reversal pH or IEP (isoelectric point) shifted towards a higher pH value, indicating greater adsorption of most hydrophobic HS. This also indicates the charge reversal is affected and influenced by solution pH and hydrophobicity of colloidal particles. We confirmed the large visual aggregates of three HSs at lower pH range and the range of pH for the appearance of large visual aggregates increases with the increase of HSs hydrophobicity. Nevertheless, the pH range of aggregation also increases with the increase of HSs hydrophobicity. The aggregates structure analysis was done by measuring the fractal dimension of HSs aggregates in TPPCl solution. The fractal dimension of all three HSs aggregates was higher in slow stirring condition than quiescent condition at low pH around 3, the highest fractal dimension was around 2.9. The result indicates the compact structural arrangement of aggregates with restructuring and/or collision between small particles and cluster makes this higher fractal aggregates at the shear condition. The findings of this charge reversal, aggregation and high fractal dimension at lower pH range clearly manifest the effect of hydrophobic interaction.

Another finding of charging and aggregation and aggregate strength evaluation of the two HSs (SRFA and LHA) in the presence of CPC and DPC as a function of pH demonstrates the charge reversal and aggregation at a wide pH range arising pronounced aggregates around IEP pH. The more charge reversal is manifested by more hydrophobic HS (LHA) interacting with longer chain cationic surfactants, CPC. This means more adsorption and hydrophobic forces are triggered by the interaction of HSs hydrophobicity and the longer alkyl tail length. We also confirmed the numerical value of HSs aggregate strength using laminar converging flow. We found the highest aggregate strength around 27.6 nN for LHA-CPC complex, which is the most hydrophobic HS and longer tail surfactant complex. In this situation, this highest aggregate strength dominantly manifests the importance and effect of hydrophobic interaction for the aggregation. This highest aggregate strength is around the IEP pH for any HSs and surfactant interaction in this investigation. The hydrophobic interaction plays a role for making large aggregates and higher aggregate strength along with the minimum electrostatic repulsion around IEP. This means the combined influence of hydrophobic and electrostatic interaction plays a role in the formation of such a large strong aggregate.

In the final investigation, we explored the charging and aggregation, and aggregate strength of most hydrophobic HS, LHA, in the presence of Ca^{2+} and Mg^{2+} ion as a function of their ionic strength and solution pH. We found an aggregation of LHA without showing any reversal of charges in any pH condition and ionic strength. We confirmed the higher strength value for Ca-induced aggregates than that of Mg induced aggregates. Nevertheless, the LHA shows aggregates at lower $CaCl_2$ concentration than $MgCl_2$ concentration. The aggregation was triggered by higher pH range. HSs have higher charge amount at higher pH. The strongest aggregates expressed as aggregate strength around 5.8 nN were formed in the presence of Ca^{2+} ion at pH around 9. This result manifests the strong divalent bridging force

induced by electrostatic attraction and counterion binding. However, the lower strength value of Mg^{2+} induced LHA aggregates indicates that the stronger hydration shell of Mg ion reduced the binding and attraction of LHA to Mg^{2+}. This finding clearly demonstrates the ion-specific interaction of these natural colloidal particles and/or substances.

The sections as mentioned earlier of this conclusion establish the effective evaluation of interaction in case of some natural organic colloids like HSs and synthetic model PSL particles. We certainly explored the application of this interacting forces in the natural system, which will help to evaluate the aggregation and fundamental charging behavior of natural organic matter (NOM) along with their real aggregate strength in natural and/ or artificial soil and water system. This study will be able to explore the NOM aggregates partly, their interaction with common soil water ions and/ or pollutants, and the transport and distribution paths and the mechanism of the withstand capacity of the pollutants in soil and water bodies.

6.2 Future research perspective

6.2.1 Hydrophobic Non-DLVO force in the synthetic polystyrene particles system

The aggregation-dispersion of HSs has been extensively discussed in the previous chapters along with the mechanisms of the NOM aggregation in different ionic and solution conditions. We thoroughly discussed the charging behavior of model polystyrene sulfate latex particles and the effects of particle surface charge density on the charge reversal and intrinsic chemical free energy of adsorption. In the first chapter of the thesis outline, we discussed that a recent study experimentally found a higher amount of attractive forces than the van der Waals forces for the adsorption of monovalent organic ions to polystyrene sulfate atex (PSL) particles (Smith et al. 2018). This additional Non-DLVO forces could be originated from the charge fluctuation force or less likely from hydrophobic interactions (Smith et al. 2018). In their experiment, they used atomic force microscopy (AFM) for the

direct force measurement. Whereas, we observed the decrease of adsorption free energy with the increase of surface charge density in case of monovalent hydrophobic organic ions to PSL particles. This means that the hydrophobic particles with the lowest charge density (-0.011 C/m^2) showed the highest adsorption free energy (11 k_BT) of TPP^+ ion to PSL particles. But in this study, we could not perform the AFM force measurement to observe the additional force in the IEP of these three PSL particles. We hope that the experimental investigation of force profile or force-distance relationship curve using AFM for the hydrophobic colloidal particles of different charge density in the presence of different hydrophobic monovalent ion of different valence and aromatic content could be able to explore the origin of this force. Our findings support the previous findings of Smith et al. (2018) that the origin of this interaction force could be hydrophobic.

6.2.2 Hydrophobic interaction in the natural HSs colloidal systems

Afterward, we considered the TPP^+ interactions with humic substances (HSs). We used three kinds of HSs of different hydrophobicity and/ or aromaticity. All the HSs showed charge reversal and aggregation, though the larger ramified aggregates were observed above the IEP or charge reversal point. We describe that this low pH aggregation and charge reversal are due to the hydrophobic interaction accompanied by higher hydrophobicity of HSs at low pH (Terashima et al., 2004). Whereas, Avena and Koopal (1999) showed that the humic acid adsorption to polystyrene latex was increased at lower pH value. So, the low pH aggregation of these three HSs at charge reversal point could be mostly explained by hydrophobic interaction, where hydrogen bonding (Jovanovic et al. 2013) and some other attractive non-DLVO forces and interactions (Gudarzi et al., 2015; Smith et al., 2018) can exist. Many previous investigations demonstrated that the chemical heterogeneity and particle morphology, and surface roughness are important factors causing the discrepancies of DLVO interaction forces (Elimelech et al., 1995; Kihira and Matijevic, 1992; Walz, 1999;

Elimelech and O'Melia, 1990). HSs also have the uneven, heterogeneous surface structure. In this situation, we need to identify the surface morphology of three different HSs and the layer thickness after TPP^+ adsorption using AFM. Although the use of AFM to liquid media is difficult and need sophisticated handling, there are some investigations using AFM for the characterization of HSs morphology (Balnois et al., 1999), the adsorption and force-distance relation of HSs on iron and alumina (Sander et al., 2004), and the adsorption on carbonaceous surfaces (Liu at al., 2011). We could not measure the amount of TPP^+ sorbed on the HSs surfaces and how the surface morphology changes with the hydrophobicity of different HSs of different sources. We demonstrated that the Leonardite humic acid formed most larger aggregates through visual, microscopic, and DLS observations. The pH range of LHA aggregation was also wider than the other two HSs (SRHA and SRFA).

We, in the third chapter, describes the causes for this larger size aggregate formation of LHA is due to the higher aromaticity and hydrophobicity of LHA than that of SRHA and SRFA. A previous investigation claimed that the intermolecular associations due to condensed aromatic structure induce the low cloud point temperature accompanied with the macroscopic aggregation of lignite humic acids (Young and Wandruszka, 2001). Whereas, in the same investigation, they demonstrated the Latahco silt loam humic acid (LSLHA) was clouded at the lowest temperature and required the lowest cation concentration of Mg^{2+} for visible phase separation (Young and Wandruszka, 2001). They explained that this lowest clouding temperature was due to the water elimination from the hydrated parts of LSLHA, and this possesses to form a hydrophobic structure (Young and Wandruszka, 2001).

This thesis provides some deep insights on NOM aggregation, the mechanism of aggregation, the effects of hydrophobic interactions and solution pH along with the effects of HSs hydrophobicity in the artificial laboratory experimental condition, from where we can get idea and insights of this phenomenon in a natural environment. In chapters 3, 4, and

5, we discussed the aggregation, charging, and aggregate strength of natural organic matters in different solution and ionic conditions. Though we can partly unveil the insight of aggregation, charging and aggregate strength of different natural colloidal particle and/or molecules, there are some lacking for the applicability of this investigation in different natural environmental conditions. Because in natural environmental conditions, the temperature and ion concentration differ from place to place, and the aggregation and charging could be affected by the local ionic condition and complex ionic systems.

In this study, we did not consider the particle concentration and temperature factors for the evaluation of HSs aggregation. In some previous studies, it was clearly demonstrated that the aggregation of colloidal silica (Sun et al., 2019) and iron oxide particles (Baalousha, 2009) in the presence of HSs were affected by particle concentration. In another investigation, temperature-induced aggregation and clouding of HSs were reported (Shaffer and Wandruszka, 2015). In the earlier sections, we already discussed the cloud point temperatures of HSs, which vary from one HS to others depending on their hydrophobic structure of the HSs. But the actual behavior of particle charging, their aggregation and aggregate strength in the natural environmental condition is our concern to study further.

6.2.3 Comparative evaluation of aggregate strength and adhesive forces

We measured the adhesion force between HSs particles stick together to form an aggregate expressed as the aggregate strength. It is the first time we have extracted this kind of force in numerical value for the NOM aggregates in CPC, DPC, Ca^{2+}, and Mg^{2+} solutions at different pH along with the charging behavior of aggregates in the designed laboratory condition. Adhesion force of particles in liquid media is usually expressed as the summation of the van der Waals force, and electrostatic force. The adhesion of the particles with other surfaces or particles occurs when the electrostatic force is attractive, or the repulsive

electrostatic force is smaller than the van der Waals force. Though the theoretical values of these forces between particles of known size could be estimated from DLVO, the experimental values of the adhesion forces were 28.4 ± 9.4 nN and 4.2 ± 1 nN in $-CH_3/-CH_3$ (methyl-methyl) and $-COOH/-CH_3$ (carboxyl-methyl) tip-sample pairs in water (Warszyński et al., 2003). These adhesion force values were measured using chemical force microscopy (Warszyński et al., 2003). These values are comparable with our findings of 27.6 nN, the maximum aggregate strength we found in LHA-CPC system around IEP. This maximum aggregate strength around IEP indicates the domination of charge neutralization due to higher attractive electrostatic interactions over repulsions. We presumed that this attractive electrostatic force around IEP exists with other attractive non-DLVO forces already mentioned in many previous investigations (Smith et al., 2018; Gudarzi et al., 2015; Cao et al., 2018) of colloidal aggregation in the presence of hydrophobic cations and anions. These non-DLVO forces in this hydrophobic environment made the strength value of HSs aggregate to much higher than the natural soil particles aggregate strength and flocs strength of polystyrene particles measured by Kobayashi (2004 and 2005). In the case of polystyrene flocs, Kobayashi (2004) explained the inter-particle/inter-molecular forces. Whereas, the origin of forces in the maximum strength of the aggregate of natural soil particles is ascribed to attractive electric double layer interactions (Kobayashi, 2005). In this situation, we think that the AFM study for force-distance relations considering some other factors such as temperature, particle concentration, and different ionic conditions could be able to minimize the limitations of our findings for the evaluation of the origin of force, the type of non-DLVO interactions and its range of presence in our experimental conditions.

In addition, this strength value will provide the insight of particle aggregation in the flow field and the adhesive forces acting on this aggregation and aggregate strength. This investigation deliberately focused on the HSs hydrophobicity, solution pH, and specific ionic

condition, but the strength of aggregates or this adhesive force could be influenced by particles concentration, temperatures, salt concentration, ion types and so on.

6.2.4 Recent environmental problems and our colloidal approach to investigate the mechanisms of aggregation and transport of these pollutants in natural soil-water systems

Nowadays microplastic pollution and their transport in surface water and the natural environment are alarming issues of the highest considerations. Some recent investigations demonstrated the effect of NOM, different electrolyte solutions and seawater salinity, and pH on the aggregation and transport of microplastic particles in different environmental condition (Dong et al., 2019; Li et al., 2018; Cai et al., 2018). In the earlier chapters, we already discussed that the transport of NOM aggregates along with pollutants deepens on the size of the aggregate. Subsequently, this size of the aggregates as a transport unit depends on the strength of aggregates in the flow field. But from the recent literature, we have seen that no studies focused on the aggregate strength of microplastic particles in the presence of NOM along with their charging. We believe that the evaluation of charging behavior along with the size and aggregate strength of micro and nano-plastic particles in the presence of NOM as a function of pH and different ionic condition could be one of the possible ways to explore the mechanisms of micro and nano-plastic aggregation in natural environmental condition. And we also believe that the exploration of their aggregation and aggregate strength in the presence of NOM will be able to unveil the mechanisms of their transport and distribution in natural environmental condition.

At this point, the consideration of real complex soil-water environment focusing the transport through soil column is one of the concerns of our further research, where we will

be able to find other natural forces and factors affecting the aggregation and transport of aggregates in such a complex natural system.

Acknowledgments

First, I express innumerable praise to Almighty for enabling me to the successful completion and preparation of this thesis paper and research.

I express my sincere and deepest sense of gratitude, heartiest appreciation and high indebtedness to my honorable supervisor Dr. Motoyoshi Kobayashi, Associate Professor, Faculty of Life and Environmental Sciences, University of Tsukuba, for his sincere guidance, active supervision and positive criticism in planning and preparation of the research project and thesis. I am also grateful to him because of his time to time monitoring, discussion, lab meeting, and valuable suggestions. He, Dr. Kobayashi gave me encouragement in the field of this colloid science and helped a lot to think in-depth about the colloid, their application, and pathways of the development of my study in this field. He always encourages me at the time of the rejection of my research papers from some journals, and always support me to think further and to overcome my bad times during my study.

I would like to express my heartfelt thanks and appreciation to Professor Yasuhisa Adachi of our laboratory in Colloid in soil and Water Environment, University of Tsukuba for his valuable suggestions, advice, and thoughtful discussion during my stay in this laboratory and weekly laboratory seminars.

I would like to express my special thanks to Associate professor Kazuyoshi Ogawa for his suggestion and recommendation to improve my thesis.

I wish to express my special thanks to Assistant professor Yuji Yamashita for his suggestion and recommendation during the laboratory seminars and presentations.

Great deals appreciation goes to Mrs. Manami Nishiya and Mr. Tomoharu Suzuki for their assistance during the experiment and planning of research, therefore they are coworkers of my two research papers during Ph.D. I am grateful to Mr. Tri Hoa Phan from Department of Chemistry, University of Iowa for his great support for the experimental work during his stay in Japan as a short time exchange research student.

I would like to express my deepest gratitude and thanks to Dr. Takuya Sugimoto, JSPS post-doctoral fellow at The University of Tokyo, for his valuable suggestions and discussion throughout my study period. I am also grateful to Prof. M. Kobayashi (my supervisor) and Dr. Takuya Sugimoto (my tutor) for their warm reception at the Narita Airport after my first arrival in Japan.

I wish to express my thanks to Wan Khairunnisa. Hence she is working and continuing the study of my findings to explore something more inclusive on the research in our collaboration.

A special thank goes to Mrs. kiyono Omija, because she initiates the study of aggregation, stability, and charging characters of a relatively new applied carbonaceous material in collaboration with me.

I would like to express my sincere thankfulness to Mrs. Chihiro Takeshita for her suggestions and help for the discarding of waste chemicals and wastewater. I am grateful to her for encouragement in the last two years.

I express my sincere thanks also to Mr. Atsushi Yamaguchi, and Mr. Huang Yi for their special guidance for the chemicals use, especially the waste management. And sometimes the discussion with Mr. Atsushi Yamaguchi helped me a lot for further thinking about my research.

I would like to extend my sincerest thanks to my laboratory members Mr, Tomokazu Yanagibashi, Zhuang Yiran, Chihiro Shimabukuro, Mr. Gao Jiahui, Lim Voon Huey, Li Maolin. Thanks go to all my lab members for their technical questions, and comments during the laboratory presentations.

I also thank our helpful secretaries and technician, Ms. Ogawa, Ms, Yamada, and Mr. Sakurai, for their kind help to arrange the conferences, events and some special seminars.

I am very much grateful to the Japan government for their support by selecting me as a MEXT scholar, and University of Chittagong, Bangladesh for the four-year leave.

Special Thanks goes to the University of Tsukuba for support during this stay and study in Japan.

Heartfelt thanks, appreciation, and gratefulness must be given to my beloved daughter Mayameen Noor Aziz (Mayanoor Aziz) for her stay in Bangladesh in the last two years without me.

Finally, I would like to thank everyone else who provided me with advice, support, and assistance throughout my study.

July 2019

Azizul Hakim (The author)

List of the publications related to this thesis

1. Azizul Hakim, Manami Nishiya & Motoyoshi Kobayashi (2016). Charge reversal of sulfate latex induced by hydrophobic counterion: effects of surface charge density. *Colloid and Polymer Science* (2016) 294:1671–1678, DOI 10.1007/s00396-016-3931-6
2. Azizul Hakim & Motoyoshi Kobayashi (2018). Aggregation and charge reversal of humic substances in the presence of hydrophobic monovalent counter-ions: Effect of hydrophobicity of humic substances. Colloids and Surfaces A: Physicochemical and Engineering Aspects, Volume 540, 5 March 2018, Pages 1-10, https://doi.org/10.1016/j.colsurfa.2017.12.065
3. Azizul Hakim, Tomoharu Suzuki, & Motoyoshi Kobayashi (2019). Strength of humic acid aggregates: Effects of divalent cations and solution pH. ACS omega, 4, 5, 8559-8567, https://doi.org/10.1021/acsomega.9b00124
4. Azizul Hakim, & Motoyoshi Kobayashi (2019). Charging, aggregation, and aggregate strength of humic substances in the presence of cationic surfactants: Effects of humic substances hydrophobicity and surfactant tail length. Colloids and Surfaces A: Physicochemical and Engineering Aspects, Volume 577, Pages 175-185, https://doi.org/10.1016/j.colsurfa.2019.05.071

References

Abe, T., Kobayashi, S., Kobayashi, M. (2011). Aggregation of colloidal silica particles in the presence of fulvic acid, humic acid, or alginate: effects of ionic composition. *Colloids Surf. A: Physicochem. Eng. Aspects,* 379 (1) 21–26. https://doi.org/10.1016/j.colsurfa.2010.11.052

Adachi, Y. (1995). Dynamic aspects of coagulation and flocculation. *Advances in Colloid and Interface Science,* 56:1-31.

Adachi, Y., Feng, L., & Kobayashi, M. (2015). Kinetics of Flocculation of Polystyrene Latex Particles in the Mixing Flow Induced with High Charge Density Polycation near the Isoelectric Point. *Colloids and Surfaces A: Physicochemical and Engineering Aspects*, 471: 38-44. doi: 10.1016/j.colsurfa.2015.02.011

Adachi, Y., Kobayashi, A., Kobayashi. M. (2012). Structure of colloidal flocs in relation to the dynamic properties of unstable suspension. *Int. J. Polym. Sci.* Volume 2012, 574878, http://dx.doi.org/10.1155/2012/574878

Ahn, W.Y., Kalinichev, A. G., & Clark, M. M. (2008). Effects of background cations on the fouling of polyethersulfone membranes by natural organic matter: Experimental and molecular modeling study. Journal of Membrane Science, 309, 128–140. https://doi.org/10.1016/j.memsci.2007.10.023

Alvarez-Puebla, R. A. & Garrido, J. J. (2005). Effect of pH on the aggregation of a gray humic acid in colloidal and solid states. *Chemosphere*, 59(5), 659–667. https://doi.org/10.1016/j.chemosphere.2004.10.021

Amjad, H., & Khan, Z. A. (2016). Comparison of Fractal Dimensions of Clay and Humic Acid Flocs under Optimum Coagulation Conditions, *Int J Environ Sci Dev.* 7, 240–3. Doi:10.7763/IJESD.2016.V7.776.

Angelico, R., Ceglie, A., Ji-Zheng, H., Yu-Rong, L., Palumbo, G., & Colombo, C. (2014). Particle size, charge and colloidal stability of humic acids coprecipitated with Ferrihydrite. *Chemospere* 99 (2014) 239-247.

Attard, P., Antelmi, D., & Larson, I. (2000). Comparison of the zeta potential with the diffuse layer potential from charge titration. *Langmuir*, 16(4), 1542–1552. https://doi.org/10.1021/la990487t

Avena, M. J., Koopal, L.K. (1999). Kinetics of humic acid adsorption at solid-water interfaces. *Environ. Sci. Technol*. 33, 2739–2744. https://doi.org/10.1021/es981236u

Baalousha, M. (2009). Aggregation and disaggregation of iron oxide nanoparticles: Influence of particle concentration, pH and natural organic matter. *Sci. Total Environ*. 407, 2093–2101. https://doi.org/10.1016/j.scitotenv.2008.11.022

Baalousha, M., Kammer, F. V. D., Motelica-Heino, M., Hilal, H. S., & Le Coustumer, P. (2006). Size fractionation and characterization of natural colloids by flow-field flow fractionation coupled to multi-angle laser light scattering. *Journal of Chromatography A*, 1104(1–2), 272–281. https://doi.org/10.1016/j.chroma.2005.11.095

Bache, D. H.., Rasool, E., Moffat, D., & McGilligan, F. J. (1999). On the strength and character of alumino-humic flocs. *Water Sci. Technol.* 40, 81–88, https://doi.org/10.1016/S0273-1223(99)00643-5

Bafana, A., Devi, S.S., & Chakrabarti, T. (2011). Azo dyes: past, present and the future. *Environmental Reviews* (19): 350–370.

Balnois, E., Wilkinson, K.J., Lead, J.R., & Buffle, J. (1999). Atomic Force Microscopy of Humic Substances: Effects of pH and Ionic Strength. *Environ. Sci. Technol.,* 33, 21, 3911-3917. https://doi.org/10.1021/es990365n

Bandyopadhyay, D., & Mehler, E.L. (2008). Quantitative expression of protein heterogeneity: Response of amino acid side chains to their local environment. *Proteins Struct. Funct. Genet.* 72, 646–659. https://doi.org/10.1002/prot.21958

Benedetti, M.F., Milne, C.J., Kinniburgh, D.G., van Riemsdijk, W.H., & Koopal, L.K. (1995). Metal-ion binding to humic substances — application of the nonideal competitive adsorption model. *Environ. Sci. Technol*. 29, 446—457, http://doi.org/10.1021/es00002a022

Besteman, K., Zevenbergen, M., & Lemay, S. (2005). Charge Inversion by Multivalent Ions: Dependence on Dielectric Constant and Surface-Charge Density. *Phys. Rev. E* 72: 061501. doi: 10.1103/PhysRevE.72.061501

Bian, S.W., Mudunkotuwa, I. A., Rupasinghe, T., & Grassian, V. H. (2011). Aggregation and dissolution of 4 nm ZnO nanoparticles in aqueous Environments: Influence of pH, Ionic Strength, Size, and Adsorption of Humic Acid. *Langmuir,* 27 (10) 6059–6068. https://doi.org/10.1021/la200570n

Blaser, S. (2000a). Break-up of flocs in contraction and swirling flows. *Colloids and Surfaces A,* 166, 215–223, https://doi.org/10.1016/S0927-7757(99)00450-1

Blaser, S. (2000b). Flocs in shear and strain flows. *Journal of Colloid and Interface Science,* 225, 273–284, https://doi.org/10.1006/jcis.1999.6671

Blaser, S. (2002). Forces on the surfaces of small ellipsoidal particles immersed in a linear flow field, *Chemical Engineering Science,* 57(2002) 515–526, https://doi.org/10.1016/S0009-2509(01)00389-X

Boller, M. & Blaser, S. (1998). Particles under stress. *Water Science and Technology*, 37, 9–29.

Bolto, B., Abbt-Braun, G., Dixon, D., Eldridge, R., Frimmel, F., Hesse, S., King, S., & Toifl, M. (1999). Experimental Evaluation of Cationic Polyelectrolytes for Removing Natural Organic Matter from Water. *Water Sci. Technol.*, 40, 71–79, https://doi.org/10.2166/wst.1999.0445

Bonn, B. A. & Fish, W. (1993). Measurement of electrostatic and site-specific associations of alkali metal cations with humic acid. *J. Soil Sci*. 44, 335—345, https://doi.org/10.1111/j.1365-2389.1993.tb00456.x

Borkovec, M., Behrens, S.H., & Semmler, M. (2000). Observation of the Mobility Maximum Predicted by the Standard Electrokinetic Model for Highly Charged Amidine Latex Particles. *Langmuir* 16**,** 5209-5212.**doi:** 10.1021/la9916373

Bouyer, F., Robben, A., Yu, W. L., & Borkovec, M. (2001). Aggregation of colloidal particles in the presence of oppositely charged polyelectrolytes: effect of surface charge heterogeneities. *Langmuir*, 17, 5225–5231, https://doi.org/10.1021/la010548z.

Brigante, M., Zanini, G., & Avena, M. (2009). Effect of pH, anions and cations on the dissolution kinetics of humic acid particles. *Colloids and Surfaces A Physicochemical and Engineering Aspects,* 347, 180–186, https://doi.org/10.1016/j.colsurfa.2009.04.003

Bryan, N. D., Jones, M. N., Birkett, J., Livens, F. R. (2001). Aggregation of humic substances by metal ions measured by ultracentrifugation. *Anal. Chim. Acta,* 437, 291−308.

Bryan, N. D., Robinson, V. J., Livens, F. R., Hesketh, N., Jones, M. N., & Lead, J. R. (1997). Metal-humic interactions: A random structural modelling approach. *Geochimica et Cosmochimica Acta*, 61(4), 805–820. https://doi.org/10.1016/S0016-7037(96)00375-4

Bryan, N.D., Jones, D.M., Appleton, M., Livens, F.R., Jones, M.N., Warwick, P., King, S., & Hall, A. (2000). A physicochemical model of metal—humate interactions. *Phys*. *Chem*. *Chem*. *Phys*. 2, 1291—1300, https://doi.org/ 10.1039/A908722B

Cai, L., Hu, L., Shi, H., Ye, J., Zhang, Y., & Kim, H. (2018). Effects of inorganic ions and natural organic matter on the aggregation of nanoplastics. *Chemosphere* 197, 142–151. https://doi.org/10.1016/j.chemosphere.2018.01.052

Calero, C., & Faraudo, J. (2011). Interaction of monovalent ions with hydrophobic and hydrophilic colloids: Charge inversion and ionic specificity, *Journal of the American Chemical Society,* 133:38 15025–15035. Doi:https://doi.org/10.1021/ja204305b

Cao, T., Trefalt, G., Borkovec, M. (2018). Aggregation of Colloidal Particles in the Presence of Hydrophobic Anions: Importance of Attractive Non-DLVO Forces. Langmuir 34, 14368–14377. https://doi.org/10.1021/acs.langmuir.8b03191

Cases, J. M., & Villieras, F. (2005). Thermodynamic model of ionic and nonionic surfactants adsorption-abstraction on heterogeneous surfaces. *Langmuir*, 8, 1251–1264, https://doi.org/10.1021/la00041a005.

Chaaban, A. A., Lartiges, B., Kazpard, V., Plisson-Chastang, C., Michot, L., Bihannic, I., Caillet, C., & Prelot, B. (2016). Probing the organization of fulvic acid using a cationic surfactant. *Colloids Surf. A Physicochem. Eng. Asp*., 504, 252–259, https://doi. org/10.1016/j.colsurfa.2016.05.032.

Chassagne, C., & Ibanez, M. (2013). Electrophoretic mobility of Latex Nanospheres in Electrolytes: Experimental Challenges. *Pure Appl. Chem.* 85(1): 41–51. doi: 10.1351/PAC-CON-12-02-12

Chen, G., Liu, X., & Su, C. (2012). Distinct effects of humic acid on transport and retention of TiO_2 rutile nanoparticles in saturated sand columns. *Environmental Science & Technology*, 46(13), 7142–7150, https://doi.org/10.1021/es204010g

Chilom, G. & Rice, J. A. (2009). Structural organization of humic acid in the solid state, *Langmuir* 25:16, 9012–5. Doi:10.1021/la900750z.

Conte, P., & Piccolo, A. (1999). Conformational arrangement of dissolved humic substances. Influence of solution composition on association of humic molecules, *Environ. Sci. Technol.* 33, 1682–1690.

D'Orazio, V., & N. Senesi. (2009). Spectroscopic properties of humic acids isolated from the rizosphere and bulk soil compartments and fractionated by size exclusion chromatography, Soil Biol. Biochem. 41, 1775–1781.

Deb, S. K. & Shukla, M. K. (2011). A Review of Dissolved Organic Matter Transport Processes Affecting Soil and Environmental Quality. *J Environment Analytic Toxicol,* 1:106. https://doi.org/10.4172/2161-0525.1000106

Dempsey, B. A., Ganho, R. M., & O'Melia, C. R. (1984). The coagulation of humic substances by means of aluminum salts. *J. Am. Water Work. Assoc,* 76,141–150, https://doi.org/10.1002/j.1551-8833.1984.tb05315.x

Derjaguin, B. & Landau, L.D. (1941) Theory of the Stability of Strongly Charged Lyophobic Sols and of the Adhesion of Strongly Charged Particles in Solutions of

Electrolytes. *Acta Physicochimica* U.R.S.S., 14, 633-662. Also available *In:* Prog. Surf. Sci., 43 (1–4) (1993), pp. 30-59. https://doi.org/10.1016/0079-6816(93)90013-L

Domingos, R. F., Tufenkji, N., & Wilkinson, K. J. (2009). Aggregation of titanium dioxide nanoparticles: Role of Fulvic Acid. *Environ. Sci. Technol.* 43: 5

Dong, Z., Zhang, W., Qiu, Y., Yang, Z., Wang, J., & Zhang, Y. (2019). Cotransport of nanoplastics (NPs) with fullerene (C 60) in saturated sand: Effect of NPs/C 60 ratio and seawater salinity. *Water Res.* 148, 469–478. https://doi.org/10.1016/j.watres.2018.10.071

Duan, J., Wang, J., Graham, N., & Wilson, F. (2002). Coagulation of humic acid by aluminium sulphate in saline water conditions. *Desalination* 150: 1, 1–14, Doi: https://doi.org/10.1016/S0011-9164(02)00925-6

Duval, J. F. L., Wilkinson, K. I., Van Leeuwen, H. P., & Buffle, J. (2005). Humic substances are soft and permeable: Evidence from their electrophoretic mobilities. *Environ. Sci. Technol.* 39, 6435–6445, https://doi.org/10.1021/es050082x

Elimelech, M. & O'Melia, C.R. (1990). Effect of Particle Size on Collision Efficiency in the Deposition of Brownian Particles with Electrostatic Energy Barriers. *Langmuir*, 6, 1153–1163. https://doi.org/10.1021/la00096a023

Elimelech, M., Gregory, J., Jia, X., & Williams, R.A. (1995). Particle Deposition and Aggregation. Measurement, Modelling, and Simulation, *Butterworth-Heinemann*, Butterworth: Oxford

Fitch, A., Stevenson, F.J., Chen, Y. (1986). Complexation of Cu (II) with a soil humic acid: response characteristics of the Cu (II) ion-selective electrode and ligand concentration effects. *Org. Geochem*. 9, 109—116, https://doi.org/10.1016/0146-6380(86)90100-2

Gaffney J. S., Nancy A. M., & Sue. B. C. (1996). Humic and Fulvic Acids and Organic Colloidal Materials in the Environment. American chemical society. *ACS symposium series,* vol. 651, pp 2-16, https://doi.org/10.1021/bk-1996-0651.ch001

Galán, J. J., González-Pérez, A., Del Castillo, J. L., Rodríguez, J. R. (2002). Thermal parameters associated to micellization of dodecylpyridinium bromide and chloride in aqueous solution. *J. Therm. Anal. Calorim.* 70, 229–234, https://doi.org/10.1023/A:1020678222376.

Ghosh, K., & Schnitzer, M. (1980). Macromolecular structures of humic substances, *Soil Sci.* 129: 5, 266–276.

Godec, A., & Kogej, K. (2007). Binding of cetyl- and dodecylpyridinium cations by poly (L - glutamic acid). *Acta Chim. Slov.*, 54, 517–522

Gregory, J. (1998). The role of floc density in solid-liquid separation. *Filtration & separation*, 35 (4), 367-371.

Gudarzi, M. M., Trefalt, G., Szilagyi, I., Maroni, P., Borkovec, M. (2015). Forces between Negatively Charged Interfaces in the Presence of Cationic Multivalent Oligoamines Measured with the Atomic Force Microscope. *J. Phys. Chem. C* 119, 15482–15490. https://doi.org/10.1021/acs.jpcc.5b04426

Hakim, A. & Kobayashi, M. (2018). Aggregation and charge reversal of humic substances in the presence of hydrophobic monovalent counter-ions: Effect of hydrophobicity of humic substances. *Colloids Surfaces A Physicochem. Eng. Asp.*, 540, 1–10, https://doi.org/10.1016/j.colsurfa.2017.12.065

Hakim, A., & Kobayashi, M. (2019). Charging, aggregation, and aggregate strength of humic substances in the presence of cationic surfactants: Effects of humic substances

hydrophobicity and surfactant tail length. Colloids and Surfaces A: Physicochemical and Engineering Aspects. https://doi.org/10.1016/j.colsurfa.2019.05.071

Hakim, A., Nishiya, M., & Kobayashi, M. (2016). Charge reversal of sulfate latex induced by hydrophobic counterion: effects of surface charge density. *Colloid and Polymer Science.* 294:10, 1671–1678. Doi: https://doi.org/10.1007/s00396-016-3931-6

Hakim, A., Suzuki, T., & Kobayashi, M. (2019). Strength of Humic Acid Aggregates: Effects of Divalent Cations and Solution pH. *ACS Omega* 4, 8559–8567. https://doi.org/10.1021/acsomega.9b00124

Heckmann, K., Schwarz, R., Strnad. J. (1987). Determination of Krafft point and CMC of hexadecylpyridinium salts in electrolyte solutions, *J. Colloid Interface Sci.*, 120, 114–117, https://doi.org/10.1016/0021-9797(87)90329-8.

Helfricht, N., Doblhofer, E, Bieber, V., Lommes, P., Sieber, V., Scheibel, T., & Papastavrou, G. (2017). Probing the adhesion properties of alginate hydrogels: a new approach towards the preparation of soft colloidal probes for direct force measurements, *Soft Matter* 13: 578–589, https://doi.org/10.1039/c6sm02326f

Higashitani, K., Inada, N., & Ochi, T. (1991). Floc breakup along centerline of contractile flow to orifice. *Colloids and Surfaces*, 56,13–23, https://doi.org/10.1016/0166-6622(91)80111-Z

Higgo, J.J.W., Kinniburgh, D., Smith, B., & Tipping, E. (1993). Complexation of Co^{2+}, Ni^{2+}, UO^{2+} and Ca^{2+} by humic substances in groundwaters. *Radiochim. Acta*, 61, 91—103, https://doi.org/10.1524/ract.1993.61.2.91

Hoekstra, L. L., Vreeker, R., & Agterof, W. G. M. T. (1992). Aggregation of nickel hydroxycarbonate studied by light scattering, *J Colloid Interface Sci.* 151 17-25.

Hussain, S., van Leeuwen, J., Chow, C., Beecham, S., Kamruzzaman, M., Wang, D., Drikas, M., & Aryal, R. (2013). Removal of organic contaminants from river and reservoir waters by three different aluminum-based metal salts: Coagulation adsorption and kinetics studies. *Chem. Eng. J.*, 225, 394–405, https://doi.org/10.1016/j.cej.2013.03.119

Hyung, H., & Kim, J. H. (2008). Natural organic matter (NOM) adsorption to multi-walled carbon nanotubes: Effect of NOM characteristics and water quality parameters, *Environ Sci. Technol.*, 42 4416–21, Doi:10.1021/es702916h.

Ibrahim, K., Salminen, A., Holappa, S., Kataja, K., Lampinen, H., Lofgren, B., Laine, J., and & Seppala, J. (2006). Preparation and Characterization of Polystyrene–Poly(ethylene oxide) Amphiphilic Block Copolymers via Atom Transfer Radical Polymerization: Potential Application as Paper Coating Materials. *Appl. Polym. Sci.*, 102: 4304 -4313

Illés, E., & Tombácz, E. (2006). The effect of humic acid adsorption on pH-dependent surface charging and aggregation of magnetite nanoparticles. *J. Colloid Interface Sci.*, 295, 115–123. https://doi.org/10.1016/j.jcis.2005.08.003

Ishiguro, M., Tan, W., & Koopal, L. (2007). Binding of cationic surfactants to humic substances. *Colloids and Surfaces A: Physicochemical and Engineering Aspects* 306, 29–39. Doi: https://doi.org/10.1016/j.colsurfa.2006.12.024

Israelachvili, J., & Pashley, R. (1982). The Hydrophobic Interaction Is Long-Range, Decaying Exponentially with Distance. *Nature*, 300, 341−342.

Ivanković, T., & Hrenović, J. (2010). Surfactants in the environment. *Arh. Hig. Rada Toksikol.* 61, 95–110. https://doi.org/10.2478/10004-1254-61-2010-1943

Jarvis, P., Jefferson, B., & Parsons, S. A. (2005). Breakage, Regrowth, and Fractal Nature of Natural Organic Matter Flocs, *Environ. Sci. Technol.* 39, 2307-2314

Jiménez, M. L., Delgado, A.V., & Lyklema, J. (2012). Hydrolysis versus ion correlation models in electrokinetic charge inversion: establishing application ranges. *Langmuir,* 28, 6786–6793, Doi:10.1021/la3010773

Jones, M. N., & Bryan, N. D. (1998). Colloidal properties of humic substances. *Advances in Colloid and Interface Science,*78(1), 1–48, https://doi.org/10.1016/S0001-8686(98)00058-X

Jovanović, U. D., Marković, M. M., Cupać, S. B., & Tomić, Z. P.(2013). Soil humic acid aggregation by dynamic light scattering and laser Doppler electrophoresis. *Journal of Plant Nutrition and Soil Science,* 176: 5 ,674–679, https://doi.org/10.1002/jpln.201200346

Kalinichev, A. G., Iskrenova-Tchoukova, E., Ahn, W. Y., Clark, M. M., & Kirkpatrick, R. J. (2011). Effects of Ca^{2+} on supramolecular aggregation of natural organic matter in aqueous solutions: A comparison of molecular modeling approaches. *Geoderma,* 169, 27–32, https://doi.org/10.1016/j.geoderma.2010.09.002

Kalinichev, A.G., & Krikpatrick, R. J. (2007). Molecular dynamics simulation of cationic complexation with natural organic matter. *European Journal of Soil Science,* 58 (4) 909–917, https://doi.org/10.1111/j.1365-2389.2007.00929.x

Kihira, H., & Matijević, E. (1992). An assessment of heterocoagulation theories. *Adv. Colloid Interface Sci*., 42, 1–31. https://doi.org/10.1016/0001-8686(92)80017-R

Kinniburgh, D. G., Riemsdijk, W. H. Van., Koopal, L. K., Borkovec, M., Benedetti, & M. F., Avena, M. J. (1999). Ion binding to natural organic matter- competition,

heterogeneity, stoichiometry and thermodynamic consistency. *Colloids and Surfaces A: Physicochemical and Engineering Aspects*, 151, 147–166. https://doi.org/10.1016/S0927-7757(98)00637-2

Kjellander, R., Marcelja, S., Pashley, R. M., & Quirk, J. P. (1990). A theoretical and experimental study of forces between charged mica surfaces in aqueous $CaCl_2$ solutions. *Journal of Chemical Physics*, 92, 4399–4407.

Kloster, N., Brigante, M., Zanini, G., & Avena, M. (2013). Aggregation kinetics of humic acids in the presence of calcium ions. *Colloids Surfaces A Physicochem. Eng. Asp.* 427, 76–82, https://doi.org/10.1016/j.colsurfa.2013.03.030

Kobayashi, M. (2004). Breakup and strength of polystyrene latex flocs subjected to a converging flow. *Colloids Surfaces A Physicochem. Eng. Asp.*, 235, 73–78, https://doi.org/10.1016/j.colsurfa.2004.01.008

Kobayashi, M. (2005). Strength of natural soil flocs. *Water Research*, 39 (14), 3273–3278, https://doi.org/10.1016/j.watres.2005.05.037

Kobayashi, M. (2008). Electrophoretic Mobility of Latex Spheres in the Presence of Divalent Ions: Experiments and Modelling. *Colloid and Polymer Science* 286: 935-940. doi: 10.1007/s00396-008-1851-9

Kobayashi, M., Adachi, Y., & Ooi, S. (1999). Breakup of fractal flocs in a turbulent flow. *Langmuir*, 15, 4351–4356.

Kobayashi, M., Adachi, Y., & Ooi, S. (2000). On the Steady Shear Viscosity of Coagulated Suspensions, *Nihon Reoroji Gakkaishi* 28, 143–144, Doi:10.1678/rheology.28.143.

Kobayashi, M., Maekita, T., Adachi, Y., & Sasaki, H. (2004). Colloid stability and cogualtion rate of polystyrene latex particles in a turbulent flow. *International Journal of Mineral Processing,* 73(2-4):177-188.

Kobayashi, M., Nitanai, M., Satta, N., & Adachi, Y. (2013). Coagulation and Charging of Latex Particles in the Presence of Imogolite. *Colloids and Surfaces A: Physicochem. Eng. Aspects* 435: 139– 146. doi: 10.1016/j.colsurfa.2012.12.057

Kobayashi, M., Ooi, S., & Adachi, Y. (2002). On the Yield Stress of Sheared Coagulated Suspensions, *Proc Hydraul Eng* 46, 637–40, Doi:10.2208/prohe.46.637.

Kobayashi, M., Skarba, M., Galletto, P., Cakara, D., & Borkovec, M. (2005). Effects of Heat Treatment on the Aggregation and Charging of Stöber-type Silica. *J. Colloid Interf. Sci*. 292, 139-147.doi: 10.1016/j.jcis.2005.05.093

Koopal, L. K., Goloub, T. P., & Davis, T. A. (2004). Binding of ionic surfactants to purified humic acid. *J. Colloid Interface Sci.,* 275, 360–367, https://doi.org/10.1016/j.jcis.2004.02.061

Kwaambwa, H. M., Hellsing, M. S., Wasbrough, M. J, & Bleuel, M. (2017). Salt induced polystyrene latex flocs investigated by neutron scattering. *Journal of Colloid and Interface Science,* 505, 9-13.

Leneveu, D. M., Rand, R. P., Parsegian, V. A., & Gingell, D. (1977). Measurement and Modification of Forces between Lecithin Bilayers. *Biophys. J.* 18, 209−230.

Li, J., Zhang, K., & Zhang, H. (2018). Adsorption of antibiotics on microplastics. *Environ. Pollut.* 237, 460–467. https://doi.org/10.1016/j.envpol.2018.02.050

Li, T., Zhu, Z., Wang, D., Yao, C.., & Tang, H. (2006). Characterization of floc size, strength and structure under various coagulation mechanisms. *Powder Technol.*, 168, 104–110, https://doi.org/10.1016/j.powtec.2006.07.003

Liu, Z., Zu, Y., Meng, R., Xing, Z., Tan, S., Zhao, L., Sun, T., & Zhou, Z. (2011). Adsorption of Humic Acid onto Carbonaceous Surfaces: Atomic Force Microscopy Study. *Microsc. Microanal*., 17, 1015–1021. https://doi.org/10.1017/s1431927611012177

Luo, W., & Gu, B. (2009). Dissolution and mobilization of uranium in a reduced sediment by natural humic substances under anaerobic conditions. *Environ. Sci. Technol.* 2009, 43:152-156. https://doi.org/10.1021/es8013979

Lyklema, J. (2006) Overcharging, Charge Reversal: Chemistry or Physics? *Colloids Surf. A* 291: 3-12.doi:10.1016/j.colsurfa.2006.06.043

MacCarthy, P. (2001). The principles of humic substances. *Soil Sci.* 166, 738–751.

Majzik, A. & Tombácz, E. (2007). Interaction between humic acid and montmorillonite in the presence of calcium ions II. Colloidal interactions: Charge state, dispersing and/or aggregation of particles in suspension. *Organic Geochemistry*, 38(8), 1330–1340. https://doi.org/10.1016/j.orggeochem.2007.04.002

Manciu, M., & Ruckenstein, E. (2001). Role of the hydration force in the stability of colloids at high ionic strengths. *Langmuir*, 17: 22, 7061–7070. Doi: https://doi.org/10.1021/la010741t

Martín-Molina, A., Calero, C., Faraudo, J., Quesada-Pérez, M., Travesset, A., & Hidalgo-Álvarez, R. (2009). The hydrophobic effect as a driving force for charge inversion in colloids. *Soft Matter*, 5: 7 , 1350, Doi: https://doi.org/10.1039/b820489f

Maryganova, V., Szajdak, L.W., & Tychinskaya, L. (2010). Hydrophobic and hydrophilic properties of humic acids from soils under shelterbelts of different ages. *Chem. Ecol*. 26, 25–33. https://doi.org/10.1080/02757540.2010.501138

Matilainen, A., Vepsäläinen, M., & Sillanpää, M. (2010). Natural organic matter removal by coagulation during drinking water treatment: A review. *Adv. Colloid Interface Sci.*, 159,189–197, https://doi.org/10.1016/j.cis.2010.06.007

Matsuda, M., Kaminaga, A., Hayakawa, K., Takisawa, N., & Miyajima, T. (2009). Surfactant binding by humic acids in the presence of divalent metal salts. *Colloids Surfaces A Physicochem. Eng. Asp*., 347, 45–49. https://doi.org/10.1016/j.colsurfa.2008.11.037

Maurice, P. A., & Namjesnik-Dejanovic, K. (1999). Aggregates structures of sorbed humic substances observed in aqueous solution, *Envron. Sci. Technol.* 33

Mccarthy, J. F. & Zachara, J. M. (1989). Subsurface transport of contaminants. *Environ. Sci. Technol.*, *23* (5), pp 496–502, https://doi.org/10.1021/es00063a602

Mei, Y., Bai, Y., & Wang, L., (2016). Effect of pH on binding of pyrene to hydrophobic fractions of dissolved organic matter (DOM) isolated from lake water. *Acta Geochim*. 35, 288–293. https://doi.org/10.1007/s11631-016-0094-6

Miklavic, S. J., Chan, D. Y. C., White, L. R., & Healy, T. W. (1994). Double-Layer Forces between Heterogeneous Charged Surfaces. *J. Phys. Chem.* 98, 9022−9032.

Milne, C. J., Kinniburgh, D. G., Van Riemsdijk, W. H., & Tipping, E. (2003). Generic NICA - Donnan model parameters for metal-ion binding by humic substances. *Environmental Science and Technology,* 37(5), 958–971. https://doi.org/10.1021/es0258879

Molina, F. V. (2014). Soil Colloids: properties and Ion binding, *CRC press, Taylor & Francis Group*

Molina-Bolívar, J. A., & Ortega-Vinuesa, J. L. (1999). How proteins stabilize colloidal particles by means of hydration forces, *Langmuir*, 15: 8, 2644–2653, https://doi.org/10.1021/la981445s

Moriguchi, S. (1987). Mathematical Formulas (Sugaku Koshikishu); Iwanami Shoten: Tokyo (in Japanese)

Myneni, S. C. B., Brown, J. T., Martinez, G. A., & Meyer-Ilse, W. (1999). Imaging of Humic Substance Macromolecular Structures in Water and Soils. *Science*, 286 (November), 1335–1338, http://doi.org/10.1126/science.286.5443.1335

Nagao, S., Matsunaga, T., Suzuki, Y., Ueno, T., & Amano, H. (2003). Characteristics of humic substances in the Kuji River waters as determined by high-performance size exclusion chromatography with fluorescence detection. *Water Research*, 37, 4159–4170, https://doi.org/10.1016/S0043-1354(03)00377-4

Nap, R. J., & Szleifer, I. (2018). Effect of calcium ions on the interactions between surfaces end-grafted with weak polyelectrolytes. *J. Chem. Phys.* 149, 163309, https://doi.org/10.1063/1.5029377

Nishiya, M., Sugimoto, T., & Kobayashi, M. (2016). Electrophoretic Mobility of Carboxyl Latex Particles in the Mixed Solution of 1: 1 and 2: 1 Electrolytes or 1: 1 and 3: 1 Electrolytes: Experiments and Modelling. *Colloids and Surfaces A: Physicochemical and Engineering Aspects*. doi:10.1016/j.colsurfa.2016.05.045

Noy, A., Vezenov, D. V., & Lieber, C. M. (1997). Chemical force microscopy. *Annual Review of Materials Sciences* 27: 381–421, https://doi.org/10.1146/annurev.matsci.27.1.381

Nozaki, Y, & Tanford, C. (1971). The Solubility of Amino Acids and Two Glycine Peptides in Aqueous Ethanol and Dioxane Solutions. *The Journal of Biological Chemistry*, 246(8), 221-2217.

O'Brien, R.W., & Hunter R.J .(1981). The Electrophoretic Mobility of Large Colloidal Particles. *Can J Chem* 59: 1878-1887. doi: 10.1139/v81-280

Ohshima, H. (2005). Approximate Expression for the Electrophoretic Mobility of a Spherical Colloidal Particle in a Solution of General Electrolytes. *Colloids Surfaces A* 267: 50-55. doi:10.1016/j.colsurfa.2005.06.036

Ohshima, H. (2006). Theory of Colloid and Interfacial Electronic Phenomena, 1st ed. *Academic Press London*

Ohshima, H., Healy, T.W., White, L.R. (1983). Approximation Analytic Expressions for the Electrophoretic Mobility of Spherical Colloidal Particles and the Conductivity of their Dilute Suspensions. J. *Chem. Soc. Faraday Trans*.2 79:1613-1628. doi: 10.1039/F29837901613

Olubukola, S., Alimi, Jeffrey Farner Budarz, Laura M. Hernandez, & Nathalie Tufenkji. (2018). Microplastics and Nanoplastics in Aquatic Environments: Aggregation, Deposition, and Enhanced Contaminant Transport. *Environ. Sci. Technol*. 52, 1704−1724

Oncsik, T., Desert, A., Trefalt, G., Borkovec, M., & Szilagyi, I. (2016). Charging and aggregation of latex particles in aqueous solutions of ionic liquids : towards an

extended Hofmeister series. *Phys. Chem. Chem. Phys.*, 18, 7511–7520. https://doi.org/10.1039/C5CP07238G

Overbeek, JThG. (1943). Theorie der Elektrophorese. Kolloid-Beihefte 54: 287. doi: 10.1007/BF02556774

Pal, S. & Sengupta, M. B. (1985). Nature and properties of humic acid prepared from different sources and its effect on nutrient availability. *Plant and Soil*, 88 (1) pp. 71-91. https://www.jstor.org/stable/42934867

Palmer, N. E. & Wandruszka, R. Von. (2001). Dynamic light scattering measurements of particle size development in aqueous humic materials. *Fresenius' Journal of Analytical Chemistry*, 371, 951–954, https://doi.org/10.1007/s002160101037

Parsons, D. F., & Ninham, B. W. (2010). Charge reversal of surfaces in divalent electrolytes: The role of ionic dispersion interactions, *Langmuir* 26: 9, 6430–6436, Doi: https://doi.org/10.1021/la9041265

Perez-Fuentes, L., Drummond C, Faraudo J, & Bastos-Gonzalez D. (2015). Anions Make the Difference: Insights from the Interaction of Big Cations and Anions with Poly(*N*-isopropylacrylamide) Chains and Microgels. *Soft Matter* 11: 5077-5086, doi**:** 10.1039/C5SM00750J

Pham, T.D., Kobayashi, M., Adachi, Y. (2015). Adsorption of Anionic Surfactant Sodium dodecyl sulfate onto Alpha Alumina with Small Surface Area. *Colloid Polymer Science* 293:217–227. doi: 10.1007/s00396-014-3409-3

Piccolo, A. (2001). The Supramolecular Structure of Humic Substances. *Soil Sci.* 166 :11, 810–832. Doi: https://doi.org/10.1097/00010694-200111000-00007

Ren, M., Horn, H., & Frimmel, F. H. (2017). Aggregation behavior of TiO_2 nanoparticles in municipal effluents: influence of ionic strengthen and organic compounds. *Water Research,* 123 678-686. Doi: http://dx.doi.org/10.1016/j.watres.2017.07.021

Rong, H., Gao, B., Dong, M., Zhao, Y., Sun, S., Wang, Y., Yue, Q., & Li, Q. (2013). Characterization of size, strength and structure of aluminum-polymer dual-coagulant flocs under different pH and hydraulic conditions. *J. Hazard. Mater.* 252–253, 330–337, https://doi.org/10.1016/j.jhazmat.2013.03.011

Russel WB, Saville DA, Schowalter WR (1989) Colloidal dispersions. Cambridge University Press, New York

Ryde, N., & Matijevic, E. (1994). Kinetics of heterocoagulation. Part 4. Evaluation of absolute coagulation rate constant using a classical light scattering technique, *Journal of Chemical Society Faraday Transactions,* 90, 167–171, https://doi.org/ 10.1039/FT9949000167

Rytwo, G., Kohavi, Y., Botnick, I., Gonen, Y. (2007). Use of CV- and TPP-montmorillonite for the removal of priority pollutants from water. *Applied Clay Science,* 36,182–190

Saar, R.A., & Weber, J.H. (1979). Complexation of cadmium (II) with water- and soil-derived fulvic acids: effect of pH and fulvic acid concentration. *Can. J. Chem.*, 57, 1263—1268. https://doi.org/10.1139/v79-206

Saito, T., Koopal, L. K., Nagasaki, S., & Tanaka, S. (2005). Analysis of copper binding in the ternary system Cu^{2+} humic acid/goethite at neutral to acidic pH. *Environ. Sci. Technol.* 39, 4886–4893, https://doi.org/10.1021/es0500308

Sander, S., Mosley, L. M., & Hunter, K. A. (2004). Investigation of interparticle forces in natural waters: Effects of adsorbed humic acids on iron oxide and alumina surface properties. *Environ. Sci. Technol*., 38, 4791–4796. https://doi.org/10.1021/es049602z

Schmitt, P., Kettrup, A., Freitag, D., Garrison, A. W. (1996). Flocculation of humic substances with metal ions as followed by capillary zone electrophoresis. *Fresenius. J. Anal. Chem.* 354, 915−920.

Senesi, N., & Loffredo, E. (1999). The chemistry of soil organic matter, In: *Spark, D.L., Ed., Soil Physical Chemistry, CRC Press*, Boca Raton, 239-370.

Shaffer, L., & Wandruszka, R. Von. (2015). Temperature Induced Aggregation and Clouding in Humic Acid Solutions, *Advances in Environmental Chemistry.* http://dx.doi.org/10.1155/2015/543614

Shang, C., & Rice, J. A. (2007). Investigation of humate-cetyltrimethylammonium complexes by small-angle X-ray scattering. J. *Colloid Interface Sci*., 305, 57–61. https://doi.org/10.1016/j.jcis.2006.09.043

Sharpless, C. M., & McGown, L. B. (1999). Effects of aluminum-induced aggregation on the fluorescence of humic substances. *Environ. Sci. Technol.* 33, 3264−3270.

Shen, J., Gagliardi, S., McCoustra, M. R. S., & Arrighi, V. (2016). Effect of humic substances aggregation on the determination of fluoride in water using an ion selective electrode. *Chemosphere*, 159, 66-71

Shimizu, T., & Kwak, J.C.T. (1994). The binding of cationic surfactants by hydrophobic alternating copolymers of maleic acid-charge density dependence, *Colloids Surfaces A Physicochem*, 82, 163–171, https://doi.org/10.1016/09277757(93)02642-R.

Shimizu, T., Seki, M., Kwak, J.C.T. (1986). The binding of cationic surfactants by hydrophobic alternating copolymers of maleic acid. *Colloids Surf.* 20, 289–301, https://doi.org/10.1016/0166-6622(86)80279-7.

Sillanpää, M., Ncibi, M. C., Matilainen, A., & Vepsäläinen, M. (2018). Removal of natural organic matter in drinking water treatment by coagulation: A comprehensive review. *Chemosphere,* 190, 54–71, https://doi.org/10.1016/j.chemosphere.2017.09.113

Sinniah, S. K., Steel, A. B., Miller, C J., & Reutt-Robey, J. E. (1996). Solvent exclusion and chemical contrast in scanning force microscopy. *J. Am. Chem. Soc.*, 118, 8925–8931, https://doi.org/10.1021/ja961295c

Sipos, P., May, P. M., & Hefter, G. T. (2000). Carbonate removal from concentrated hydroxide solutions. *Analyst,* 125: 5, 955–958

Smith, A. M., Maroni, P., & Borkovec, M. (2018). Attractive non-DLVO forces induced by adsorption of monovalent organic ions. *Phys. Chem. Chem. Phys*., 20, 158–164. https://doi.org/10.1039/c7cp06383k

Sobeck, D. C., & Higgins, M. J. (2002). Examination of three theories for mechanisms of cation-induces bioflocculation. *Water Research,* 36, 527–538.

Somasundaran, P., Healy, T.W., & Fuerstenau, D.W. (1964). Surfactant Adsorption at the Solid-Liquid Interface—Dependence of Mechanism on Chain Length. The Journal of Physical Chemistry 68(12): 3562-6.

Song, J., Jin, P., Jin, X., & Wang, X. C. (2019). Synergistic effects of various in situ hydrolyzed aluminum species for the removal of humic acid. *Water Research,* 148, 106–114, https://doi.org/10.1016/j.watres.2018.10.039

Sonntag, R. C., & Russel, W. B. (1987). Structure and breakup of flocs subjected to fluid stresses: III. Converging flow. *Journal of Colloid and Interface Science*, 115, 390–395, https://doi.org/10.1016/0021-9797(87)90054-3

Sposito, G. (1984). The Surface Chemistry of Soils, *Oxford University Press*, New York, 1984.

Stevenson, F.J. (1982). Humus Chemistry: Genesis, Composition, Reactions. *John Wiley & Sons*, New York.

Sugimoto, T., Kobayash M, & Adachi Y. (2014). The Effect of Double Layer Repulsion on the Rate of Turbulent and Brownian Aggregation: Experimental Consideration. Colloids and Surfaces A: Physicochem. Eng. Aspects 443: 418-424. doi:10.1016/j.colsurfa.2013.12.002

Sugimoto, T., Nishiya, M., & Kobayashi, M. (2017). Electrophoretic mobility of carboxyl latex particles: effects of hydrophobic monovalent counter-ions. *Colloid. Polym. Sci.* 295 (12), 2405–2411, http://dx.doi.org/10.1007/s00396-017-4219-1.

Sugimoto, T., Nishiya, M., & Kobayashi, M. (2019). Charge reversal of sulfate latex particles in the presence of lanthanum ion. Colloids and Surfaces A, 572, 18-26. https://doi.org/10.1016/j.colsurfa.2019.03.077

Sun, C., Yue, Q., Gao, B., Mu, R., Liu, J., Zhao, Y., Yang, Z., & Xu, W. (2011). Effect of pH and shear force on flocs characteristics for humic acid removal using polyferric aluminum chloride-organic polymer dual-coagulants. *Desalination*, 281, 243–247, https://doi.org/10.1016/j.desal.2011.07.065

Sun, H., Jiao, R., Xu, H., An, G., & Wang, D. (2019). The influence of particle size and concentration combined with pH on coagulation mechanisms. *J. Environ. Sci. (China)*, 82, 39–46. https://doi.org/10.1016/j.jes.2019.02.021

Sung, S. S., Ju, S.P., Hsu, C., Mujumdar, A.S., & Lee, D. J. (2008). Floc strength evaluation at alternative shearing with presence of natural organic matter. *Drying Technology*, 26(8), 996–1001. https://doi.org/10.1080/07373930802115669

Swift, S.R. (1999). Macromolecular properties of soil humic substances: fact, fiction, and opinion. *Soil Science*, 164, 790–802.

Szilágyi, I., Trefalt, G., Tiraferri, A., Maroni, P., & Borkovec M. (2014). Polyelectrolyte Adsorption, Interparticle Forces, and Colloidal Aggregation. *Soft Matter* 10: 2479-2502. doi: 10.1039/c3sm52132

Tambo, N. & Hozumi, H. (1979). Physical characteristic of flocs. 2. Strength of floc. *Water Research*, 13, 421–427.

Tan, L., Tan, X., Mei, H., Ai, Y., Sun, L., Zhao, G., Hayat, T., Alsaedi, A., Chen, C., Wang, X., & Wang, X. (2018). Coagulation behavior of humic acid in aqueous solutions containing Cs^{+}, Sr^{2+} and Eu^{3+}: DLS, EEM and MD simulations. *Environ. Pollut.* 236, 835−843.

Tan, W. F., Koopal, L. K., & Norde, W. (2009). Interaction between humic acid and lysozyme, studied by dynamic light scattering and isothermal titration calorimetry. *Environmental Science and Technology*, 43(3), 591–596, https://doi.org/10.1021/es802387u

Tan, W. F., Koopal, L. K., Weng, L. P., van Riemsdijk, W. H., & Norde, W. (2008). Humic acid protein complexation. *Geochimica et Cosmochimica Acta,* 72(8), 2090–2099, https://doi.org/10.1016/j.gca.2008.02.009

Tan, W., Norde, W., Koopal, L.K. (2014) Interaction between Lysozyme and Humic Acid in Layer-by-Layer Assemblies: Effects of pH and Ionic Strength. *Journal of Colloid and Interface Science* 430: 40–46. doi10.1016/j.jcis.2014.05.029

Terashima, M., Fukushima, M., &Tanaka, S. (2004). Influence of pH on the surface activity of humic acid : micelle-like aggregate formation and interfacial adsorption. *Colloids and Surfaces A: Physicochem. Eng. Aspects*, 247, 77–83. https://doi.org/10.1016/j.colsurfa.2004.08.028

Thieme, J., & Niemeyer, J. (2008). Interaction of colloidal soil particles, humic substances and cationic detergents studied by X-ray microscopy, *Struct. Dyn. Prop. Disperse Colloid. Syst.* 193–201, https://doi.org/10.1007/bfb0118132.

Tipping, E. & Hurley, M. A. (1992). A unifying model of cation binding by humic substances. *Geochimica et Cosmochimica Acta,* 56 (10), 3627-3641, https://doi.org/10.1016/0016-7037(92)90158-F

Tipping, E. (2002). Cation binding by humic substances, Cambridge University press (2002)

Torres, F. E., Russel, W. B., & Schowalter, W. R. (1991). Floc structure and Growth Kinetics for rapid shear Coagulation of polystyrene colloids, *J Colloid Interface Sci.* 142, 554

Treeby, M., Chitanu, G.C., & Kogej, K. (2005). Association of cationic surfactants with maleic acid copolymers: Dependence of binding on the nature of the neutral

comonomer unit. *J. Colloid Interface Sci*., 288, 280–289. https://doi.org/10.1016/j.jcis.2005.02.069

Valsesia, A., Desmet, C., Ojea-Jiménez, I., Oddo, A., Capomaccio, R., Rossi, F., & Colpo, P. (2018). Direct quantification of nanoparticle surface hydrophobicity. *Commun. Chem. 1*. https://doi.org/10.1038/s42004-018-0054-7

Van Os, N.M., Haak, J.R., & Rupert, L.A.M. (1993). Physico-Chemical Properties of Selected Anionic, Cationic and Nonionic Surfactants, Physico-Chemical Properties of Selected Anionic, Cationic and Nonionic Surfactants, Elsevier Science, 1993.

Vezenov, D. V., Noy, A., Rozsnyai, L.F., & Lieber, C. M. (1997). Force titrations and ionization state sensitive imaging of functional groups in aqueous solutions by chemical force microscopy. *J. Am. Chem. Soc.*, 119, 2006–2015, https://doi.org/10.1021/ja963375m

Wall, N. A., & Choppin, G. R. (2003). Humic acids coagulation: influence of divalent cations. *Appl. Geochem.* 18, 1573−1582.

Walz, J.Y., Suresh, L., & Piech, M. (1999). The effect of nanoscale roughness on long range interaction forces. J. *Nanoparticle Res*., 1, 99–113. https://doi.org/10.1023/A:1010065714589

Wang, D., Wu, R., Jiang, Y., & Chow, C.W.K. (2011). Characterization of floc structure and strength: Role of changing shear rates under various coagulation mechanisms. *Colloids and Surfaces A: Physicochemical and Engineering Aspects,* 379 (1–3),36–42, https://doi.org/10.1016/j.colsurfa.2010.11.048

Wang, L. F., Wang, L. L., Ye, X. D., Li, W. W., Ren, X. M., Sheng, G. P., Yu, H. Q., & Wang, X. K. (2013). Coagulation Kinetics of Humic Aggregates in Mono- and Di-

Valent Electrolyte Solutions. *Environ. Sci. Technol.*, 47 (10), 5042-5049. https://doi.org/10.1021/es304993j

Wang, S. & Mulligan, C.N. (2009). Enhanced mobilization of arsenic and heavy metals from mine tailings by humic acid. *Chemosphere*, 74(2):274-9, http://doi.org/ 10.1016/j.chemosphere.2008.09.040

Wang, W., Zhao, S., Yue, Q., Gao, B., Song, W., & Feng, L. (2017). Purification, Characterization and application of dual coagulants containing chitosan and different Al species in coagulation and ultrafiltation process. *Journal of Environmental Sciences*, 51, 214-221

Wang, Y., Gao, B.Y., Xu, X. M., Xu, W.Y., & Xu, G.Y. (2009). Characterization of floc size, strength and structure in various aluminum coagulants treatment. *Journal of Colloid and Interface Science*, 332(2), 354–359. https://doi.org/10.1016/j.jcis.2009.01.002

Warszyński, P., Papastavrou, G., Wantke, K. D., & Möhwald, H. (2003). Interpretation of adhesion force between self-assembled monolayers measured by chemical force microscopy. *Colloid and Surface A: Physicochemical and Engineering Aspects*, 214: 61–75, https://doi.org/10.1016/S0927-7757(02)00362-X

Weng, L., Fest, E. P. M. J., Fillius, J., Temminghoff, E. J.M., & Riemsdijk, W. H. V. (2002). Transport of Humic and Fulvic Acids in Relation to Metal Mobility in a Copper-Contaminated Acid Sandy Soil. *Environ. Sci. Technol., 36* (8), pp 1699–1704. https://doi.org/10.1021/es010283a

Weng, L., Van Riemsdijk, W. H., Koopal, L. K., & Hiemstra, T. (2006). Adsorption of Humic Substances on Goethite: Comparison between Humic Acids and Fulvic Acids. *Envron. Sci. Technol.* 40, 7494-7500

Winterwerp, J.C. (1998). A simple model for turbulence induced flocculation of cohesive sediment. *Journal of hydraulic Research*, 36(3): 309-326

Xia, W., Wang, Y., Yang, A., & Yang, G. (2017). DNA compaction and charge inversion induced by organic monovalent ions. *Polymers* 9:4. https://doi.org/10.3390/polym9040128

Yamaguchi, A. & Kobayashi, M. (2016). Quantitative Evaluation of Shift of Slipping Plane and Counterion Binding to Lysozyme by Electrophoresis Method. *Colloid and Polymer Science*, doi: 10.1007/s00396-016-3852-4

Yamashita, Y., & Saito, T. (2015). Effects of weak organic acids on the size distribution and size-dependent metal binding of humic substances as studied by flow field-flow fractionation. *J. Environ. Chem. Eng.*, 3, 3024–3029, https://doi.org/10.1016/j.jece.2015.03.026

Yee, M. M., Miyajima, T., & Takisawa, N. (2009). Study of ionic surfactants binding to humic acid and fulvic acid by potentiometric titration and dynamic light scattering. *Colloids Surfaces A Physicochem. Eng. Asp.*, 347,128–132, https://doi.org/10.1016/j.colsurfa.2009.02.010

Young, C., & Wandruszka, R. von. (2001). A Comparison of aggregation behavior in aqueous humic acids. *Geochem. Trans*., 2, 16. https://doi.org/10.1039/b100038l

Yu W. L. & Borkovec, M. (2002). Distinguishing heteroaggregation from homoaggregation in mixed binary particle suspensions by multiangle static and dynamic light scattering. *Journal of Physical Chemistry B* 106, 13106–13110, https://doi.org/10.1021/jp021792h

Yu, W. Z., Gregory, J., & Campos, L. (2010). Breakage and regrowth of Al-humic flocs - Effect of additional coagulant dosage. *Environmental Science and Technology*, 44(16), 6371–6376. https://doi.org/10.1021/es1007627

Zachara, J.M., Resch, C.T, & Smith, S.C. (1994). Influence of humic substances on Co^{2+} sorption by a subsurface mineral separate and its mineralogic components. *Geochim. Cosmochim. Acta.*, 1994, 58 (2), 553—566. https://doi.org/10.1016/0016-7037(94)90488-X

Zhu, C., Gao, Y., Li, H., Meng, S., Li, L., Francisco, J.S., & Zeng, X.C. (2016). Characterizing hydrophobicity of amino acid side chains in a protein environment via measuring contact angle of a water nanodroplet on planar peptide network. *Proc. Natl. Acad. Sci.* 113, 12946–12951. https://doi.org/10.1073/pnas.1616138113

Zhu, S., Avadiar, L., & Leong, Y.K. (2016). Yield stress- and zeta potential-pH behaviour of washed α-Al2O3 suspensions with relatively high Ca (II) and Mg (II) concentrations: Hydrolysis product and bridging. *International Journal of Mineral Processing*, 148, 1-8. https://doi.org/10.1016/j.minpro.2016.01.004